UNIVERSITY OF PARDUBICE
FACULTY OF CHEMICAL TECHNOLOGY

DOCTORAL DISSERTATION

2022 Jaroslav Charvot

UNIVERSITY OF PARDUBICE
FACULTY OF CHEMICAL TECHNOLOGY

Organic selenium compounds and their modern applications

Doctoral thesis
2022

Author: Ing. Jaroslav Charvot
Supervisor: prof. Ing. Filip Bureš, Ph. D.
Co-supervisor: Dr-Ing. Jan Macák, Ph. D.

PROHLÁŠENÍ

Prohlašuji:

Tuto práci jsem vypracoval samostatně. Veškeré literární prameny a informace, které jsem v práci využil, jsou uvedeny v seznamu použité literatury.
Byl jsem seznámen s tím, že se na moji práci vztahují práva a povinnosti vyplývající ze zákona č. 121/2000 Sb., autorský zákon, zejména se skutečností, že Univerzita Pardubice má právo na uzavření licenční smlouvy o užití této práce jako školního díla podle § 60 odst. 1 autorského zákona, a s tím, že pokud dojde k užití této práce mnou nebo bude poskytnuta licence o užití jinému subjektu, je Univerzita Pardubice oprávněna ode mne požadovat přiměřený příspěvek na úhradu nákladů, které na vytvoření díla vynaložila, a to podle okolností až do jejich skutečné výše.

Souhlasím s prezenčním zpřístupněním své práce v Univerzitní knihovně.

V Pardubicích dne

Jaroslav Charvot

ACKNOWELEDGEMENT

Although, that dissertation thesis is bearing name of just only one author, the number of essential people to present this work in its final form is much higher. Here, I would like to thank all those scientists, that cooperated with me during the whole realization process, starting with experiments and data processing to support during writing phase.

Namely, I would like to thanks to my supervisor Filip Bureš. As my guide since bachelor thesis, he always gave me valuable hints and knowledge, how to pursue my chemistry goals. But most importantly, I always received enough freedom, to do my research in a way, that I considered the best. This of course comes with giving me enough space, to let me make my own mistakes and finding a way, how to correct them.

Members of our group are always helpful and creates enjoyable environment and I am glad that our activities expand beyond common workplace interactions. Big thank belong to my colleague Daniel Pokorný, who cooperated with me during the syntheses of various products.

My gratitude belongs to the research team of Jan Macák and mostly to the Raúl Zazpe, who spend humongous part of his lifetime testing the prepared materials. Their work gave me a valuable information about the utility of the compounds and giving me a lot of motivation.

The significant part of this thesis was made during my internship at FAU Erlangen-Nürnberg in a group led by prof. Julien Bachmann. Julien is exceptional person worth to follow and I am grateful for opportunity to work in his team. The great thanks belongs also to the whole groups for teaching me a lot of stuff, that I didn't know a single thing about before, but most importantly very warm and welcoming environment.

In the end, I would like to thank the Czech science foundation (18-03881S) and the Technology Agency of the Czech Republic (TH80020009) for funding. University of Pardubice for the space and opportunity to study and be a part of research. And my family, which always gives me endless support.

ANNOTATION

This dissertation work is focused on selenium compounds and their utilization in modern materials sciences. Selected thin film deposition techniques with emphasis on Atomic Layer Deposition (ALD) are briefly introduced along with possible utilization of manufactured nanolayers. The latter part of the thesis is devoted to various organic selenides as potential ALD precursors. Several cyclic silyl-selenides, linear silylselenides, silylselenols, stanylselenides and one silyltelluride were prepared using described, modified, and newly developed synthetic pathways. All target molecules were characterized by GC/MS and multinuclear NMR. DSC and TG analyses were employed to determine fundamental thermal behaviour, as a key parameter of ALD precursors. The last part of the work is dedicated to testing selected selenides in ALD to produce $MoSe_2$ and Sb_2Se_3 thin films.

KEYWORDS

Selenium, synthesis, ALD, depositions, thin films

NÁZEV

Organické sloučeniny selenu a jejich moderní využití.

ANOTACE

Tato disertační práce se zabývá sloučeninami selenu a jejich aplikací při tvorbě tenkých vrstev. První část práce představuje vybrané depoziční metody s bližším zaměřením na technologii Atomic Layer Deposition (ALD), její charakteristiky, využití a obecné požadavky na ALD prekurzor. Ve větším detailu je pak studována příprava a vlastnosti organických sloučenin selenu s již popsaným či potenciálním využitím v ALD. V experimentální části práce bylo připraveno několik silylselenidů, silylselenolů, stanylselenidů a jeden silyltelurid. Charakterizace cílových molekul byla provedena pomocí GC/MS a multinukleární magnetické rezonance. Syntéza a strukturní analýza je doplněna o studii základních termických vlastností (DSC a TGA), které jsou pro využití v ALD zcela klíčové. Vybrané selenidy byly v poslední části práce testovány při tvorbě tenkých vrstev $MoSe_2$ a Sb_2Se_3.

KLÍČOVÁ SLOVA

Selen, syntéza, ALD, depozice, tenké vrstvy

1 Table of content

List of figures

List of schemes

List of tables

List of abbreviations

AFM – Atomic Force Microscopy
ALD – Atomic Layer Deposition
CBD – Chemical Bath Deposition
CVD – Chemical Vapor Deposition
CZTS – Copper Zinc Tin Sulphide
DSC – Differential Scanning Calorimetry
EDX – Energy Dispersive X-Ray Analysis
GC/MS – Gas Chromatography/Mass Spectrometry
GPC – Growth Per Cycle
HAAFD-STEM – High-angle Annular Dark-field Scanning Transmission Electron Microscopy
HER – Hydrogen Evolution Reaction
MLD – Molecular Layer Deposition
NMR – Nuclear Magnetic Resonance
OER – Oxygen Evolution Reaction
SEM – Scanning Electron Microscopy
SILAR – Successive Ionic Layer Adsorption and Reaction
STEM – Scanning Transmission Electron Microscopy
TMDC – Transition Metal Dichalcogenides
TE – Thermoelectrics
TGA – Thermogravimetric Analysis
THF – Tetrahydrofuran
TMA – Trimethylaluminum
XPS – X-Ray Photoelectron Spectroscopy
XRD – X-Ray Diffraction

2 Introduction

Nanotechnology, as a scientific discipline studies the properties, preparation and application of objects with the size up to 100 nm. These unimaginably tiny dimensions possess characteristics that are often completely different from the properties observed in a bulk of the same material. It is unnecessary to describe current fields affected by application of nanotechnologies, because there is almost no domain of human endeavour, where nano-scale materials are not applied in some way.

Although preparation of thin films, nanoparticles or other smaller than microscopic species are steadily gaining more and more interest, many challenges still emerge in scientists' minds and efforts. This work intends to deal with one of such calls – fabrication of high quality nanofilms of materials that were scarcely investigated so far. For this purpose, Atomic Layer Deposition (ALD) was chosen, as its unique abilities and high demands of ALD community ensure preparation of outstanding nanofilms.

On the upcoming pages, the ALD along with its sister technology CVD (Chemical Vapour Deposition) and selected solvent-based deposition techniques are briefly introduced. Established and potential applications of selected materials will be summarized in the next part.

ALD precursors are chemical substances utilized in the ALD reactor for deposition. Precursors must possess specific properties such as reactivity, volatility and thermal stability, while finding a trade-off between these properties represents a key point for successful thin film fabrication. Therefore, considerable part of this literature research is focused on ALD precursors and attempts to describe an ideal ALD precursor.

Metal selenides are interesting materials with application in various technologies such as photovoltaics, thermoelectrics or phase change transistors. Nevertheless, selenium ALD precursor portfolio is very limited, to only few options, namely toxic H_2Se, not sufficiently reactive Et_2Se and bis(trimethyl)silyl selenide. The latter is the most established selenium precursor so far. This work aims to focus closer on the existing and potential selenium precursors, their synthetic routes, yields and difficulties during preparation. The most important properties of precursor, such as sufficient reactivity, volatility and thermal stability, are also discussed.

3 Aims of the dissertation

The main aims of this work are as follows:

- To perform literature search focusing on principles of ALD and selenium ALD precursors; especially their preparation and utilization.
- To prepare organic selenides with possible application in ALD.
- To characterize prepared organic selenides including their fundamental thermal behaviour.
- To test applicability of the prepared organic selenides in ALD.

4 Vapor deposition methods - Chemical Vapor Deposition (CVD)

Although this work is mostly focused on ALD, CVD is also briefly introduced. The reason is that ALD community and literature often refers to different types of film mechanism deposition as “CVD (or ALD) - like growth.” Therefore, these characteristics and terms needs to be clarified for both methods.

A CVD process may be defined as a deposition of a solid by chemical reaction in the vapor phase near or on a heated substrate surface.[1] *Figure 1* illustrates this process graphically. In the first step, typically two precursors are simultaneously introduced into the reaction chamber with the heated substrate, where their mutual reaction leads to the deposition of material until precursors are entirely consumed or equilibrium is established. This means that the control of thickness is only maintained by the precursors selection, their amount, temperature and reaction time (exposure of precursors to the substrate). Composition of the material is mostly dependent on the used precursors, however other properties such as their stoichiometry or temperature play also a role. The last step is purging or evacuating the chamber to ensure removal of by-products and unreacted precursors.

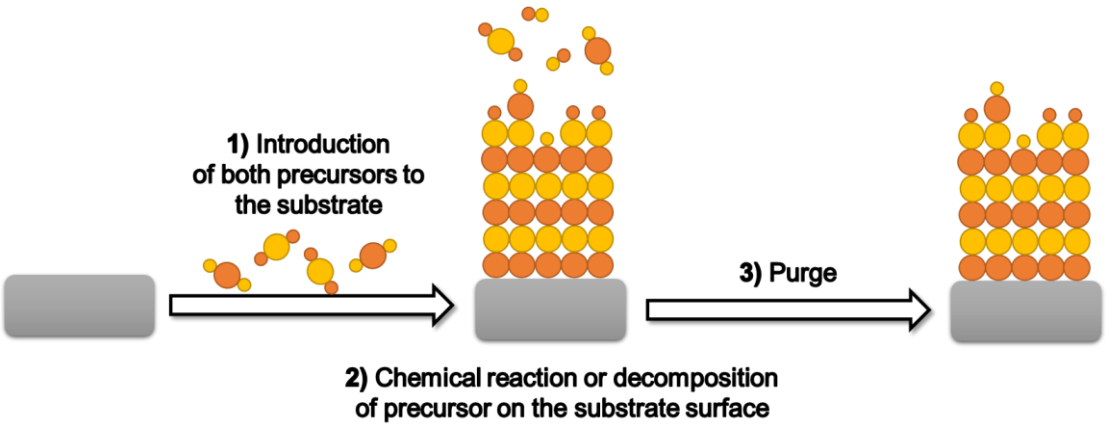

Figure 1. Simplified CVD process.

The chemical reaction in the case of CVD includes wide variety of mechanisms such as reduction, oxidation, nitridation and very often also thermal decomposition (pyrolysis). To activate the precursors, high temperature is often needed. The high temperature means above 500 °C, but temperatures up to 1000 °C or even more are also applied in some cases. Even though the temperature could be lowered with the use of plasma or UV-light, the temperature lower than 300 °C is not commonly used,[1] which prevents depositions on thermally labile substrates. On the other hand, CVD offers deposition using inexpensive precursors with high deposition rates and very thick films (micrometres or more)

can be obtained readily with fair conformality and purity.[2] High temperatures also allow deposition of materials such as metal carbides, nitrides or diamond.[3]

5 Vapor deposition methods – Atomic Layer Deposition (ALD)

5.1 Introduction to ALD

ALD was simultaneously discovered by two teams: prof. Aleskovskii research group from the former USSR and the group led by Dr. Suntola from Finland, who's technique was later in the 1977 patented. The history of ALD was nicely summarized by Puurunen.[4]

The first ALD success was demonstration of its abilities in commercial deposition of ZnS thin films in electroluminescent displays technology, because other methods like sputtering or vacuum evaporation failed. Since that, a great boom of advanced processes, ALD tools and precursor portfolio for various materials is encountered both in academic and industrial research.[5] The importance and increasing interest is easily visible in ALD semiconductor equipment market. *Figure 2*[6] shows that its size overgrowth forecasts in several past years and the ALD semiconductor business is now multibillion worth market.

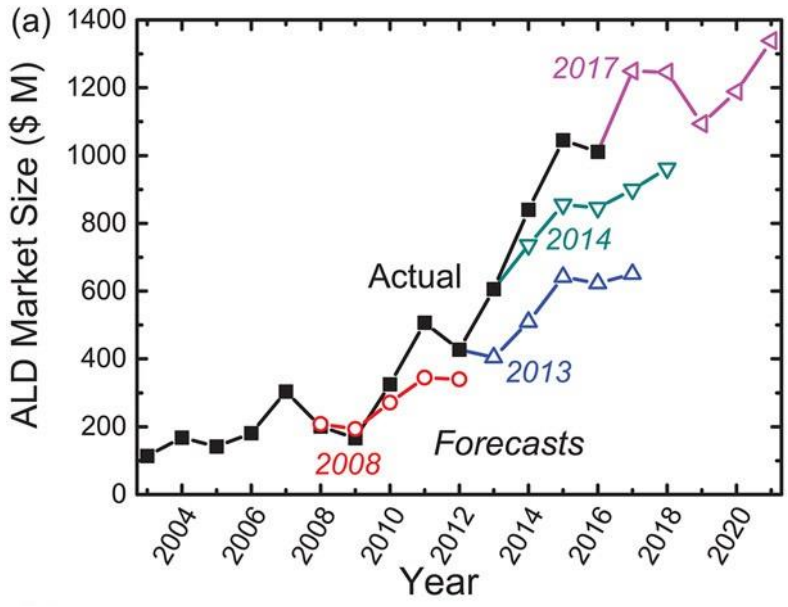

***Figure 2**. ALD semiconductor equipment market size.*[6] *(Reused with AIP Publishing permission)*

5.2 ALD thin film growth mechanism and characteristics

Its fundamental characteristics make ALD very precise and unique among other deposition methods. These features originate from the deposition nature itself; a simplified reaction mechanism shown in *Figure 3* may give an initial idea about cyclic process consisting of few simple steps. Firstly, the precursor (gaseous species including an atom that is going to

be deposited) is transferred to the reaction chamber containing the selected substrate. Here, the precursor undergoes gas-solid chemical reaction with free functional groups of the substrate, until all of the reaction sites are occupied. This is the key factor of a successful ALD process because self-limiting reaction of the precursor with the substrate surface ensures growth of only one atomic layer. To prevent mixing of the precursors in gas phase, the reaction chamber is evacuated and (or) purged by an inert gas making it ready for introduction of the second precursor. Again, a single atomic layer is deposited and upcoming purge finishes the deposition of the first cycle.[7] Thus, the number of cycles precisely controls the thickness within an Angstrom level precision.

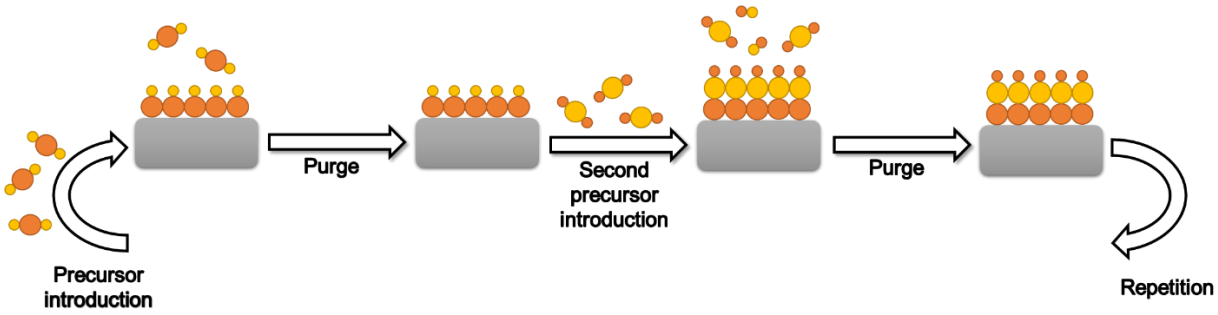

Figure 3. Simplified ALD mechanism scheme.

Nevertheless, various deviations from this ideal model may appear resulting in more or less pronounced defects. To ensure that the deposition is "really ALD" and a solely self-limiting growth is present, a series of experiments with different parameters needs to be carried out. The most common ones involve study of linearity, saturation and ALD window. Moreover, the prepared layer should also display uniformity and conformality, the same thickness over the whole substrate area, the same thickness along the 3D-structures and a constant growth rate at the initial and later stages of deposition.[8]

The saturative ALD process should always provide the same amount of deposited material per cycle, thus the increase of thickness (or mass) must be linearly dependent on the number of cycles. This is commonly referred as Growth Per Cycle (GPC), however it is important to understand that this term does not describe the reality precisely. The incisive description of the GPC can be found in the book entitled *Atomic Layer Deposition in Energy Conversion Applications,*[9] in which the following quote by J. Dendooven and C. Detavernier can be found:

"*GPC value does not reflect in any way the chemical reaction kinetics during the deposition process, but is determined by the number of chemisorption sites on the growth surface, which will depend on the reactivity and number of accessible surface sites and even on surface morphology (…) The apparent GPC is substrate dependent at the start of the ALD process and that it takes a certain number of cycles before a steady-state GPC value is*

obtained. This is caused by the fact that the chemical sites on the original substrate can have a different reactivity compared to the chemical sites on the surface of the as-grown material."

Figure 4 shows three cases that may happen during the deposition process.[9] The green curve (a) is situation, where substrate enhances the growth rate level. For instance, this behaviour was observed during the deposition of Co on SiO_2[10] or Ti on platinum.[11] The blue curve (b) depicts linear ALD growth with smooth continuous layer and homogeneous increase of material deposited per every cycle. Third situation shown by the orange curve (c) demonstrates the inhibition effect of the substrate with typical island structure growth, if the incoming precursor preferentially chemisorbs on already deposited material rather than substrate surface.[12] Nevertheless, after certain number of cycles, while the whole surface area is covered and materials grows on "itself", the deposition rate is stabilized at a constant rate.[13]

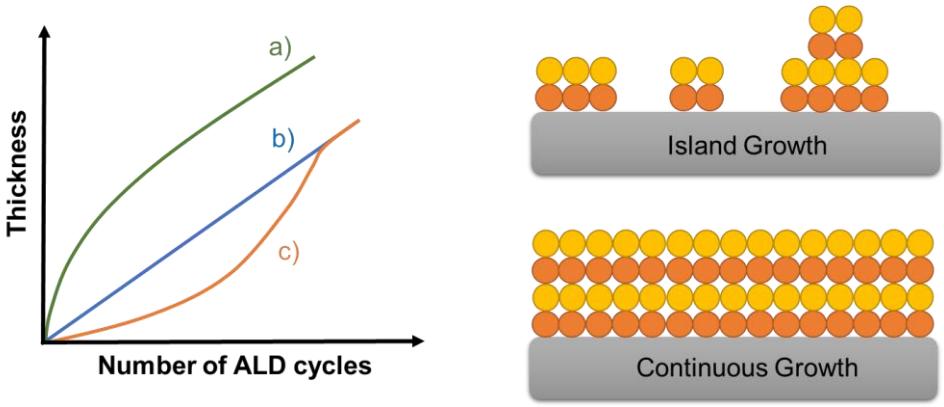

Figure 4. GPC curves and film morphology.

The saturative reaction can only take place, if there is sufficient amount of precursor to cover the whole substrate. The amount of evaporated precursor may be difficult to determine, however the saturation effect is easily observed on thickness increase while the dosage time of precursor (Pulse length) is plotted as a function of GPC (all experiments need to be done at the same temperature), which should fetch stable value after particular pulse length, see *Figure 5*. A purge time study is another prerequisite as remaining precursor in the reaction chamber may cause a CVD type reaction with higher growth rates upon dosing the second precursor.

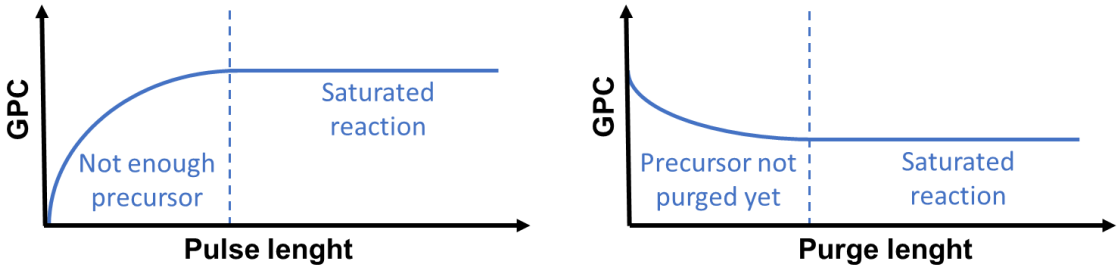

Figure 5. ALD saturation curves.

Temperature of the substrate (chamber) is also very important attribute during the thin film preparation. If the temperature is too low, the energy might be insufficient to allow the reaction between precursor and substrate and exchange of ligands will not happen. Another possibility is that low temperature causes physisorption of precursor on the surface, which will appear as increased growth, but not in the self-saturation manner. Similar situation could be observed also with too high temperature. Growth rate might be higher as the precursors are thermally decomposing or lower if the deposited material evaporates from the surface. An ideal ALD temperature, also called as "ALD window", is depicted in *Figure 6*, however the GPC can vary at different temperatures even though self-limited growth is maintained. This is happening, because the number (density) of free functional groups on substrate surface might be directly dependent on temperature.[9]

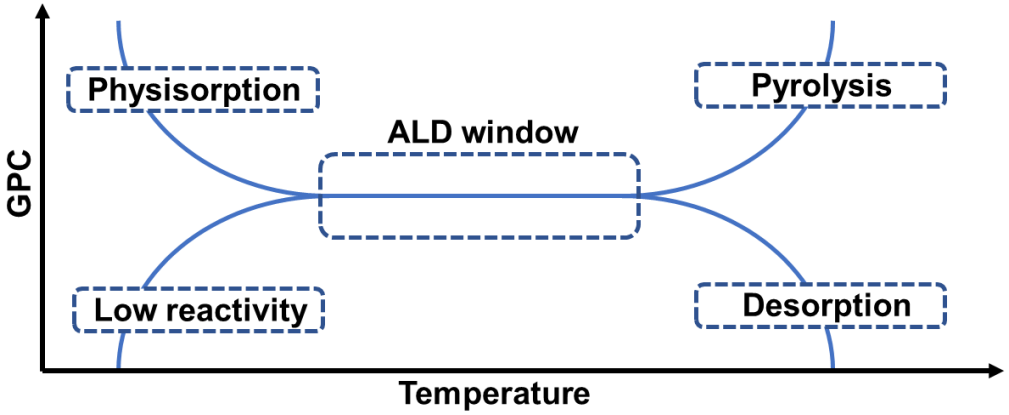

Figure 6. Growth rate dependency on temperature; the "ALD window".

5.3 Uniformity, conformality and selectivity of ALD

Equal distribution of precursor along the reaction chamber leads to equal thickness increase along the whole substrate surface. If the thickness varies among the substrate, then ALD growth is not maintained. The reason could be in wrong parameters or rather ALD reactor flaws like "gas dead pockets," temperature gradients or uneven distribution of precursor in the chamber.[14] By avoiding such a flaws, the ALD process offers great uniformity bearing the same thickness among the flat substrate, but also conformality, which is described as the same thickness on the three dimensional species surface. Conformal deposition of various materials on heterostructures like tubes, trenches, spheres and others is rapidly growing topic in nanotechnology and it is also one of the best opportunities for ALD to stand up among the other deposition techniques. This feature is exploited by fields with high demands on thickness control such as semiconductor industry[15] or large surface area substrates that are typical for photovoltaics or catalysis.

The difference between uniformity and conformality is schematically depicted on *Figure 7*. As an example, *Figure 8* shows real representation of the ALD conformality capabilities.[16, 17]

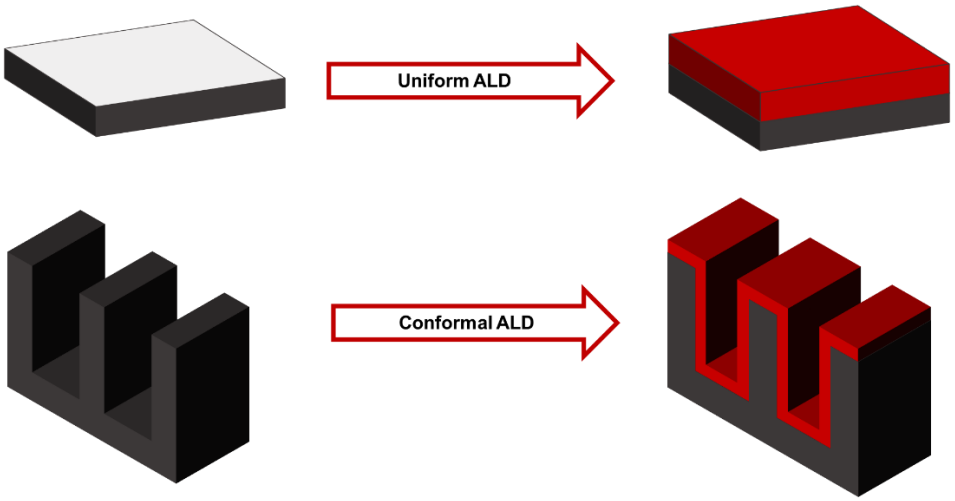

***Figure 7**. ALD uniformity and conformality.*

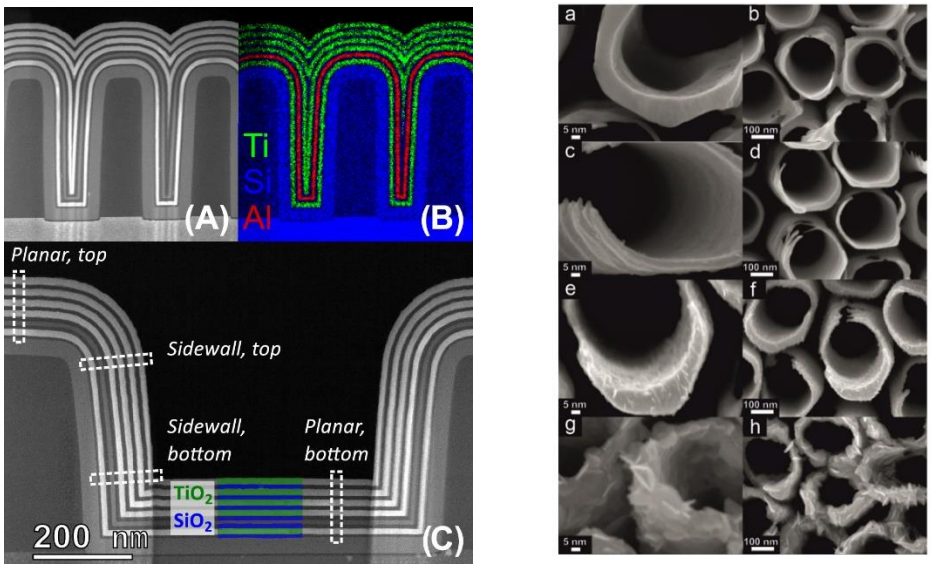

Figure 8. **Left:** Cross-sectional HAADF-STEM images (A, C) and an EDX map (B) of a stack of alternated TiO_2 and SiO_2 layers and a single layer of Al_2O_3, deposited on vertical trenches.[16] (ACS Publications, Under Creative Commons License). **Right:** SEM top-view images at two different magnifications of TiO_2 nanotubes decorated with (a,b) 20, (c,d) 60, (e,f) 180, and (g,h) 540 $MoSe_2$ ALD cycles.[17]

Selective deposition is another unique ability of ALD. It becomes a “real hot topic” because of increasing demands by electronics and semiconductor industry. Patterned substrate containing two materials that possess different affinity towards the precursor may demonstrate deposition on only one type of material, meanwhile the other is left without any change.[18] Hydroxylated silicon Si-OH usually acts as growth area and hydrogen terminated silicon Si-H as a non-growth area[19] even though the exactly opposite situation might occur.[20] Other specifications like crystal orientation or reaction temperature also play the role during

selective deposition.[21] *Figure 9* shows scheme of selective ALD (*top*) accompanied with STEM and EDX images of preferential TiN deposition onto different substrates (*bottom*).[22]

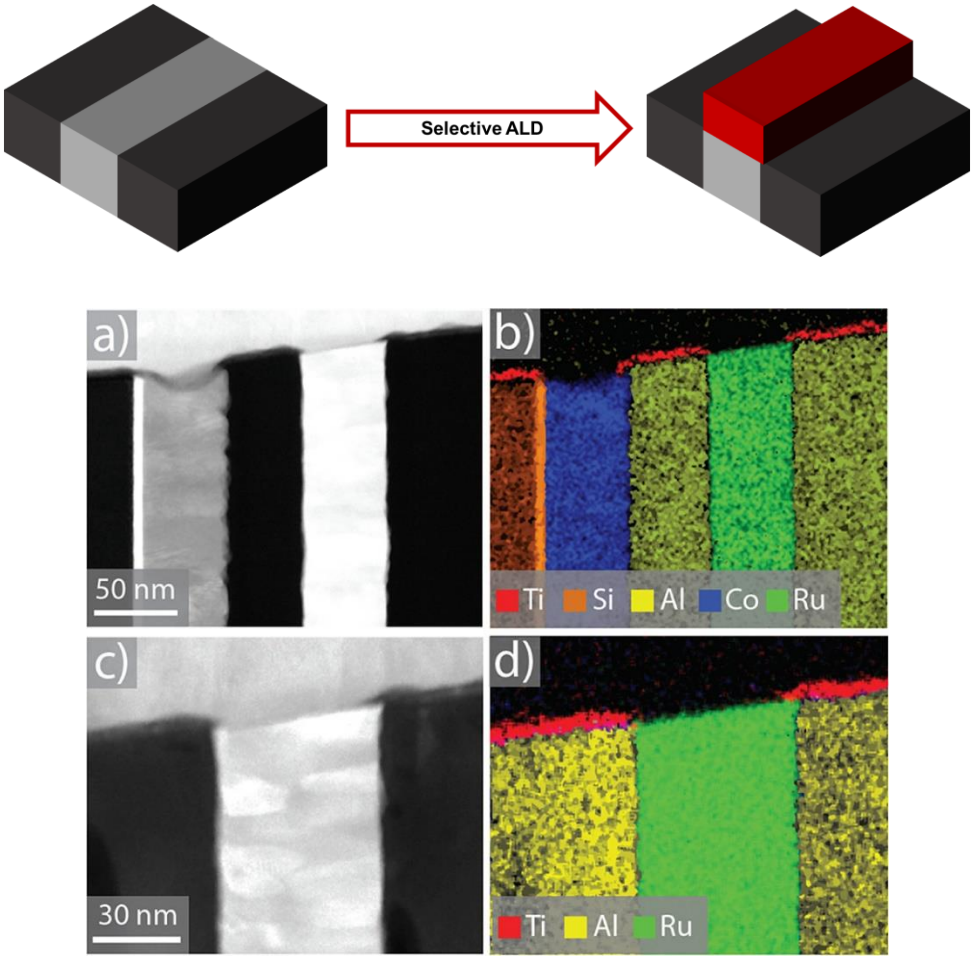

Figure 9. Top: Schematic representations of selective ALD. **Bottom**: (a,c) HAAFD-STEM images and (b,d) EDX mappings of the cleaved multilayer sample after 200 TiN ALD cycles.[22] (ACS Publications, Under Creative Commons License)

5.4 Limitations of ALD

The effective and precise coatings offered by ALD come with some disadvantages and challenges to deal with. The first problem might be price of ALD reactor itself and maintenance expenses due to demand on high vacuum and thus precisely working valves, sealings and other sensitive parts, that need to be replaced regularly. The ALD operation also requires high energy, inert gas and precursor consumption, where 60–90 % or more of precursor is usually wasted.[23,24] Mentioned problems leads to low and difficult sustainability of ALD. The ecologic and economic drawbacks in ALD were recently reviewed and discussed with suggestions to optimize the environmental drain.[24]

Often mentioned limit is deposition rate. This is naturally true, as the highest possible growth per cycle corresponds to thickness (radius) of one atomic layer, which is in the most

cases in units of Angstroms. A deposition of tens or hundreds of nanometres might take even thousands of cycles lasting several hours. Next drawback is seen in a selection of materials and available portfolio of ALD precursors. Even though several new precursors appear every year, finding a suitable precursor pair that will possess satisfactory growth on selected substrate might be difficult. The high reactivity demanded by ALD process is often accompanied with pyrophoricity or toxicity increasing safety risks. More details on precursor design and selections is given in the next chapter.

In summary, ALD is very efficient deposition technique in specific areas, especially for deposition with low number of defects, coating of variously shaped nanostructures or sensitive substrates. On the other hand, if higher thickness or lower quality of deposited material is required/sufficient, less demanding deposition techniques should be used.

6 ALD precursors

6.1 General characteristics

ALD precursor is a substance containing an element or molecule to be deposited. Usually, it is an organic or inorganic molecule carrying metal atom, however even larger molecules (Molecular Layer Deposition – MLD) can be used to prepare organic polymer or organic-inorganic hybrid thin films.[25] A reaction between two precursors is most commonly employed, but materials using three or more precursors could also be combined in so called super cycle. Deposition of $GeSb_xSe_yTe_z$ using four different precursors, $Ge(OEt)_4$, $Sb(OEt)_3$, $Se(SiMe_3)_2$ and $Te(SiMe_3)_2$, is an example.[26] Alternatively, using two (or more) precursors in pairs allows to form sandwich structures, for instance deposition of $PbSe_xTe_y$ with subsequent layering of PbSe and PbTe.[27]

A selection of the right precursors is crucial for successful ALD process. In general, an ideal precursor should fulfil all of the listed basic requirements:

- Sufficient and desired reactivity with the second precursor and the substrate surface.
- Sufficient volatility at selected temperature and the pressure.
- Thermal stability without decomposition during the whole process.
- Generation of non-corrosive by-products.
- Accessibility – simple synthesis and purification, low purchase prices.
- Easy handling, including low air-sensitivity, non-toxicity or pyrophoricity.

Even though the most of the elements in periodic table have at least one reported precursor[8] with the exception of radioactive materials and thallium, finding the right molecule for desired process might be very challenging and a compromise have to be made during the precursor design. Typically, high reactivity and volatility is usually accompanied by low air-stability or pyrophoricity. On the other hand, using bulkier ligands might lead to low volatility or insufficient deposition rates. Moreover, a preparation of complicated ligands is often complemented by lower yields and increased expenses disallowing their use beyond laboratory scale.

6.2 Inorganic ALD precursors

In principle, the pure element itself is the simplest possible precursor. The most important representatives are O_2 and O_3 used to produce metal oxide layers.[28] Other chalcogenides including elemental S,[29–31] Se[32–34] and Te[35,36] were also reacted with metals like Zn, Cd or Mg. In general, elements are cheap precursors and possess great purity of deposited materials, obviously because no other elements are present.

However, with exception of O_2 (O_3), their use is limited to few materials such as ZnX and CdX (X = S, Se, Te) and their principally low volatility and reactivity is often redeemed by higher reaction temperature.

Along with elements, hydrides and halides belong to the group of inorganic precursors. Dihydrochalcogenides H_2O,[28] H_2S[37] are commonly used. H_2Se[38] is more problematic due to its toxicity and instability. Another often used "hydrides" are NH_3 for deposition of nitrides,[39] SiH_4 (Si_2H_6), and even AsH_3 despite its extreme toxicity. Deposition of phosphides may be accomplished by PH_3 and plasma activation.[8] Halides, mostly chlorides and less often fluorides, are abundant class of precursors for metals ($AlCl_3$, WCl_5, WF_6, $MoCl_5$, $TiCl_4$) and non-metals ($SiCl_4$, $SbCl_3$, PCl_3, etc.). Chlorides are often endowed by sufficient volatility, thermal stability and high reactivity. Their low price also comes with higher sustainability as structurally more complicated ALD precursors are often prepared by ligand-to-halide exchange, while skipping preparation of another precursor significantly simplify and reduce subsequent ALD.[24] Nevertheless, the main disadvantage of halides is seen in their corrosive nature and formation of potential by-products like HCl, both damaging the ALD equipment.

6.3 Organometallic, Oxygen and Nitrogen coordinated ALD precursors

Some alkylated metals are very volatile and reactive, thus potentially very good ALD precursors. Indeed, Me_3Al along with Et_2Zn are well-established and studied precursor for ALD.[40] Besides serving as a metal source during deposition, these compounds may also be applied as drying or passivating agent and indicator of leaks. Depositions with Me_3In,[41] Me_3Ga[42] and others were also performed. A significant part of alkyl derivatives are based on transition metal cyclopentadienyls like $(EtCp)_2Mg$,[43] Cp_2Fe[44] or $(MeCp)_2Ni$.[45] A general drawback of this class of precursors is enhanced reactivity, rather too high for some derivatives such as Me_3Al, Me_2Zn. This fact requires careful manipulation with strict safety measures to obey. On the other hand, typically cyclopentadienyls (Cp_2Fe) or $SnEt_4$ are not enough reactive and require activation with plasma or H_2.

Alkoxides are also commonly employed in ALD, $Ti(O\mathit{i}Pr)_4$ for deposition of TiO_2 is a typical example.[46] Alkaline metal thin film manufacturing with ALD is difficult, because of ionic nature and thus very low volatility and thermal stability, but *tert*-butoxides of whole column of alkali metals were successfully used.[47] β-Diketonates were proposed and used as volatile materials for metal separation by sublimation and gas chromatography,[15] so these properties were later re-inspected in CVD and ALD. Wide range of *d*-block metals were used as simple acetylacetonate (Ni^{+2}, Cu^{+2}, Pt^{+2}),[48] di-*tert*-butylacetoacetonate (Cu^{+2},[49] Co^{+2}[50]) or hexafluoro acetylacetonate (Pd^{+2},[51] Ag^{+1}[52]). While their chemical stability and resistance to air are high enough, the reactivity is too low along with poor deposition rates and oxygen or carbon impurities.

Nitrogen based ligands consist mostly of dialkylamides or bis(trimethylsilyl)amides widely used for *d*-block metals such as $Zr(NMe_2)_4$ or $Hf(NMe_2)_4$[53] as well as metal amidinates. The latter can be considered as analogues to β-diketonates, where metal atom is coordinated with two nitrogen atoms. Deposition of $GdSc_xO_y$ using gadolinium and scandium alkylamidinates is an example.[54] Unlike alkoxides and β-diketonates, amides and amidinates possess higher reactivity, which is however usually accompanied by lower thermal stability.

Figure 10 summarizes the aforementioned groups of ALD precursors with their common abbreviations. It shows main ideas and possibilities rather than comprehensively review available precursors. Some classes are combined together (e.g. $CpZr(NMe_2)_3$),[55] while some less usual precursors (e.g. $Me_2Au(S_2CNEt_2)$[56] and very recent g-DAS ligand with promising possibilities for Li, Mg and several other transition metals deposition,[57] are presented. Even though almost all elements from the periodic table were screened as ALD precursors, the results of their depositions are sometimes unsatisfactory, which opens room for new precursor development.

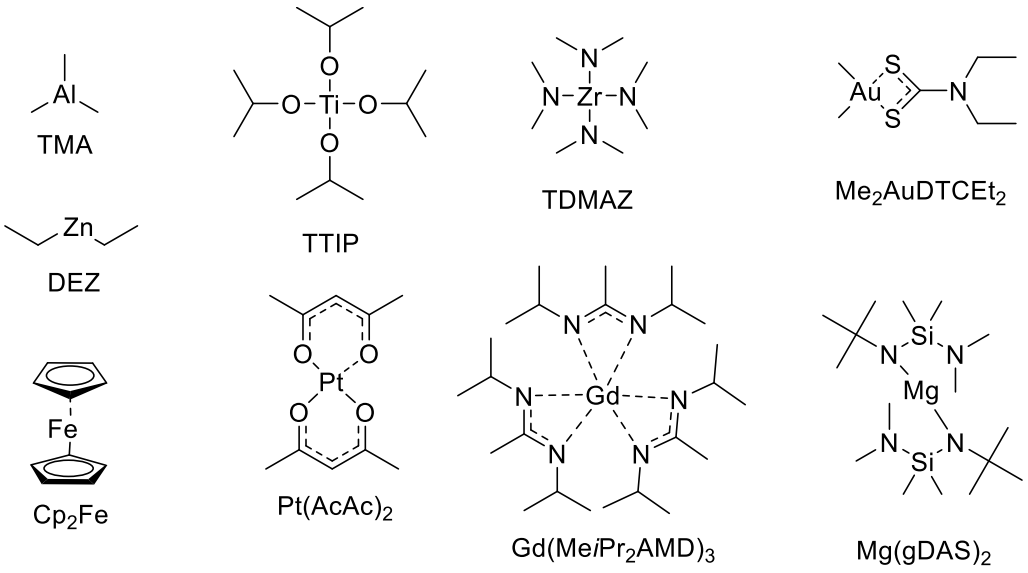

Figure 10. Examples of ALD precursors with commonly used abbreviations.

7 Selenium precursors

7.1 Se, H_2Se and dialkyl(di)selenides

Up to date, deposition of 15 different selenides was reported. This list includes Sr, Mo, W, Cu, Zn, Cd, In, Ge, Sn, Pb, Sb and Bi[8,58] with Fe, Co and Ni as the most recently presented materials.[59]

The first depositions using elemental selenium as a precursor afforded CdSe[31] and ZnSe[32] thin films. Another approach during deposition of SrS_xSe_y and ZnS_xSe_y is preparation of strontium and zinc sulfides using H_2S with following exchange of sulfur by elemental selenium.[34] Unfortunately, the aforementioned disadvantages of pure elements, such as low volatility and reactivity, hold true also for elemental selenium.

Hydrogen selenide H_2Se is very reactive gaseous compound reported to be suitable as ALD precursor several times. Deposited materials includes ZnSe by reacting H_2Se and Et_2Zn, $Zn(N(SiMe_3)_2)_2$,[60] or $ZnCl_2$.[61] The reaction with Me_2Cd gave CdSe.[62] $SbCl_3$ affords smooth Sb_2Se_3 thin films and $InCl_3$ surprisingly InSe.[63] A similar situation has been observed for Et_4Sn affording SnSe,[64] while WSe_2 has also been mentioned.[38] A reaction of hydrogen selenide with metal halides generates corrosive HX, which is generally not suitable for sensitive ALD parts. The principal limitation of H_2Se application is its high toxicity, while serious precautions and measures must be followed, especially for large scale depositions during eventual industrial manufacturing.

Alkyl selenides or diselenides are often employed by CVD for depositions at higher temperatures starting around 500 °C. CVD for example use Et_2Se and WCl_6 for WSe_2 depositions[65] or tBu$_2$Se reaction with $MoCl_5$ yielding $MoSe_2$[66] at temperatures from 500 to 650 °C. Even CVD of ZnSe using reactive Et_2Zn has to be carried out at 500 °C with NF_3 as co-reactant.[67] This fact implies that the C–Se bond is strong and the growth mechanism is based on decomposition rather than saturated reaction. Activation with H_2 plasma allows to use these molecules as an inexpensive selenium source but hamper depositions on labile substrates. Et_2Se_2 along with plasma activation was used for deposition of ZnSe[68] and recently for $FeSe_2$, $CoSe_2$ and $NiSe_2$.[59]

7.2 Bis(trialkylsilyl)selenides

Bis(trialkylsilyl)selenides with a general formula of $R_3Si\text{-}Se\text{-}SiR_3$ were presented in 2009[69] by Pore and became one of the most versatile selenium precursors. In contrast to dialkylsilyl selenides, fairly polarized Si-Se bond ensures enough reactivity with metal halides, alkoxides or amides. These reactions yield trialkylsilylchloride, trialkylsilylamine or trialkylalkoxysilane as by-products; all of them are ALD-approved due to their non-corrosive nature. The exchange of ligands depicted on *Scheme 1* is favored, because silicon center

(hard Lewis acid) is bonded to selenium atom (soft Lewis base) and after ligand recombination, preferred hard-hard (Si-Cl) and soft-soft (Se-M) pairs are generated.

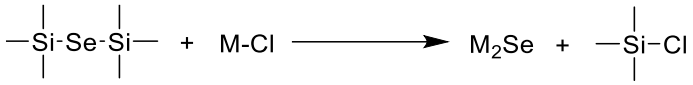

Scheme 1. A representative reaction of bis(trimethylsilyl)selenide with metal chloride.

Table 1 summarizes metal selenides deposited so far using $(R_3Si)_2Se$ precursors. Except these binary compounds, some ternary or tertiary structures were also prepared including $GeSb_xSe_yTe_z$,[26] $MoSe_xO_y$,[70] $SbSe_xTe_y$[71] and $PbSe_xTe_y$.[27]

Table 1. Binary selenides reported using bis(trialkylsilyl)selenides.

Prepared material	Metal precursor	Selenium precursor	Reference
Bi_2Se_3	$BiCl_3$	$(Et_3Si)_2Se$	Ref.[69,72]
Cu_xSe_y	CuCl	$(Et_3Si)_2Se$	Ref.[69]
	$Cu(O_2CtBu)_2$	$(Et_3Si)_2Se$	Ref.[69,73]
$GeSe_x$	$Ge(N(SiMe_3)_2)_2$	$(Me_3Si)_2Se$	Ref.[74]
	$HGeCl_3$	$(Me_3Si)_2Se$	Ref.[75]
In_2Se_3	$InCl_3$	$(Et_3Si)_2Se$	Ref.[69]
$MoSe_2$	$Mo(CO)_6$*	$(Me_3Si)_2Se$	Ref.[76]
	$MoCl_5$	$(Me_3Si)_2Se$ $(Et_3Si)_2Se$ $(iPr_3Si)_2Se$	Ref.[77]
ZnSe	$ZnCl_2$	$(Et_3Si)_2Se$	Ref.[69]

**High amount of MoO_x was present*

A series of systematically enlarged bis(trialkylsilyl)selenides $(R_3Si)_2Se$ has been designed and prepared during the authors diploma work.[78] The alkyl residues involved Me, Et, *i*Pr and *t*Bu. The volatility and thermal stability of $(R_3Si)_2Se$ were studied by TGA[79] as well as DSC (*Figure 11*). The measured TGA curves revealed zero residues and gradual evaporation with onset temperature dependent on the molecule weight and alkyl chain branching. The same structure-property relationships are seen in the DSC curves featuring

higher boiling points for heavier substances with smooth evaporation maintained. High thermal stability is also confirmed during high temperature depositions of $MoSe_2$ at 350 °C[77] or ZnSe and Cu_2Se at 400 °C.[69]

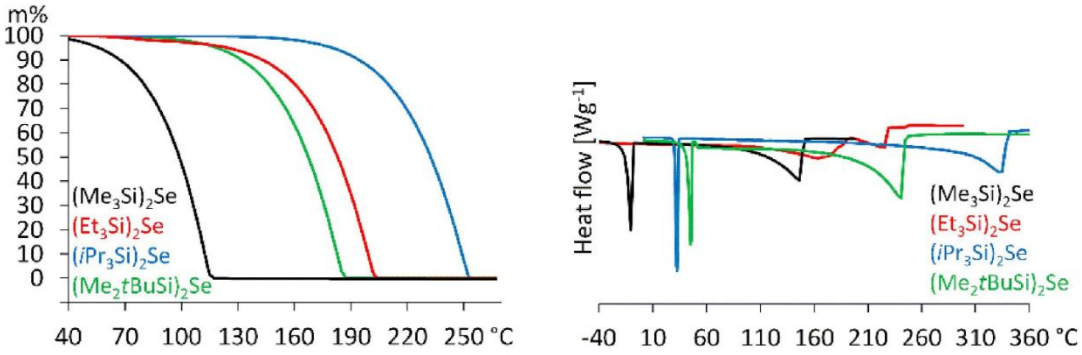

Figure 11. TG (left) and DSC (right) analyses showing thermal behaviour of selected bis(trialkylsilyl)selenides.[77] (Under Creative Commons License, Modified)

Preparation of bis(trialkylsilyl)selenides is a two-step reaction initiated by reduction of the elemental selenium to reactive selenide (*Scheme 2*). This could be achieved by direct reaction with alkaline metal (M = Li, Na, K) in THF. Naphthalene or diphenylacetylene improve the conversion, reaction rate and yield of M_2Se.[79,80] Another method, employed by Gladysz[81] and later Detty,[82] consists of a direct selenium reduction by Super-Hydride® solution, which is 1M $LiBHEt_3$ in THF. This method is faster and generally possesses higher yields. Despite the Li_2Se preparation using pure elements requires reflux at 70 °C and longer reaction time up to 72 h, the starting materials are readily available and inexpensive.

In the next step, two equivalents of selected trialkylsilylchloride are added to this *in-sittu* prepared Li_2Se affording the final bis(trialkylsilyl)selenide. The reaction is accelerated by addition of catalytic amount of $BF_3{\cdot}OEt_2$. Syper[80] has mentioned that if selenium is added in an excess, Li_2Se_2 instead of Li_2Se is being formed. Nevertheless, bis(trialkylsilyl)selenide is always the only product without detection of bis(trialkylsilyl)diselenide. The yield is dependent on the used trialkylsilylchloride and Li_2Se generation method. *Scheme 2*[58] depicts the overall reaction pathways and yields for both syntheses.

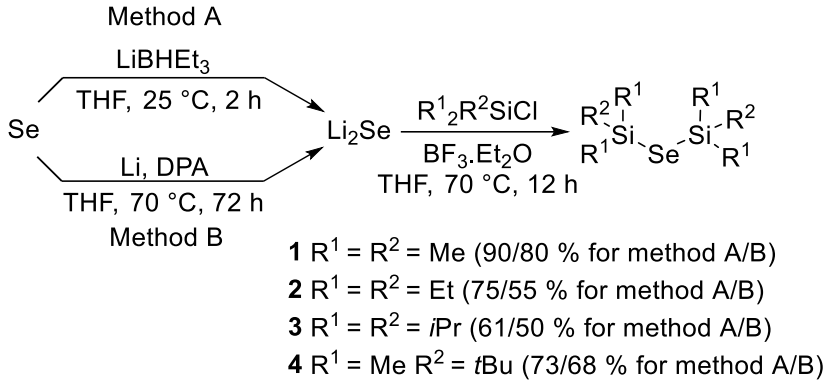

Scheme 2. Synthetic pathways to bis(trialkylsilyl)selenides and their reaction yields.[58]

Alternatively, Drake[83] prepared silyl selenides with lower number of attached alkyls as shown in *Scheme 3*. $(H_nMe_{3-n}Si)_2Se$ compounds are accessible *via* synthetic route using lithium selenoaluminate and selected $(alkyl)_n$silyl iodide.

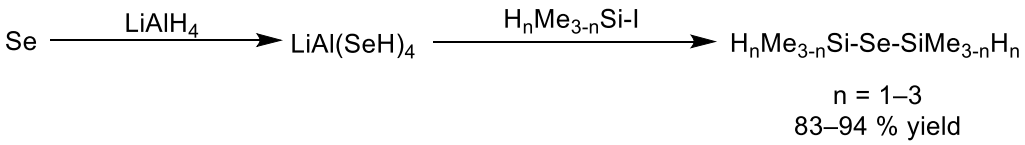

Scheme 3. Drake's preparation of $(H_nMe_{3-n}Si)_2Se$ using selenoaluminate.[83]

7.3 Bis(trialkylstannyl)selenides

In 2020, I have proposed bis(trialkylstannyl)selenides bearing tin instead of silicon as an alternative to bis(trialksilyl)selenides with lower air-sensitivity.[77] Three bis(trialkylstanyl)selenides (with alkyl = Me, Et and Bu) were tested for $MoSe_2$ deposition. These molecules are distinctly heavier as compared to their silicon predecessors, therefore lower volatility was generally observed. TGA and DSC shown in *Figure 12* revealed lower thermal stability of molecules with bulkier alkyls at temperatures higher than ~ 220 °C. However, trimethyl derivative $(Me_3Sn)_2Se$ seems to be fairly volatile with no residues after TG measurements even though some unidentified thermal process takes place during the evaporation (as revealed by the DSC).

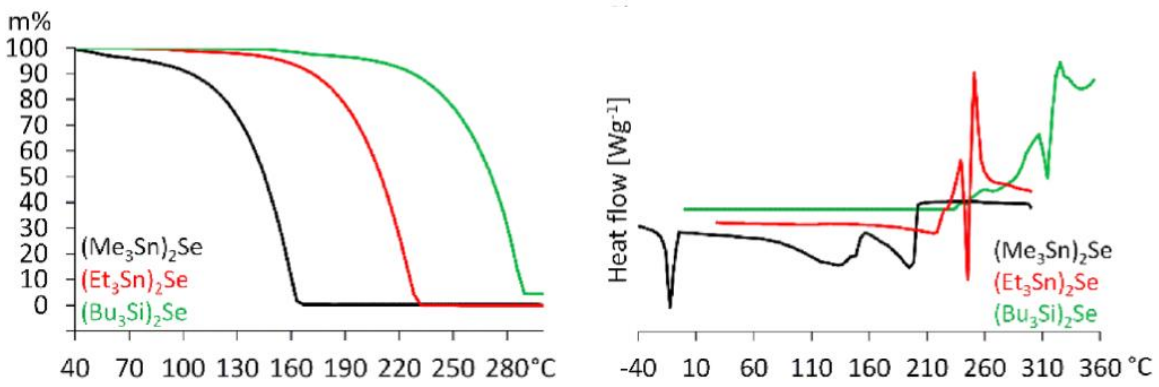

Figure 12. TGA (left) and DSC (right) records showing thermal behaviour of selected bis(trialkylstanyl)selenides.[77] (Under Creative Commons License, Modified)

As mentioned previously, $(Me_3Sn)_2Se$ was tested as an ALD precursor for $MoSe_2$ deposition by reaction with $MoCl_5$ while the bulkier derivatives (Et and Bu) were discarded because of their low volatility and thermal instability. Indeed, experiments using $(Me_3Sn)_2Se$ were successful and $MoSe_2$ structure was confirmed by XPS, XRD and Raman spectroscopy with complementary structure studies by AFM, SEM and HR-TEM.[77] *Figure 13*[77] shows typical flaky structure of $MoSe_2$ and its differences using various silyl precursors besides $(Me_3Sn)_2Se$.

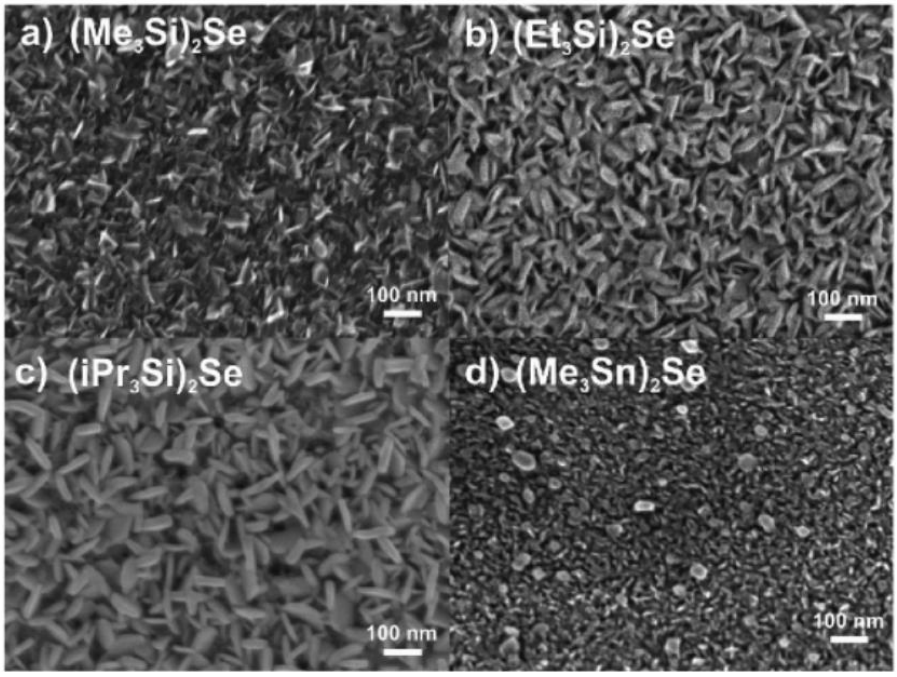

Figure 13. SEM top-view images of $MoSe_2$ nanostructures deposited on glass using $MoCl_5$ and different Se precursors: (a) $(Me_3Si)_2Se$ (400 cycles), (b) $(Et_3Si)_2Se$ (400 cycles), (c) $(iPr_3Si)_2Se$ (400 cycles), and (d) $(Me_3Sn)_2Se$ (200 cycles).[77] (Elsevier, Under Creative Commons License)

Scheme 4[77] shows the synthesis of stannylselenides, which can be carried out similarly to silylselenides (*Scheme 1*). The *in-situ* prepared Li_2Se reacted with selected trialkylstanylchloride and catalytic amount of $BF_3{\cdot}OEt_2$.

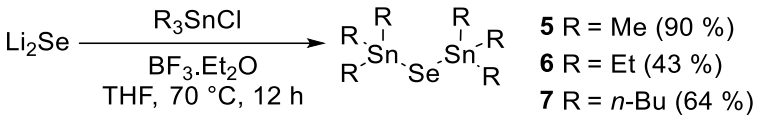

Scheme 4. Preparation of bis(trialkylstanyl)selenides.[77]

Another examined synthetic route involved insertion of the elemental selenium into the Sn-Sn bond in a catalytic cycle mediated by R_3P in benzene at 80 °C for 5 h (*Scheme 5*).[84]

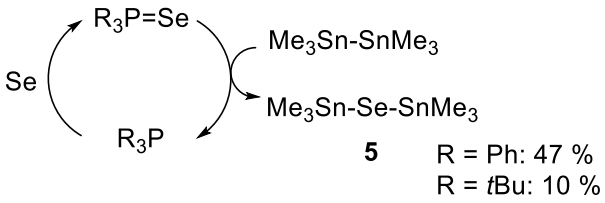

Scheme 5. R_3P-catalyzed preparation of bis(trialkylstanyl)selenides.[78,84]

A direct reduction of selenium or diethylselenide is possible with trialkyltinhydrides as demonstrated by Vyazankin (*Scheme 6*).[85] Bis(triethylstannyl)selenide **6** can be prepared this way (yield not given).

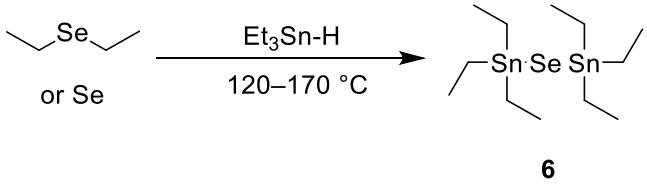

Scheme 6. Reduction of Se or Et_2Se by triethyltinhydride.

7.4 Selenium dimethyldithiocarbamate (SDMDTC)

SDMDTC **8** is a precursor recently used for deposition of Sb_2Se_3 by a reaction with $Sb(NMe_2)_3$.[86] TGA study shows smooth evaporation within 120–160 °C range with decomposition starting at 165 °C indicating quite narrow ALD window. Nevertheless, deposition maintained at 150 °C gives polycrystalline Sb_2Se_3 with growth rate 0.28 Å/c on ZnS substrate. This selenium precursor is air stable and commercially available, because of its use as rubber vulcanization accelerator with patented synthesis as shown in *Scheme 7*.[87]

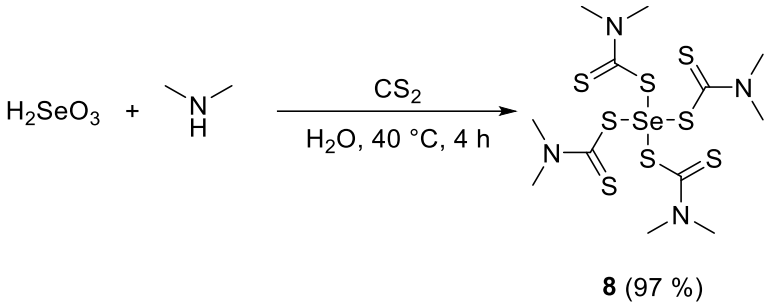

8 (97 %)

Scheme 7. Patented preparation of SDMDTC.[87]

8 Other silyl-selenides as potential ALD precursors

This chapter aims to review reported cyclic selenides that might be utilized in ALD as a selenium source. Most of the attention is devoted to the synthesis and its possible simplification compared to benchmark bis(trialkylsilyl)selenides. The cyclic structure certainly affects their reaction behaviour, while a trade-off between reactivity, air-sensitivity and volatility might appear.

8.1 Cyclic silylselenides containing one or more Se atoms

An extensive study on heteronuclear NMR properties of variously substituted silylchalcogenides was reported by Herzog.[88,89] Unfortunately, no experiments on thermal behaviour were carried out, therefore the following selection of selenium compounds is based on small derivatives that would possess sufficient volatility. The main focus is directed to five membered carbon bridged cyclic selenide **9** (*Scheme 8*). Its preparation involves generation of Li_2Se followed by the reaction with $ClMe_2Si\text{-}CH_2CH_2\text{-}SiMe_2Cl$ providing **9** as a slightly yellow liquid; a yield was not given.[89] Likewise are the preparations of symmetric silylselenide **10** (64 % yield)[88] containing two Se atoms, by reaction of two equivalents of Li_2Se and $ClMe_2Si\text{-}SiMe_2Cl$, and asymmetric silylselenide **11** (50–70 % yield),[88] prepared by using a mixture of $ClMe_2Si\text{-}SiMe_2Cl$ and Me_2SiCl_2 and Li_2Se.

A reaction of M_2Se (M = Li, Na) with R_2SiCl_2 is more complicated as six- or four-membered cycle can be formed depending on the alkyl bulkiness (*Scheme 8*). Herzog[88] reported a generation of six-membered cyclic silyl selenide **12** (50 % yield) when Li_2Se was treated with Me_2SiCl_2. On the other hand, Thompson[90] reacted Na_2Se with Et_2SiCl_2 and obtained mixture of six-membered cycle **13** (40 % yield) and four-membered cycle **14** (30 % yield). This work also proposed a reaction mechanism. It comprises nucleophile attack of the selenide anion to silicon atom accompanied by elimination of two NaCl molecules leading to reactive [Et_2Si=Se], which underwent [2+2] or [2+2+2] cycloaddition. Interestingly, UV- irradiation (λ = 254 nm) of **13** initiates its conversion to **14** with 90 % yield.

Weidenbruch[91] also employed UV photochemistry (UV lamp Heraeus TQ 150) during preparation of four-membered silylselenide (*Scheme 8*). Selenophene is irradiated together with hexa*tert*butyl-cyclotrisilane giving product **15** with 11 % yield.

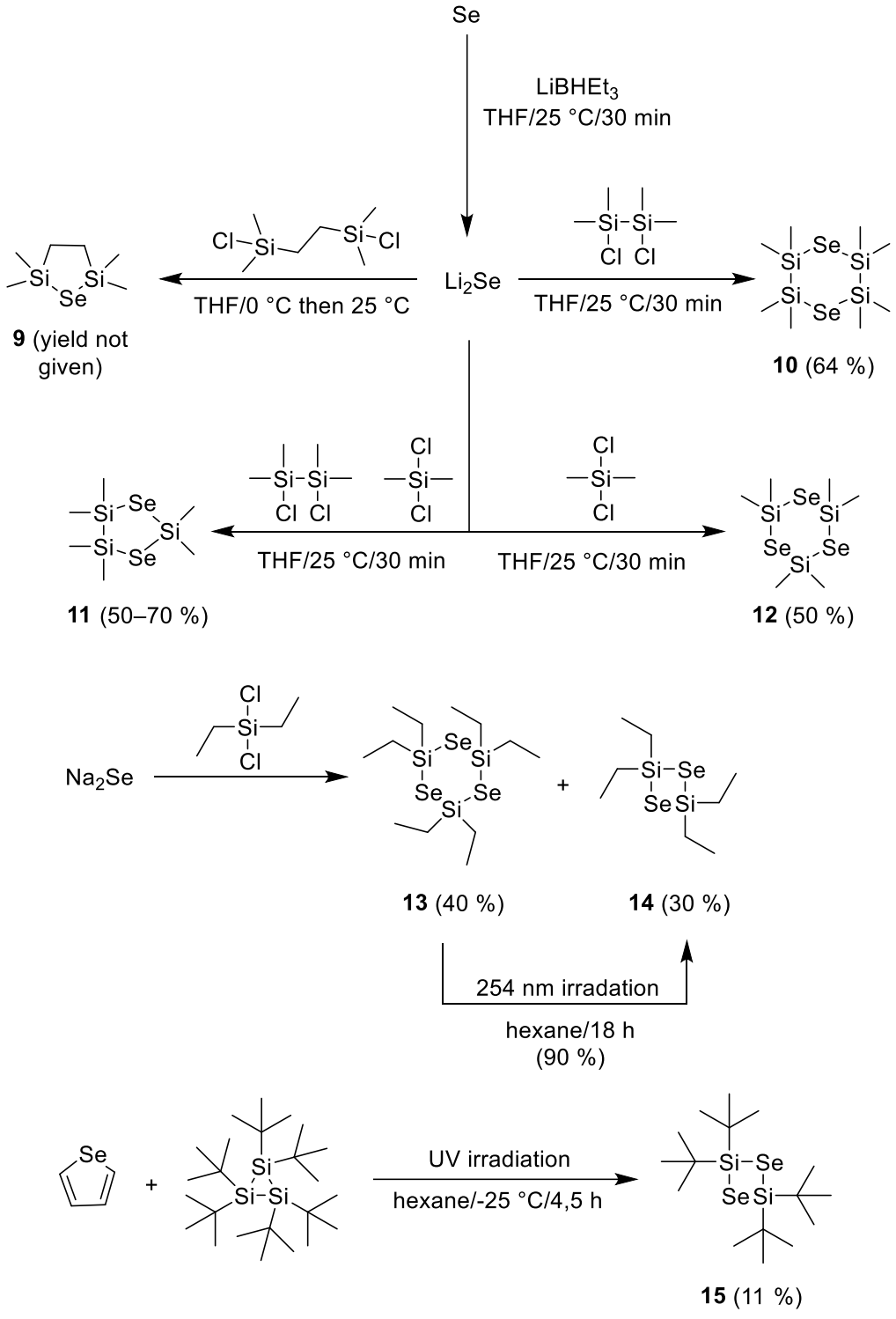

Scheme 8. Reported syntheses of cyclicsilylselenides: **9**;[89]**10**–**12**;[88]**13**,**14**;[90]**15**.[91]

8.2 Silylselenoles

In principle, silylselenoles of a general formula R_3Si-SeH can bring new possibilities for deposition of selenides by ALD. They feature low molecular weight and thus potentially high volatility, while the reactivity is maintained by acidity of the proton attached to the selenium.

Drake[83] reported generation of Me_3Si-SeH **16** by treating H_2Se with $(Me_3Si)_2Te$ (*Scheme 9*). Kuckmann[92] applied a different approach, where *t*Bu_3Si-Na reacts with selenium affording selenium salt *t*Bu_3Si-SeNa, which was acidified by F_3C-COOH to **17**. However, these preparations seem to be less convenient as starting materials are not commercially available and their preparation might be cumbersome.

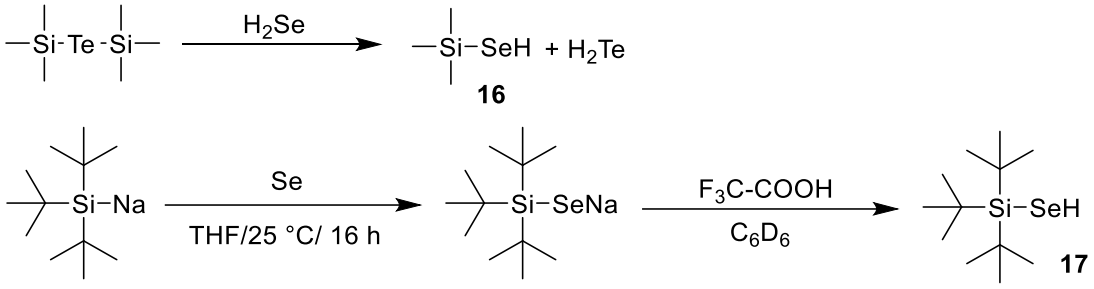

Scheme 9. Preparation of Me_3SiSeH[83] and *t*Bu_3SiSeH.[92]

A reduction of selenium with trialkylsilanes is possible similarly to trialkyltinhydrides as observed during the reaction of Se and Et_3Si-H affording Et_3Si-SeH.[93] *Scheme 10* shows preparation of $cHex_3Si$-SeH **18** by Grenader.[94] Authors have also mentioned similar preparation of *i*Pr_3Si-SeH, but no further details were given. It is obvious that exploitation of silanes as reducing agents requires harsh conditions as compared to the trialkyltinhydrides. Nevertheless, simple and inexpensive silane starting materials represent an interesting choice among the trialkylsilylselenoles preparation methods.

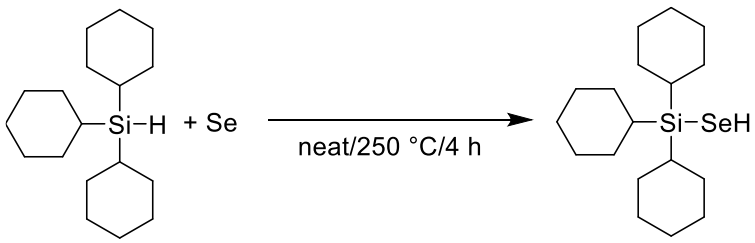

18 (70 %)

Scheme 10. Preparation of the $cHex_3Si$-SeH.[94]

9 Solution-based thin film deposition methods

First deposition of thin films came up to several thousand years before Christ in ancient civilizations like Egypt or Roman empire. The precise craftsmanship of these cultures was surprisingly efficient and the great work reviewing the history of thin film preparations is summarized by Greene.[95]

Modern liquid deposition methods were developed later in nineteenth century with increasing demand of industry. Chemical Bath Deposition (CBD), electrodeposition, sol-gel (suspension of colloidal particles) and SILAR are the most prominent. The upcoming pages will briefly present CBD (as an analogue to CVD), SILAR and solution ALD (sALD). The two latter employ step-by-step deposition with great control characteristic for ALD process. The overview of ALD methods using liquid phase was recently released by Graniel.[96]

9.1 Chemical Bath Deposition (CBD)

Chemical Bath Deposition (CBD) is one of the simplest methods among deposition techniques. It is a convenient method for manufacturing thin films on large substrates, because only elementary inexpensive equipment and available chemicals are usually needed. This method allows preparation of 0.05–0.5 μm thick films with good reproducibility.[97]

The CBD mechanism is pretty straightforward. Selected substrate is immersed in solution containing cations and anions of atoms that are used as building blocks for desired material which grows on the surface. Activation of initial nucleation and growth continuation depends on maintained conditions. Therefore, other characteristics like definitive thickness, morphology, electronic properties and crystallinity depend mostly on used substrate and chemicals as a source of ions, length of reaction, solubility, temperature, pH, stirring intensity, present complexation agents and many more.[98] From the certain point of view, CBD mechanism is very similar to CVD growth, because building blocks are not introduced sequentially and growth is mostly dependent on deposition conditions.

Metal chalcogenides are materials often deposited by CBD. An example might be CdSe used in solar energy applications.[97] *Scheme 11* represents process of CdSe deposition using simple $Cd(NO_3)_2$ and *N*,*N*-dimethylselenourea. Thickness of obtained layer is controlled by the reaction time and differs between 0.5 to 0.65 μm.[99]

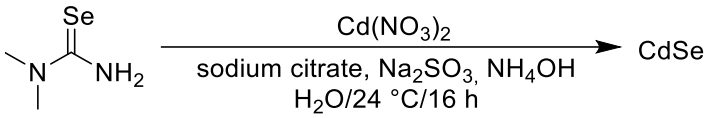

Scheme 11. Chemical Bath Deposition of CdSe.

9.2 Successive Ionic Layer Adsorption and Reaction (SILAR)

Nicolau[100] initiated sequential solution-based deposition in 1985 with intention to "grow polycrystalline or epitaxial thin films of water-insoluble ionic or ionocovalent compounds of the C_mA_n type by heterogeneous chemical reaction at the solid-solution interface between adsorbed C^+ cations and A^- anions". In this first case, CdS and ZnS layers were prepared by reacting Na_2S and $CdSO_4$ or $ZnSO_4$ providing 2 nm per hour deposition rate (250 nm in 6 days).

The course of deposition is very simple. The substrate is poured into the solution of cations, where the first layer of ions adheres to negatively charged substrate surface terminal groups. Then, substrate is moved to pure solvent, which ensures removal of all excess cations. After upcoming immersion to the solution of anions, the reaction takes place and the first layer is deposited. The cycle is again finished by rinsing step in solvent.

SILAR comes with several advantages. Mainly it is precise control of thickness increase, low equipment cost, low deposition temperatures and simple precursors. On the other hand, the most problematic is immersion and rinsing time duration, which leads to very low deposition rates.

For deposition of metal chalcogenides, SILAR is convenient method. The overview was made some time ago by Pathan.[101] Interesting is also work by Ratnayake,[102] where authors compare SILAR with CBD, ALD and CVD.

9.3 Atomic Layer Deposition from dissolved precursors (solution ALD - sALD)

ALD from liquid solutions of precursors, so-called solution ALD (sALD), was firstly presented by Bachmann research group in 2015.[103] This work demonstrated that self-limiting growth and other ALD characteristics are not limited just to gaseous phase.

Figure 14 represents simplified scheme of the sALD system and design of the reaction chamber. Precursors A and B dissolved in suitable solvent are introduced one by one to the reaction chamber by peristaltic (or other) pump. The purging step with pure solvent after each precursor pulse ensures that the precursors do not mix and only a saturative reaction on the substrate surface is present. Uniform distribution of solutions is maintained by the reaction chamber design. Concentration of precursors and pulse/purge lengths are crucial to achieve self-limiting growth. These attributes are identified by the series of experiments carried out using different sequences, until the steady growth per cycle is observed. This procedure is comparable with finding the "ALD window" described in the previous chapter.

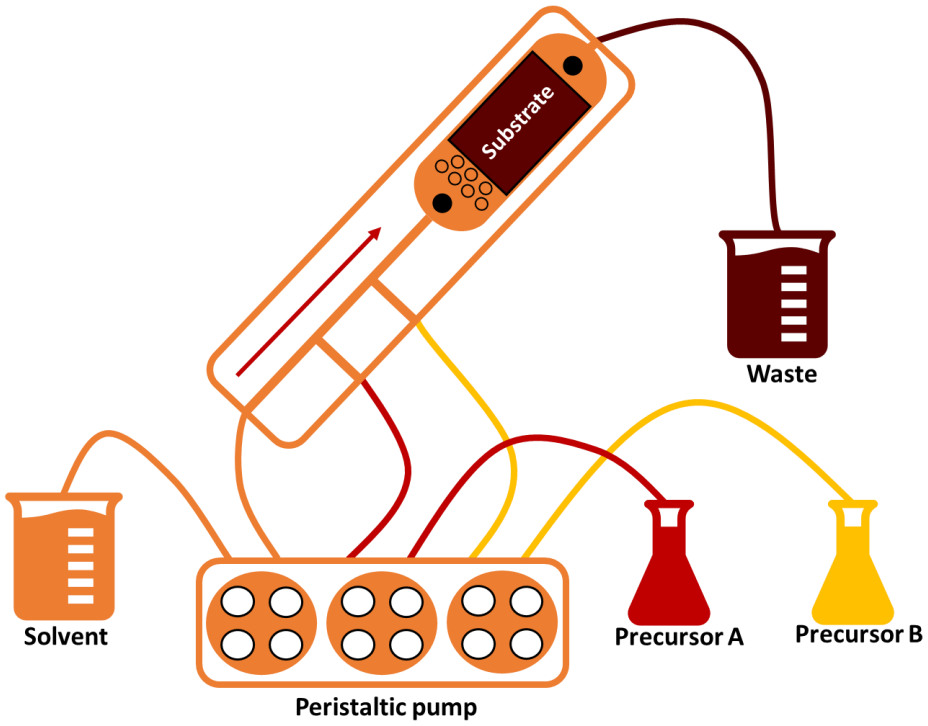

Figure 14. Simple scheme of sALD setup.

In contrast to a complicated vacuum system of gas ALD (gALD), sALD uses simple pump and common Schlenk techniques, if an inert atmosphere needs to be maintained. Moreover, purchase price of sALD is far below that of gALD and is also accompanied with low maintenance needs and easy control. Reaction chamber design and used material (stainless steel, Teflon etc.) can be easily tuned for specific substrate size, shape or other requirements such as variable number of precursor inlets for deposition of multi-layered materials. The pioneering sALD work[103] focused on deposition of TiO_2, SiO_2 and MgO. Hydrolysis of $Ti(OiPr)_4$ in Et_2O as a solvent produced amorphous TiO_2 films with 0.3 Å/c growth rate. The reaction was performed at 25 °C, while gALD usually use temperatures equal or over 200 °C for TiO_2 depositions. MgO thin film fabrication employing unstable and non-volatile EtMgCl with 1 Å/c is one of the most interesting sALD abilities. Typical limitations of gALD precursors - volatility and thermal stability are overcame in sALD as it requires only sufficient reactivity and solubility. This brings great potential for thin films depositions, not just because of simplifying the chemistry and lowering the costs, but also tunning the selectivity and properties of deposited material with used solvent or additives (pH, surfactants etc.). Ability to produce films, that are tricky for gALD, was later confirmed again with deposition of LiH by hydrolysis of BuLi,[104] polycrystalline PbS[105] and HfS_2[106] at mild conditions.

ALD unique capability to produce conformal thin films on the surface of nanostructures was also investigated with sALD. First, a reaction of H_2O with $HSiCl_3$ was studied on planar Si wafer giving SiO_2 with 1.7 Å/c growth rate (determined by ellipsometry). Second part of this work[103] examined deposition on porous silica substrate (30 nm in diameter

and approximately 30 μm long pores) and saturative behaviour was observed also in this case (determined by EDX). The deposited thin film was smooth and continuous, thus comparable to the gALD results.

There are two concerns about sALD so far. The length of deposition process usually takes one to several minutes per cycle, therefore deposition of thick films (100 and more nanometers) is very time and solvent consuming. Even though that purge lengths and solvent volumes can be greatly reduced by optimized chamber design and flow rates, one might pick other deposition method rather than ALD for thicker films in general. The second concern considers consumption of solvent, which depends on pulse and purge lengths and usually ranges between units to tens of millilitres per one cycle. On the other hand, the solvents might be often easily recycled by common laboratory methods (distillation, filtration etc.), so further optimization of the process and system design could minimize the wasted materials.

10 Application of metal selenides thin films

Metal selenides possess many interesting properties among various fields. Some of them are known for a long time, meanwhile other still awaits to be discovered or investigated deeper. The upcoming pages will briefly introduce selected metal selenides and applications in exciting technologies, which might possibly attract interest in the near future.

10.1 Transition metal dichalcogenides (TMDCs)

TMDCs are compounds composed of *d*-block metal or tin (M) and the chalcogenide (S, Se, Te = X) with a general formula MX_2. TMDCs possess 2D layered structure, where chalcogen-metal-chalcogen single monolayers are bound by weak van der Waals. TMDCs with known layered structure and a showcase of possible crystal shapes are displayed in *Figure 15*.[107]

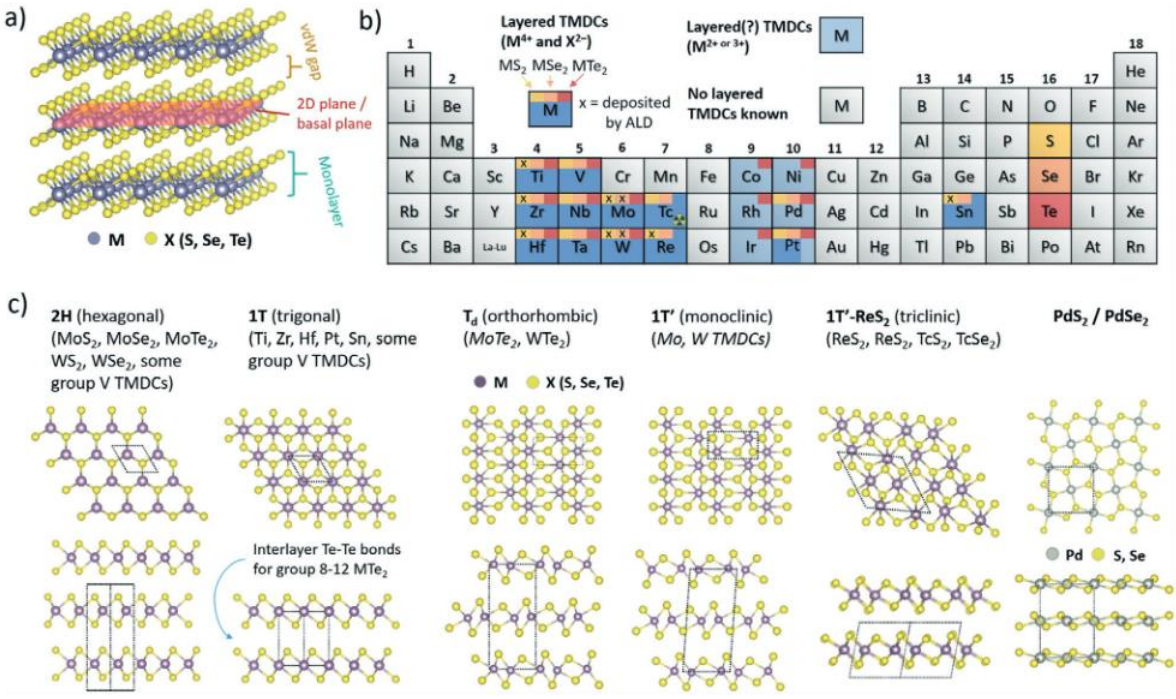

Figure 15. a) Layered structure of TMDCs exemplified by the 1T phase and terminology used to describe the structure. **b)** Periodic table highlighting metals that form layered TMDCs. TMDCs deposited by ALD are marked with an x. **c)** Top (top row) and side (bottom row) views of crystal structures of the different TMDC phases and examples of materials crystallizing in each structure. Metastable phases are written in italics.[107] (Reused with permission, Copyright Wiley-VCH GmbH)

A proper combination of metal and chalcogenide allows to tune band gap from very low (metallic behaviour) to wide exceeding 2 eV such as in semiconductors. A precise engineering of desired properties for a specific application can be even more pronounced by mixing

different TDMCs together. The reader is further referred to recent review articles summarizing properties of TMDCs prepared by ALD.[107–109]

2D materials find manifold use in optoelectronics[110] as they are capable to transform electric signal to light or vice versa. Light emitting diodes, light detectors and photovoltaic cells are typical examples. Catalytic properties of transition metal dichalcogenides are gaining pronounced interest. One of the most studied processes is electrochemical Hydrogen Evolution Reaction (HER) and Oxygen Evolution Reaction (OER) during the so-called water splitting, when water molecule broke into the elements. Both, H_2 and O_2 are greatly utilized by the industry, however its large-scale preparation is very energy-demanding and often, the amount of generated hydrogen does not correspond to the electricity consumed. The most efficient electrode material for HER and OER is elemental platinum, which low abundance and high prices disallow its wide application. Some of the TMDCs however, shown to be suitable and efficient catalyst for this type of reaction.[111,112] One of the most studied is MoS_2[113] and also $MoSe_2$ revealed good efficiency.[114] Metal sulphides or selenides were also successfully tested for the electrochemical reduction of CO_2, SO_2 or NO_x[115,116] and their optical properties make them suitable for photocatalytic HER or pollutant decomposition reactions. The effect is even more pronounced when the catalyst is deposited on large area heterostructures.[17,70]

10.2 Photovoltaics – thin light absorbing layers

Solar cell is a device that converts light energy into the electricity by the photovoltaic effect. The first solar cell ever was reported by Charles Fritts in 1883 and his device was composed of gold plate and thin film of elemental selenium as a photoactive layer. Even though this device reached less than one percent conversion efficiency, the upcoming research in 1980´s increased this number to 5 %. Later, experiments in 2017 optimized the device composition reaching 6.5 % with 100 nm thick layer of selenium as inexpensive and stable material.[117] More renowned are, however, CIGS ($CuIn_xGa_{1-x}Se_2$) solar cells. With 16.5 % efficiency they took around 1 % of the total solar cell market in 2020.[118]

Interest in antimony sulphide and selenide and their mixtures is growing every year as depicted on *Figure 16*.[119] Although some compounds of these elements might be very dangerous, Sb_2S_3 and Sb_2Se_3 toxicities are estimated to be low and neither of these molecules are on the list of highly toxic or carcinogenic materials by Chinese, American or European Union regulation authorities.[120] Preparation of antimony chalcogenides is relatively cheap including deposition, because very low thickness (tens of nanometres) are sufficient to absorb enough of light. The suitable band gaps of antimony sulphide (1.7 eV) and selenide (1.1 eV) are accompanied with high absorption index and the theoretical efficiency could reach around 30 % for simple single-junction device (based on Schockley-Queisser theory). In contrast to

Sb_2S_3, antimony selenide by ALD was not reported for solar cells application up to date. Nevertheless, Mahuli[86] tested SDMDTC as a novel selenium precursor by investigating Sb_2Se_3 photo-harvesting properties with promising results. Li[121] used Close Spaced Sublimation (CSS) method for deposition of 1200 nm long Sb_2Se_3 nanorod arrays getting 9.2 % efficient photovoltaic device. Gharibshahian[122] then propose optimization of mentioned solar cell by the substitution of CdS buffer layer with $Zn_{0,93}Mg_{0,07}O/ZnO_{0,4}S_{0,6}$ double buffer layers raising energy yield to 15.46 %. Similar suggestions and ideas show, that Sb_2Se_3 solar cells are in early stage of development and further investigations could lead to preparation of very efficient and inexpensive energy generator.

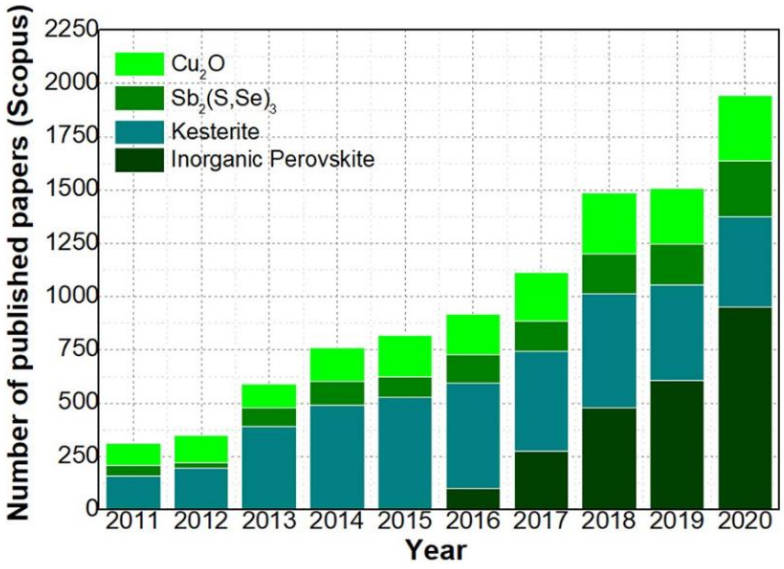

Figure 16. Number of papers published in last ten years with selected materials.[119](IOP Publishing, Under Creative Commons License)

10.3 Thermoelectric devices

Thermoelectric (TE) technology mediates the generation of electrical energy through the difference of temperature on two sides of the device (heat flux). This is called thermoelectric or Seebeck´s effect. *Figure 17*[123] shows scheme of a TE device. Thermoelectric materials play the key role – positive (p) and negative (n) charge carriers of semiconductors that are connected to the closed circuit. If one side of the TE module is heated, then created heat gradient develops voltage between the junctions, which is proportional to the difference in the temperatures. Reverse mechanism called as Peltier´s effect on the other side, causes heating of the one side and cooling the other side of the module, if voltage is applied.

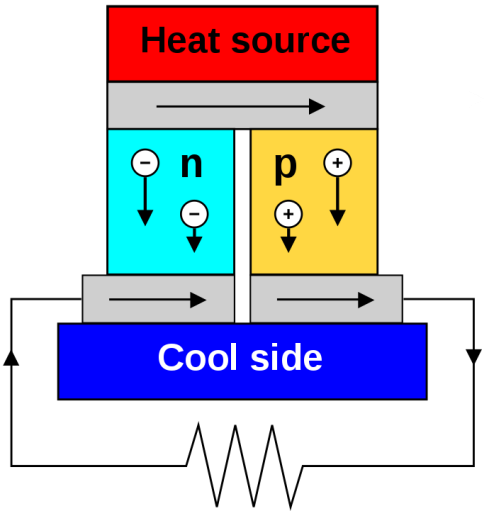

Figure 17. Scheme of the thermocouple.[123] (Wikimedia, By Ken Brazier, Under Creative Commons License)

The thermocouples may (and already do) find various applications, wherever the waste heat is produced. That means industrial facilities, computer parts or transportation units like cars or airplanes could utilize waste heat to lower their energy consumption. The very simple construction with no liquids or moving parts make TE devices suitable even for very harsh conditions like space or ocean depths with long expected lifespan. Production of TE units is scalable from very small to hundreds of kW.[124]

Ideal TE material has high electrical conductivity allowing charge carriers to flow. Very important is also low thermal conductivity, which ensures that hot side and heat sink (cold side) are separated. The efficiency is dependent on arbitrary unit "*zT*" referred as a "figure of merit" which is the correlation between Seebeck´s coefficient, thermal and electrical conductivity and temperature. This means that design of the right material varies by selected operating temperature and thus the application.[125]

Metal chalcogenides are convenient TE materials. Bi_2Te_3 is suitable for lower temperatures under 150 °C, PbTe is the most efficient at temperatures from 150 to 500 °C and for high heat conditions (700–900 °C), while LaTe might be also a material of choice.[125] Large portion of industry and transportation operates at the temperatures below 300 °C, therefore materials providing high efficiency at this range needs to be explored. Nevertheless, tellurium scarcity has initiated interest in metal selenides, which show high figure of merit at different temperatures. Binary materials like Ag_2Se or Bi_2Se_3 operate at lower temperatures, while Cu_2Se and SnSe possess high efficiencies at 800 °C and more. *Figure 18*[126] illustrates that a combination of different materials into a complex system enables fine tuning of TE material properties.[126]

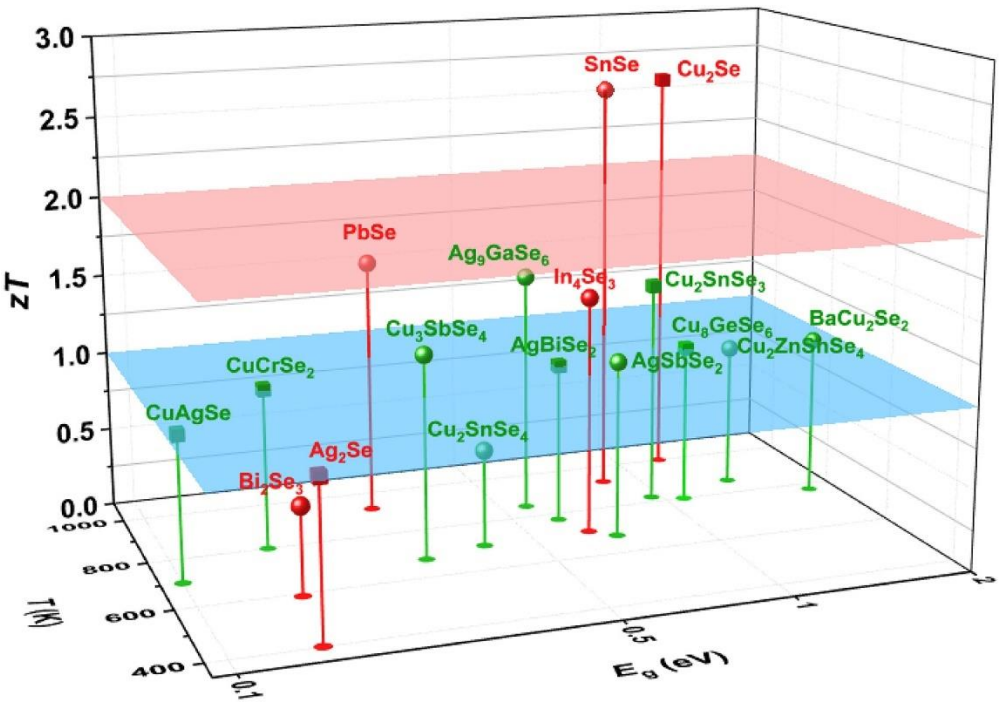

Figure 18. 3D graph representing correlation between figure of merit (*zT*), operating temperature (*T*) and the energy value of band gap (E_g).[126] (Elsevier, Under Creative Commons License)

11 Further applications of organo-selenium compounds in material sciences

11.1 Metal selenides-based nanocrystals (Quantum dots)

Semiconductor nanocrystals (NC) also commonly called as quantum dots (QD) gained huge attention in the last decade. This is mostly attributed to their unique electronic, optical and other properties, that are easily tuneable by its composition, shape, surface characteristics and most importantly size. The applications span wide variety of fields such as light-emitting diodes, photovoltaics or sensing. *Figure 19*[127] illustrates difference in emitted wavelength of CdSe nanoparticles of different sizes upon their excitation by UV light.

The resulting NC material is highly dependent on used chemical precursors and reaction conditions. Temperature, reaction duration, used solvent and surfactants are the most prominent ones, however the way of preparation is also important and can significantly change the properties of harvested nanocrystals.[128] High-temperature organo-metallic injection method of two precursors is the most common way how to produce QD. One precursor is dissolved in solvent preheated to the high temperature (150–250 °C) and the second precursor is then rapidly injected giving immediate reaction and nucleation of crystals.

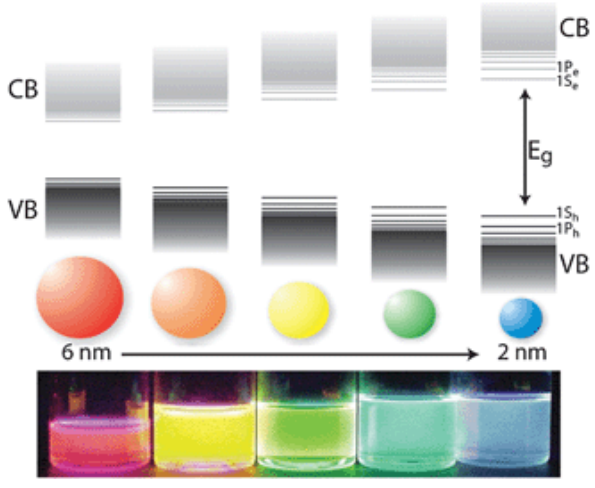

Figure 19. Schematic representation of the quantum confinement effect on the energy level structure of a semiconductor material. The lower panel shows colloidal suspensions of CdSe NC of different sizes under UV excitation.[127] (Reproduced with permission of RSC publications)

To prepare metal selenide QD, various materials are utilized, where one of the most favourite source of selenium is trioctylphosphine selenide (TOPSe), which is generated *in-situ* by a reaction of trioctylphosphine with elemental selenium.[129] Bis(trimethylsilyl)selenide, previously mentioned as an ALD precursor, is also being employed in QD preparation. High reactivity of this molecule allows lowering the reaction temperature to 0 °C.[130]

The reproducible preparation of nanocrystal is very challenging, especially when scaling-up the reaction. One of the reasons includes non-homogeneous distribution of precursor solutions and temperature changes during the injection, causing different crystallite sizes. This problem is bypassed by using single-source precursor method. Here, instead of an intermolecular reaction between two precursors, only one molecule containing both atoms, metal and selenium, is decomposed to the desired material. Decomposition is usually initiated by temperature increase. As an example, dialkyldiselenocarbamate metal salts were used for preparation of ZnSe[131] or InSe[132] spherical nanocrystals and Bi_2Se_3 nanosheets were prepared by tris(selenobenzoato)bismuth thermal decomposition at 200 °C.[133] Even very simple precursor like Ag or Cu salt of dodeca-1-selenol worked for Ag_2Se and Cu_2Se nanocrystal synthesis.[134] Molecular representations of the aforementioned molecules are given in *Figure 20.*

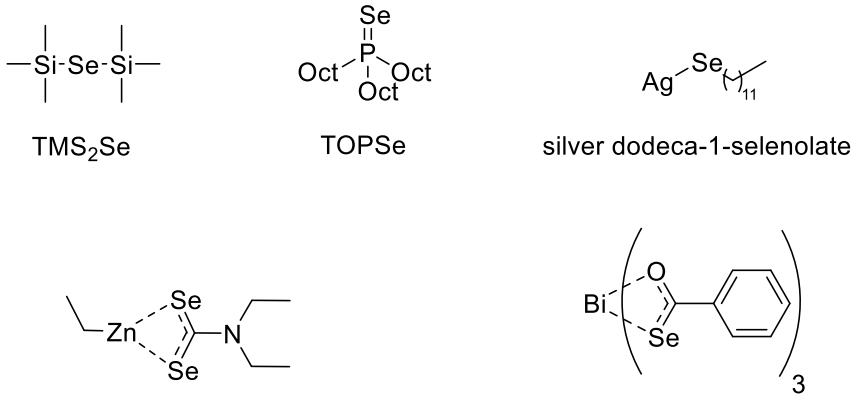

Figure 20. Selenium compounds used in nanocrystal synthesis.

11.2 Coordinating compounds based on selenium

Crown ethers play an important role in coordination chemistry as separation agents utilized in analysis, sensing or biological sciences. Binding capabilities depend on crown ether radius and composition, while their fine-tuning may render high selectivity towards specific ion(s). For example, selena-crown ethers proved excellent selectivity to Ag^+ [135] or Tl^+ [136] ions as compared to other heavy or alkali/alkaline-earth metals. Jung[137] demonstrated that replacement of two oxygens in 18-crown-6 ether affords 1,10-diselena-18-crown-6, with diminished ability to chelate other cations than Pb^{+2}, Cd^{+2} and Hg^{+2}. A similar N→Se exchange in porphyrins led to pronounced changes in metal ions binding affinities.[138] *Scheme 12* shows typical preparations of selected selena-crown ether[139] and selena-porphyrin.[140]

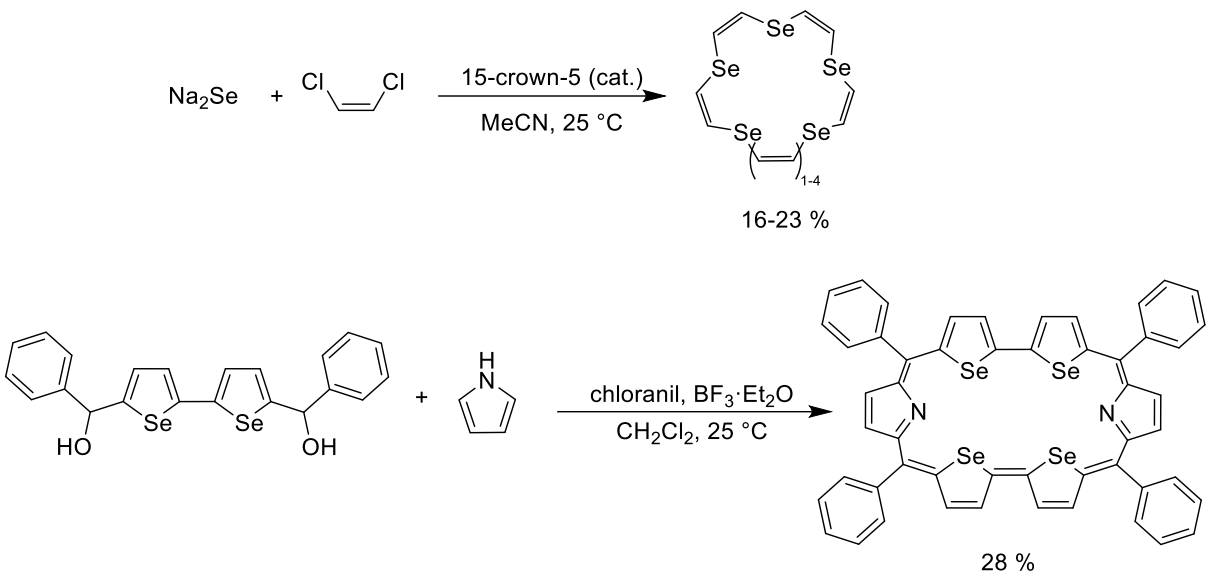

Scheme 12. Preparation of selena-crown ether[140] and selena-porphyrin.[141]

12 Experimental part

12.1 General methods

Starting materials for reactions were purchased from Acros, Alfa-Aesar, Fluka, Penta, Sigma-Aldrich and TCI and were used without any further purification. Dry THF was distilled over Na/K alloy and benzophenone under inert atmosphere of argon. ^{1}H, ^{13}C, ^{29}Si, ^{77}Se and ^{125}Te NMR spectra were recorded in d_6-benzene at 25 °C on a Bruker AVANCE III (frequencies 400/100 MHz) and a Bruker AscendTM (frequencies 500/125 MHz) spectrometers. Chemical shifts (δ) are provided in parts per million as compare to signal of $(CH_3)_4Si$, which was used as an internal standard for ^{1}H, ^{13}C and ^{29}Si (0 ppm). Me_2Se (0 ppm) and Ph_2Te_2 (421 ppm in d_6-benzene) were used as external standards for ^{77}Se and ^{125}Te NMR spectra. Interaction constants (*J*) are given in Hz. The observed signals are described as s (singlet), d (doublet) and m (multiplet). Mass spectra were measured on a GC/EI-mass spectrometer, which consists of a gas chromatograph Agilent Technologies 6890N (HP-5MS, column length 30 m, I.D. 0.25 mm, film 0.25 μm) and a Network MS detector 5973 (EI 70 eV, range 33–550 Da). The thermal properties of final derivatives were studied through DSC measurements with a Mettler-Toledo STARe system DSC 2/700 equipped with a FRS 6 ceramic sensor and HUBER TC100-MT RC 23 cooling system. The thermal behaviour of target compounds was measured in open aluminous crucible under an inert nitrogen atmosphere. DSC curves were determined at a scanning rate of 3 or 5 °C/min^{-1} within the range of –60 to 500 °C. Boiling point was recorded during vacuum distillation. Thermogravimetric analysis (TGA) was carried out using a Mettler-Toledo STARe System TGA 2 equipped with a horizontal furnace LF (400 W, 1100 °C), balance XP5 (resolution 1 μg) and cooling system HUBER Minichiller 600.

12.2 General preparation methods

The synthesis and workup were performed under Ar atmosphere or in a nitrogen-filled glovebox. All used solvents were properly dried before use. The used glassware was poured into sodium hypochlorite bath to destroy remaining organic selenides before cleaning.

Method A (molecules **9**–**11**, **14**, **15**, **19**, **20**):

Dry THF (40 ml) and fine selenium powder (1.0 g, 12.6 mmol) were placed to a 100 ml Schlenk flask. The suspension was cooled to 0 °C and $LiBHEt_3$ (25.2 ml, 25.2 mmol, 1 M solution in THF) was added slowly. The mixture was stirred at 25 °C for 2 h forming white suspension of Li_2Se. One molar equivalent of corresponding dialkyldichlorosilane or carbon-bridged dialkyldichlorodisilane dissolved in THF (10 ml) was added dropwise. In the case of **9** and **19**, $BF_3{\cdot}OEt_2$ (0.1 ml) was introduced. The mixture was stirred at room temperature (or 65 °C for **10**) for 15 h. The solvent was evaporated in vacuo, dry hexane (30 ml) was added, and

the solution was filtered via cannula. The hexane solutions were evaporated in vacuo affording crude selenium compounds.

Method B (**15**, **20**):

Elemental selenium (1.0 g, 12.6 mmol) along with dialkylchlorosilane (12.6 mmol) and EtN*i*Pr_2 (2.2 ml, 1.64 g, 12.6 mmol) were introduced into a pressure vessel filled with argon and containing a magnetic stir bar. The mixture was stirred at 120 °C for 3 h and was cooled to 25 °C accompanied by solidification. A second stirrer was added along with hexane (15 ml) and the mixture was vigorously stirred and shook until a yellow solution with a white precipitate was formed. The mixture was filtered via cannula and cooled to –78 °C to afford yellowish crystals, while the hexane was removed via a syringe. The crystalline product was dried in vacuo.

Bis(triethylsilyl)selenide (**2**)

Selenium powder (0.5 g; 6.33 mmol), Et_3SiH (1.5 g; 2.0 ml; 12.66 mmol), Ph_3SiH (30 mg), and Ph_3P (10 mg) were placed into a sealed tube and the reaction mixture was heated to 250 °C for 48 hours. After cooling to room temperature, the mixture was filtered and purified by vacuum distillation at 120–125 °C (3 torr) to give 0.7 g (35 %) of orange liquid.
^{1}H-NMR (500 MHz, 25 °C, $CDCl_3$): δ(^{1}H) = 0.81 (q, *J* = 8.0 Hz, 12H, CH2), 1.01 (t, *J* = 8.0 Hz, 18H, CH_3) ppm. ^{13}C-NMR APT (125 MHz, 25 °C, $CDCl_3$): δ(^{13}C) = 7.70, 8.16 ppm. ^{29}Si-NMR (99 MHz, 25 °C, $CDCl_3$): δ(^{29}Si) = 23.41 ppm. ^{77}Se-NMR (95 MHz, 25°C, $CDCl_3$): δ(^{77}Se) = –485.70 ppm. EI-MS: *m/z* = 310 (20, M+), 281 (100), 253 (60), 115 (70), 87, 59.

Bis(trimethylstannyl)selenide (**5**)

Me_6Sn_2 (5.0 g; 15.26 mmol) and fine selenium powder (1.4 g; 17.73 mmol) were placed into a sealed tube and heated to 180 °C for 5 hours. After cooling to room temperature, the selenium excess was filtered off to give 6.1 g (98 %) of $(Me_3Sn)_2Se$ as yellow liquid.

^{1}H-NMR (500 MHz, 25 °C, $CDCl_3$): δ(^{1}H) = 0.51 (s, 18H, CH_3) ppm. ^{13}C-NMR APT (125 MHz, 25 °C, $CDCl_3$): δ(^{13}C) = –1.86 ppm. ^{119}Sn-NMR (186 MHz, 25 °C, $CDCl_3$): δ(^{119}Sn) = 50.06 ppm. ^{77}Se-NMR (95 MHz, 25 °C, $CDCl_3$): δ(^{77}Se) = –550.76 ppm. EI-MS: *m/z* = 408 (10, M+), 391 (40), 165 (100), 135.

Bis(tributylstannyl)selenide (**7**)

Bu_6Sn_2 (5.0 g; 8.62 mmol) and fine selenium powder (0.82 g, 10.34 mmol) were placed into a sealed tube and heated to 180 °C for 12 hours. After cooling to room temperature, the selenium excess was filtered off to give 5.6 g (98 %) of $(Bu_3Sn)_2Se$ as yellow oil.

Bu_3SnH (3.7 g; 12.71 mmol) and selenium powder (0.6 g; 7.6 mmol) were placed into the sealed tube and heated to 180 °C for 12 hours. After cooling to room temperature, the selenium excess was filtered off to give 4 g (98 %) of $(Bu_3Sn)_2Se$ as yellow oil.

^{1}H-NMR (500 MHz, 25 °C, $CDCl_3$): δ(^{1}H) = 0.91 (t, *J* = 7.5 Hz, 18H, CH_3), 1.12 (t, *J* = 8.2 Hz, 12H, CH_2), 1.30–1.38 (m, 12H, CH_2), 1.53–1.60 (m, 12H, CH_2) ppm. ^{13}C-NMR APT (125 MHz, 25 °C, $CDCl_3$): δ(^{13}C) = 13.61, 15.44, 27.08, 29.00 ppm. ^{119}Sn-NMR (186 MHz, 25 °C, $CDCl_3$): δ(^{119}Sn) = 57.14 ppm. ^{77}Se-NMR (95 MHz, 25 °C, $CDCl_3$): δ(^{77}Se) = –651.72 ppm. EI MS: m/z = 545 (20), 317, 291 (90), 235 (50), 179 (100).

2,2,5,5-Tetramethyl-1,2,5-selenadisilolane (**9**)

Prepared by Method A from 1,2-bis-(chlorodimethylsilyl)ethane (2.7 g, 12 mmol). Purified by vacuum distillation, b. p. = 85 °C (20 torr). Yellowish liquid, yield: 2.3 g (83 %). ^{1}H-NMR (500 MHz, 25 °C, C_6D_6): *δ*(^{1}H) = 0.36 (s, 12H, CH_3), 0.85 (s, 4H, CH_2) ppm. ^{13}C-NMR APT (125 MHz, 25 °C, C_6D_6): *δ*(^{13}C) = 2.92, 14.84 ppm. ^{29}Si-NMR (99 MHz, 25°C, C_6D_6): *δ*(^{29}Si) = 33.63 ppm. ^{77}Se-NMR (95 MHz, 25 °C, C_6D_6): *δ*(^{77}Se) = –428.19 ppm. EI-MS: *m/z* = 224 (30, M^+), 209 (100), 181 (30), 73 (60).

2,2,3,3,5,5,6,6-Octamethyl-1,4,2,3,5,6-diselenatetrasilinane (**10**)

Prepared by Method A from 1,2-dichlorotetramethyldisilane (2.4 g, 12 mmol). Colourless crystals upon crystallization from hexane at –78°C, yield: 2.1 g (42 %). ^{1}H-NMR (500 MHz, 25 °C, C_6D_6): *δ*(^{1}H) = 0.46 (s, 24H, CH_3), ppm. ^{13}C-NMR APT (125 MHz, 25 °C, C_6D_6): *δ*(^{13}C) = 1.47 ppm. ^{29}Si-NMR (99 MHz, 25°C, C_6D_6): *δ*(^{29}Si) = -9.34 ppm. ^{77}Se-NMR (95 MHz, 25 °C, C_6D_6): *δ*(^{77}Se) = –369.08 ppm. EI-MS: *m/z* = 392 (10), 116 (100), 73 (80).

2,2,4,4,5,5-Hexamethyl-1,3,2,4,5-diselenatrisilolane (**11**)

Prepared by Method A from 1,2-dichlorotetramethyldisilane (1.2 ml, 1.2 g, 6.3 mmol) and dimethyldichlorosilane (0.8 ml, 0.8 g, 6.3 mmol). Purified by vacuum distillation, b. p. = 95–100 °C (1 torr). Yellowish liquid, yield: 1.6 g (75%). ^{1}H-NMR (400 MHz, 25 °C, C_6D_6): *δ*(^{1}H) = 0.45 (s, 12H, CH_3), 0.78 (s, 6H, CH_3) ppm. ^{13}C-NMR APT (100 MHz, 25 °C, C_6D_6): *δ*(^{13}C) = 0.6, 9.9 ppm. ^{29}Si-NMR (80 MHz, 25°C, C_6D_6): *δ*(^{29}Si) = 13.9, 24.9 ppm. ^{77}Se-NMR (76 MHz, 25 °C, C_6D_6): *δ*(^{77}Se) = –303.5 ppm. EI-MS: *m/z* = 319 (30), 211 (20), 73 (100).

2,2,4,4-Tetraethyl-1,3,2,4-diselenadisiletane (**14**)

Prepared by Method A from diethyldichlorsilane (1.9 ml, 1.99 g; 12.6 mmol). Purified by vacuum distillation, b. p. = 120–140 °C (1 torr). Yellow oil, yield: 1.9 g (92 %).

Preparation by modified Method A: Dry THF (40 ml) and fine selenium powder (1.0 g, 12.6 mmol) were placed to a 100 ml Schlenk flask. The suspension was cooled to 0 °C and then $NaBHEt_3$ (25.2 ml, 25.2 mmol, 1M solution in THF) was added slowly. The mixture was stirred

at 25 °C for 2 h forming dark violet suspension of Na_2Se. The remaining procedure is similar to the Method A. Yield: 0.9 g (43 %) of **14**.

EI-MS: *m/z* = 332 (20, M^+), 303 (100), 275 (30), 245 (20), 217 (20), 59 (10). NMR revealed mixture of products, which were not separable by further fraction vacuum distillation or crystallization from hexane at –78 °C (further discussed in next chapter). Obtained spectra correspond for both experiments.

2,2,4,4-Tetratertbutyl-1,3,2,4-diselenadisiletane (**15**)

Attempts to prepare **15** by Method A from di*tert*butyldichlorosilane (2.7 g; 126 mmol) failed. Extending reaction time to several days, refluxing the mixture or addition of $BF_3{\cdot}OEt_2$ did not gave the desired product neither.

Prepared by Method B from tBu$_2$SiHCl (2.6 ml, 2.3 g; 12.6 mmol). Product **15** was obtained as orange crystals. Yield = 1.7 g (61 %). ^{1}H-NMR (400 MHz, 25 °C, C_6D_6): δ(^{1}H) = 1.23 (s, 36H, CH_3) ppm. ^{13}C-NMR APT (100 MHz, 25 °C, C_6D_6): δ(^{13}C) = 25.12, 29.19 ppm. ^{29}Si-NMR (80 MHz, 25°C, C_6D_6): δ(^{29}Si) = 19 ppm. ^{77}Se-NMR (76 MHz, 25 °C, C_6D_6): δ(^{77}Se) = –321.9 ppm. EI-MS: *m/z* = 387 (100), 345 (80), 246 (20), 57 (20).

2,2,6,6-Tetramethyl-1,2,6-selenadisilinane (**19**)

Prepared by Method A from 1,2-bis-(chlorodimethylsilyl)propane (2.9 g; 12 mmol). Yellowish liquid, yield: 2.9 g (95 %), pure enough after pentane evaporation, b. p. = 95 °C (20 torr). ^{1}H-NMR (500 MHz, 25 °C, C_6D_6): δ(^{1}H) = 0.36 (s, 12H, CH_3), 0.71–0.73 (m, 4H, CH_2), 1.78–1.80 (m, 2H, CH_2) ppm. ^{13}C-NMR APT (125 MHz, 25 °C, C_6D_6): δ(^{13}C) = 3.30, 18.71, 18.97 ppm. ^{29}Si-NMR (99 MHz, 25°C, $CDCl_3$): δ(^{29}Si) = 8.09 ppm. ^{77}Se-NMR (95 MHz, 25 °C, C_6D_6): δ(^{77}Se) = –387.64 ppm. EI-MS: *m/z* = 238 (30, M^+), 223 (100), 195 (50), 73 (20).

2,2,4,4-Tetraisopropyl-1,3,2,4-diselenadisiletane (**20**)

Prepared by Method A from iPr$_2$SiCl$_2$ (2.3 ml, 2.3 g; 12.6 mmol). Purified by crystallization from hexane at –78 °C. Yellowish liquid forming colourless crystals upon standing at room temperature, yield = 2.4 g (99 %).

Preparation by modified Method A: Dry THF (40 ml) and fine selenium powder (1.0 g; 12.6 mmol) were placed to a 100 ml Schlenk flask. The suspension was cooled to 0 °C and then $NaBHEt_3$ (25.2 ml, 25.2 mmol, 1M solution in THF) was added slowly. The mixture was stirred at 25 °C for 2 h forming dark violet suspension of Na_2Se. The remaining procedure is similar to Method A. Yield: 1.8 g (72 %) of **20**.

Prepared by Method B from iPr$_2$SiHCl (2.2 ml, 1.9 g, 12.6 mmol) yielding 1.9 g (81 %) of **20**.

^{1}H-NMR (400 MHz, 25 °C, C_6D_6): δ(^{1}H) = 1.15 (d, J = 7 Hz, 24H, CH_3), 1.21–1.30 (m, 4H, CH) ppm. ^{13}C-NMR APT (100 MHz, 25 °C, C_6D_6): δ(^{13}C) = 17.72, 18.37 ppm. ^{29}Si-NMR (80

MHz, 25°C, C_6D_6): $\delta(^{29}Si)$ = 18.1 ppm. ^{77}Se-NMR (76 MHz, 25 °C, C_6D_6): $\delta(^{77}Se)$ = –402.33 ppm. EI-MS: *m/z* = 388 (10, M^+), 345 (100), 303 (20), 275 (20), 231 (20), 59 (10). Obtained spectra correspond to all experiments.

Triisopropylsilylselenole (**22**)

iPr_3Si-H (3.86 g, 5.0 ml; 24,4 mmol), Se powder (2.3 g; 29.29 mmol), and Ph_3P (50 mg; 0.19 mmol) were placed into a sealed tube and the reaction mixture was heated to 250 °C for 48 hours. After cooling to room temperature, the selenium excess was filtered off. The residue was purified by vacuum distillation at 80–85 °C (5 torr) to give 4.68 g (81 %) of *i*Pr_3SiSeH as orange liquid.

Using Et*i*Pr_2 as a Lewis base instead of Ph_3P yielded 3.13 g (54 %) of **22**. Yield of non-catalysed reaction is around 0.3 g (5 %).

^{1}H-NMR (400 MHz, 25 °C, C_6D_6): $\delta(^1H)$ = –2.81 (s, 1H, SeH), 0.98–1.04 (m, 21H, CH, CH_3) ppm. ^{13}C-NMR APT (100 MHz, 25 °C, C_6D_6): $\delta(^{13}C)$ = 13.96, 18.72 ppm. ^{29}Si-NMR (99 MHz, 25°C, C_6D_6): $\delta(^{29}Si)$ = 32.22 ppm. ^{77}Se-NMR (95 MHz, 25 °C, C_6D_6): $\delta(^{77}Se)$ = –420.7 (d, *J* = 47.17 Hz) ppm. EI MS: *m/z* = 238 (20, M^+) 195 (100), 153 (60), 125 (65), 59 (15).

Triisopropylsilyl-trimethylsilylselenide (**23**)

Hexane (30 ml), *i*Pr_3SiSeH (1.22 g; 5.14 mmol) and Et*i*Pr_2 (0.67 g, 0.9 ml; 5.14 mmol) were placed into a Schlenk flask and the reaction mixture was cooled to 0 °C. Me_3SiCl (0.56 g, 0.65 ml; 5.14 mmol) was added dropwise and the mixture was stirred at 25 °C for 12 hours. Upon filtration and vacuum distillation at 100–105 °C (2 torr), 1.12 g (70 %) of yellow liquid was obtained.

One-pot preparation: *i*Pr_3SiH (3.86 g, 5.0 ml; 24.4 mmol), Se powder (2.3 g; 29.29 mmol), and Ph_3P (50 mg; 0.19 mmol) were placed into a sealed tube and the reaction mixture was heated at 250 °C for 48 hours. After cooling to room temperature, hexane (30 ml) and Et*i*Pr_2 (3.15 g, 4.26 ml, 24.4 mmol) were added. The mixture was cooled to 0 °C and Me_3SiCl (2.64 g, 3.58 ml; 24.4 mmol) was added dropwise. After stirring for 12 hours at 25 °C, the mixture was filtered, and hexane was evaporated in vacuo. The residue was purified by vacuum distillation at 100–105 °C (2 torr) to give 3.6 g (50 %) of yellow liquid.

^{1}H-NMR (400 MHz, 25 °C, C_6D_6): $\delta(^1H)$ = 0.40 (s, 9H, CH_3), 1.01 (s, 3H, CH), 1.11–1.15 (m, 18H, CH_3) ppm. ^{13}C-NMR APT (100 MHz, 25 °C, C_6D_6): $\delta(^{13}C)$ = 4.97, 14.67, 19.09 ppm. ^{29}Si-NMR (99 MHz, 25°C, C_6D_6): $\delta(^{29}Si)$ = 10.41, 30.24 ppm. ^{77}Se-NMR (95 MHz, 25 °C, C_6D_6): $\delta(^{77}Se)$ = –447.10 ppm. EI MS: *m/z* = 310 (10, M^+), 267 (95), 224 (45), 183 (20), 129 (20), 101 (25), 73 (100).

Bis(dimethylphenylsilyl)selenide (**24**)

Selenium powder (0.5 g; 6.33 mmol), $PhMe_2SiH$ (2.6 g, 3.0 ml; 19 mmol), and Ph_3P (10 mg) were placed into a sealed tube and the reaction mixture was heated to 250 °C for 48 hours. Vacuum distillation of the crude product at 160–165 °C (2 torr) gave 1 g (43 %) of colourless oil.

^{1}H-NMR (400 MHz, 25 °C, C_6D_6): $\delta(^{1}H)$ = 0.45 (s, 12H, CH_3), 7.14–7.16 (m, 6, Ph), 7.50–7.52 (m, 4H, Ph) ppm. ^{13}C-NMR APT (100 MHz, 25 °C, C_6D_6): $\delta(^{13}C)$ = 127.93, 129.66, 133.94, 138.44 ppm. ^{29}Si-NMR (99 MHz, 25°C, C_6D_6): $\delta(^{29}Si)$ = 5.44 ppm. ^{77}Se-NMR (95 MHz, 25 °C, C_6D_6): $\delta(^{77}Se)$ = –341.15 ppm. EI MS: *m/z* = 350 (10, M^+), 257 (10), 197 (20), 135 (100).

2,2,3,3,5,5,6,6-Octamethyl-1,4,2,3,5,6-ditelluratetrasilinane (**25**)

Dry THF (200 ml) and fine tellurium powder (5 g; 39.2 mmol) were placed to a 500 ml Schlenk flask. $LiBHEt_3$ (78.4 ml; 78.4 mmol; 1 M sol. in THF) was added and the mixture was stirred for 14 h at 25 °C to afford pink solution with a white precipitate. The mixture was cooled to 0 °C whereupon 1,2-dichlorotetramethyldisilane (7.4 g; 39.2 mmol) dissolved in THF (50 ml) was added dropwise within 20 minutes. The colour turned dark brown immediately followed to clear yellow after 14 h at 25 °C. The solvent and all volatiles were removed by distillation and vacuum drying to afford white crystals that were taken up in hexane (50 ml) and warmed to 50 °C with vigorous stirring. The warm yellow mixture was filtered through cannula and the remaining solids were extracted with hexane once again. Both combined hexane fractions were cooled to –78 °C to provide crystals of **25** while the hexane supernatant was removed with a syringe. The colourless needles were dried in vacuum yielding 6.5 g (68 %) of cyclic silyltelluride **25**.

^{1}H-NMR (400 MHz, 25 °C, C_6D_6): $\delta(^{1}H)$ = 0.65 (s, 24H, CH_3) ppm. ^{13}C-NMR APT (100 MHz, 25 °C, C_6D_6): $\delta(^{13}C)$ = 1 ppm. ^{29}Si-NMR (80 MHz, 25°C, C_6D_6): $\delta(^{29}Si)$ = –29.1 ppm. ^{125}Te-NMR (126 MHz, 25 °C, C_6D_6): $\delta(^{125}Te)$ = –885.53 ppm. EI-MS: *m/z* = 487.9 (M+, 10), 288.9 (10), 116 (40), 73 (100).

Attempted preparation of bis(trimethylsilyl)selenide (**1**)

Selenium powder (0.5 g; 6.3 mmol) and Me_6Si_2 (1.3 ml, 0.93 g; 6,3 mmol) were placed to a pressure vessel. Heating to temperature up to 250 °C for several days did not afford any reaction.

Attempted preparation of 2,2,4,4-tetramethyl-1,3,2,4-diselenadisiletane (**25**)

Both Methods A and B starting from Me_2SiCl_2 (1.6 ml, 1.6 g, 12.6 mmol) and MeSiHCl (1.4 ml, 1.2 g, 12.6 mmol) provided a yellow oil. EI-MS revealed a rich mixture of several selenium products (see Results and discussion chapter). The reaction lacked reproducibility

and abundance of each product varied within the particular experiments. Attempts to separate products by vacuum distillation or crystallization from hexane at –78 °C were not successful.

13 Results and discussion

Silyl- and stanylselenides have proven as convenient ALD precursors. Their volatility, high reactivity, and thermal stability, however, come with some drawbacks. The most pronounced is high air-sensitivity, which complicates handling during the synthesis, purification, and subsequent deposition. Another questionable limitation is their synthesis. Even though that the established preparation utilizing Li_2Se is straightforward, the high price of $LiBHEt_3$ and safety issues connected with the aforementioned hydride or elemental lithium along with high demand for dry solvents and inert atmosphere limit its application beyond the laboratory scale. Hence, the experimental part of this work aims to investigate cyclic silyl-selenides and silylselenoles as an alternative to bis(trialkylsilyl)selenides. These derivatives would potentially bring improved air-sensitivity along with novel synthetic routes using inexpensive starting materials. Thorough structural analysis confirming predicted structure and purity as well as investigation of fundamental thermal properties, as an important characteristic of ALD precursor, are integral part of this experiment work. The last part focuses on testing selected molecules for deposition of metal selenides employing both gALD and sALD. Quality of manufactured thin films, deposition conditions, and effect of precursor structure to the resulting layer properties are discussed.

13.1 Preparation of selenium compounds

The most straightforward way to prepare silylselenides is a reaction between Li_2Se and desired alkyldichlorodisilane or dialkyldichlorosilane. In this work, Li_2Se is readily prepared by the established reaction of elemental selenium with $LiBHEt_3$ solution. The alternative reaction of elemental Se with Li is sluggish and usually provides lower yields.

Scheme 13 depicts the first attempts on cyclic silylselenides **9,**[89] **10** and **11**[88] that were formerly reported by Herzog. The synthesis of six-membered cycle **19** was not reported up to date. Whereas products **9** and **19** were prepared with the aid of $BF_3{\cdot}OEt_2$ as a catalyst in good yields, target compounds **10** and **11** rather decomposed in the presence of $BF_3{\cdot}OEt_2$. Target compounds were purified by vacuum distillation or crystallization from hexane at –78 °C in the case of **11**. In general, these preparations were without major difficulties.

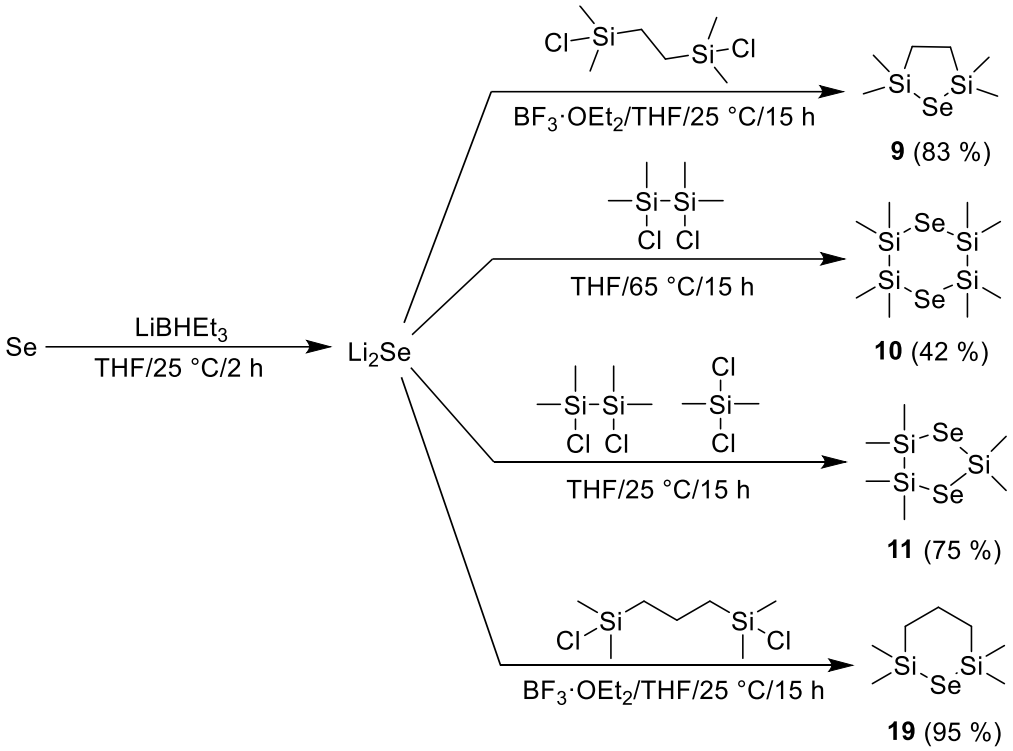

Scheme 13. Preparation of cyclic silylselenides **9**–**11** and **19**.

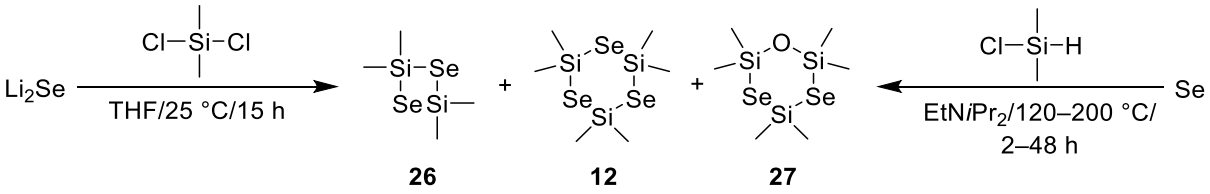

Scheme 14. Attempted preparation of selenide **26**.

In contrast to five- and six-membered cycles, a synthesis of four-membered cyclic silylselenides containing two selenium atoms such as **26** was not reported so far. A reaction between Li_2Se and Me_2SiCl_2 affording six-membered cycle **12** containing three selenium atoms is known from the literature.[88] However, attempts to reproduce this procedure was not successful while a mixture of products was always obtained. Vacuum distillation, fraction vacuum distillation, sublimation, and crystallization from hexane at 0 °C or –78 °C failed to separate single molecules. In addition, *Scheme 14* also shows alternative method towards products **12**, **26** and **27** by employing Me_2HSiCl, elemental selenium, and $EtNiPr_2$ as a base. Analogously to the reaction of Me_2SiCl_2, the reaction provided mixture of products; the corresponding GC/MS records of the reactions at 100 °C and 250 °C are shown in *Figure 21*. As a general feature, these experiments lacked reproducibility and ratios of products usually varied. Four-membered cycle **26** can be clearly identified at 100 °C, while low amount of six-membered cycle **12** appeared if the reaction was carried out at elevated temperature.

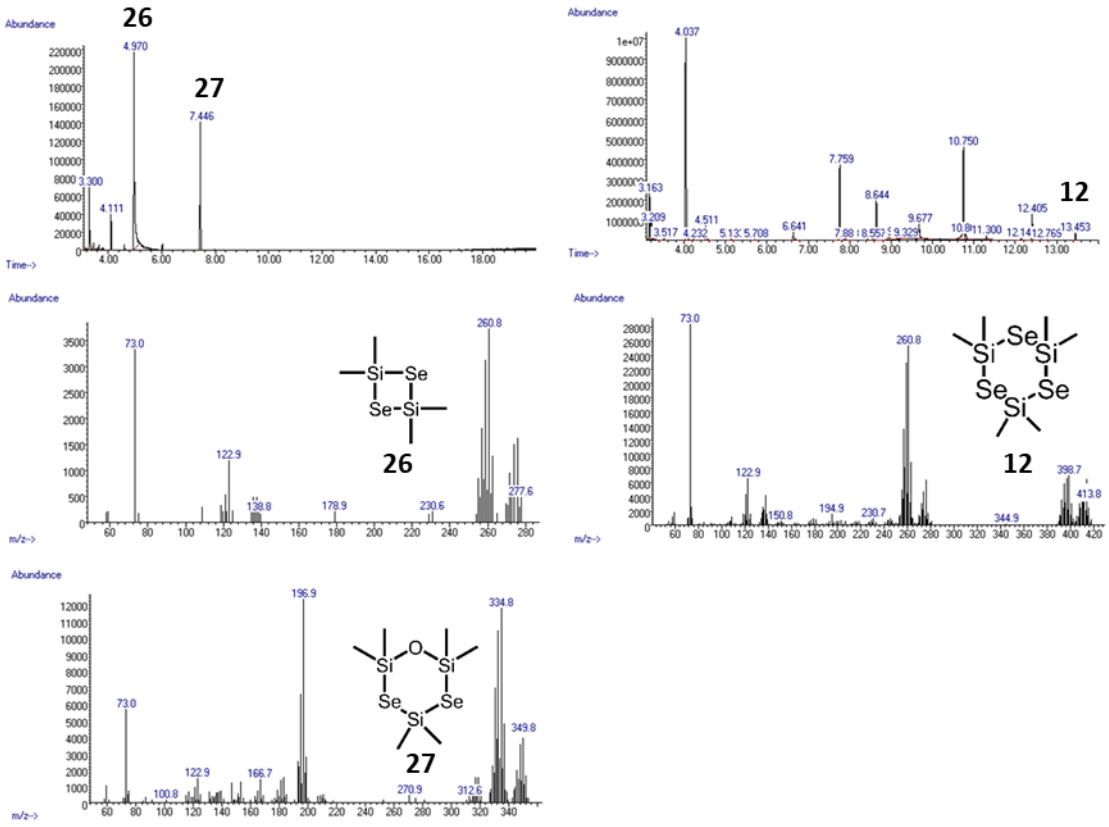

Figure 21. GC/MS record of crude reaction mixture during attempted preparation of 2,2,4,4-tetramethyl-1,3,2,4-diselenadisiletane by reaction Me_2HSiCl_2, elemental selenium and Et*N*iPr_2 at 100 (left) and 250 °C (right).

Heterocycle **27** containing oxygen was always observed as a major impurity, but source of the oxygen was not identified. Hence, motivated by development and synthesis of new selenium precursor in simple and efficient manner, I stopped further investigation of these products.

Thompson[90] reported reaction of Na_2Se (its preparation was not specified) with Et_2SiCl_2 giving mixture of four- (30 % yield) and six-membered (40 % yield) cycles. A separation method was also not specified in this work. Experimental reproduction of this reaction afforded a yellow oil in 43 % yield. However, the yield was significantly improved to 92 % by using Li_2Se. In contrast to GC/MS record detecting only four-membered product **14** (*Scheme 15*), ^{1}H, ^{13}C, ^{29}Si, and ^{77}Se NMR spectra showed several products. All separation attempts failed, the mixture composition is unknown so far, six-membered cycle **13** (see *Scheme 8*) is suspicious, but NMR spectra given by Thompson[90] do not correspond precisely. These difficulties again caused loss of interest in molecule **14**. On the other hand, the corresponding *iso*propyl derivate **20** was prepared quantitatively from Li_2Se, whereas its synthesis from Na_2Se can be carried out with lower yield of 72 %. Newly developed method starting from elemental

selenium and *i*Pr_2HSiCl in a basic environment provided **20** in 81 % yield. This method excludes solvent, uses readily available and inexpensive starting materials, and the separation of **20** was very easy. Hence, compound **20** would become an attractive Se-precursor for application in ALD. Analogous *tert*butyl derivative **15** was also examined. Whereas its preparation from Li_2Se completely failed, the synthesis using *t*Bu_2HSiCl provided **15** in 61 % yield.

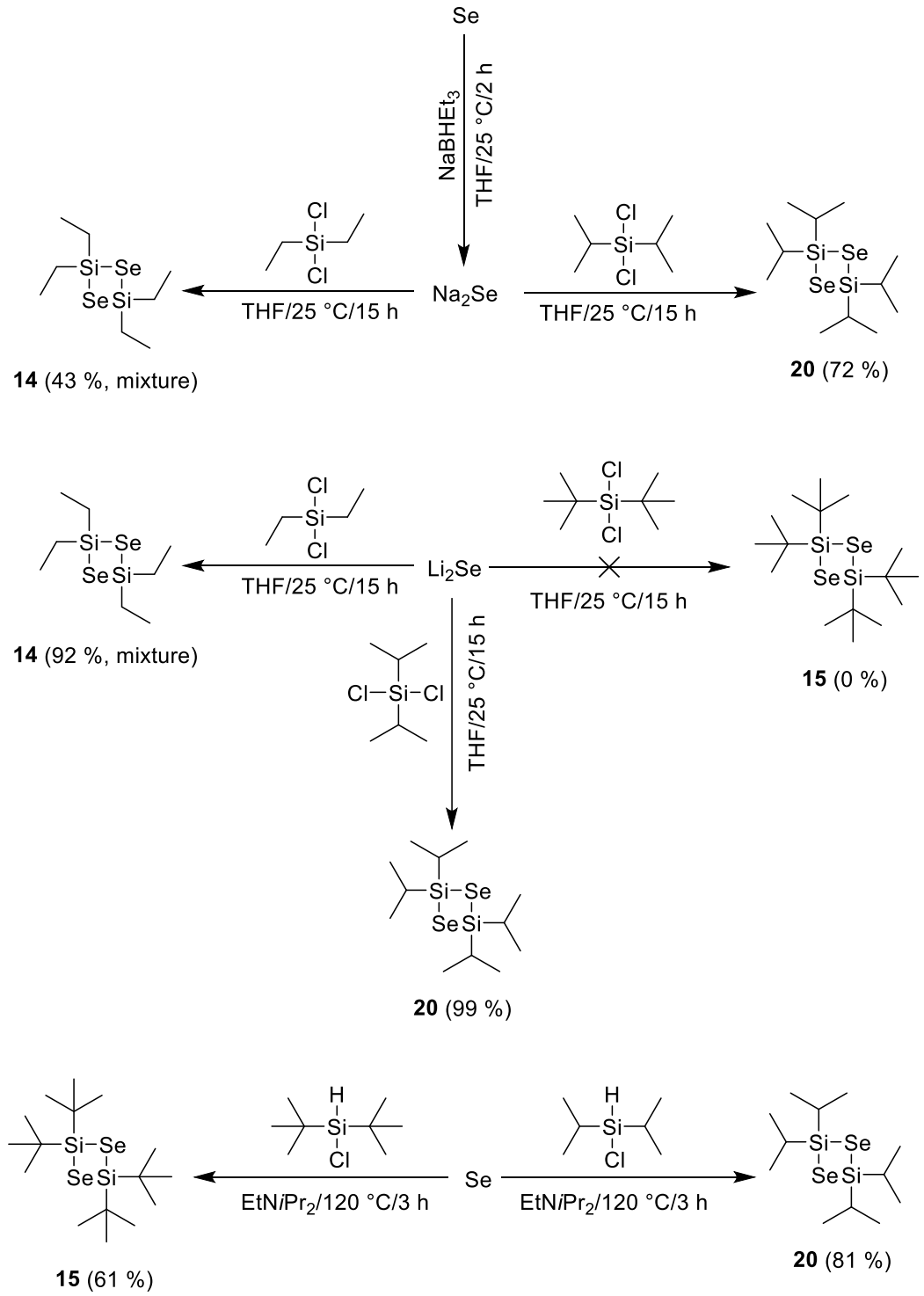

Scheme 15. Preparation of four-membered silylselenides.

Direct insertion of selenium into R_3Si-H bond forming trialkylsilylselenole R_3Si-SeH is another attractive option towards potential Se-precursors as synthetically demonstrated by Grenader.[94] His work reported a reduction of selenium with $cHex_3Si$-H at 250 ° and also briefly but with no further details mentions preparation of $i Pr_3Si$-SeH **22**. My attempt to prepare **22** starting from $i Pr_3Si$-H afforded only poor yield around 5 % even after heating at 250 °C for 48 hours (*Scheme 16*). Further investigation revealed that the yield can be dramatically increased by adding a Lewis base. When Ph_3P was used, tri*iso*propylsilylselenole **22** was obtained in 81 % yield. Compound **22** possesses high volatility and very inexpensive synthesis and, therefore, might be an interesting Se-precursor for ALD. Nevertheless, the proton attached to selenium may generate ALD-undesired HX by-product when treated with metal halides. A transformation of **22** to asymmetric silylselenide **23** bearing additional trimethylsilyl group may overcome this drawback. The reaction of selenole **22** with trimethylsilylchloride or one-pot reaction starting from $i Pr_3SiH$ gave **23** in 70 or 55 %. Interestingly, using even a large excess of tri*iso*propyl silane gave exclusively **22** and only traces of bis(tri*iso*propylsilyl)selenide, which was detected by GC/MS.

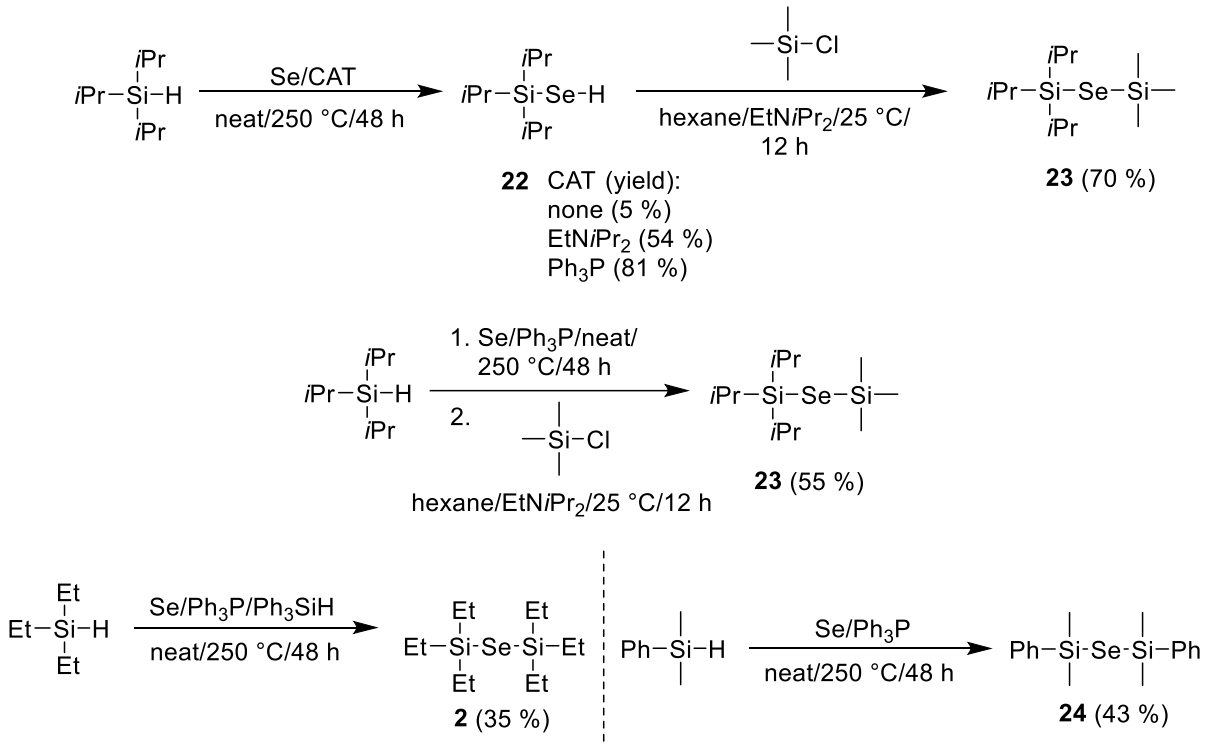

Scheme 16. Reduction of selenides by silanes.

Reduction of selenium with Et_3Si-H was also published by Vyazankin.[93] However, my attempts to reproduce this reaction failed even with addition of Ph_3P, elevated temperature or extended reaction time. Further experiments on preparation of Et_3Si-SeH or $(Et_3Si)_2Se$ via this method led to an idea of employing transmission, which is known phenomenon for 14 group elements. Indeed, when treating two equivalents of Et_3Si-H with selenium and small amount

of Ph_3Si-H, bis(triethylsilyl)selenide **2** was obtained in 35 % yield (*Scheme 16*). Only traces of Et_3Si-SeH were detected by GC/MS. Selenide **24** was isolated in 43 % yield along with only minor amount of Me_2PhSi-SeH when treating bulkier silane Me_2PhSi-H with selenium.

Vyazankin[85] described also reduction of selenium with Et_3Sn-H to bis(triethylstanyl)selenide at 120 °C. I have examined this reaction with nBu$_3$Sn-H (*Scheme 17*). When the reaction temperature was increased to 180 °C, bis(tributylstanyl)selenide **7** was obtained in almost quantitative yield after 12 hours.

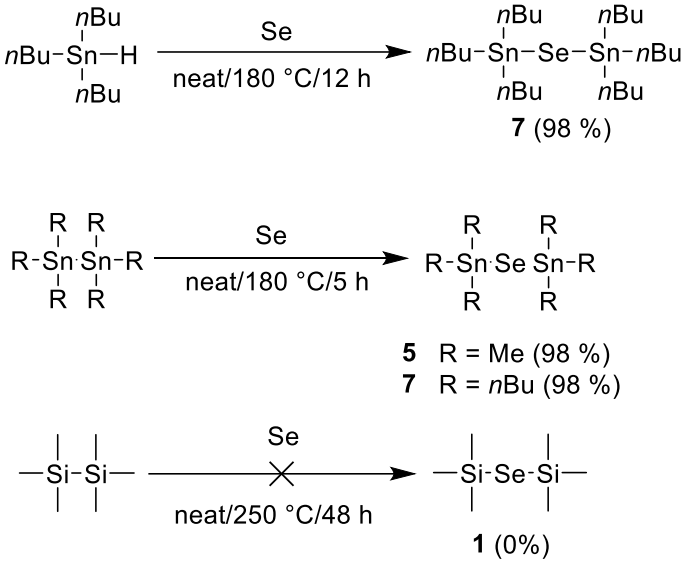

Scheme 17. Insertion of selenium to Sn-Sn/H bond.

Scheme 17 also shows modified synthesis by Han.[84] In this work, selenium is inserted to Sn-Sn bond in a catalytic cycle involving oxidation of triphenylphosphine to Ph_3P=Se, which reacts with Me_6Sn_2 at laboratory temperature in benzene to bis(trimethylstanyl)selenide **5** in 47 % yield after 5 hours. Further elaboration with this method revealed, that elevated reaction temperature to 180 °C afforded **5** and **7** in nearly quantitative yields even without catalyst or solvent present. It is wort to note that both starting Me_6Sn_2 and Bu_6Sn_2 are commercially available, air stable, and inexpensive starting materials.

A similar reaction using Me_6Si_2 was also attempted but even at very harsh reaction conditions (250 °C for seven days) and presence of Ph_3P of EtN*i*Pr_2 did not afford any product.

13.2 Structural analysis

The structure of all target compounds and eventual intermediates was studied and determined with a combination of GC/MS and heteronuclear NMR. *Figure 22* shows representative EI-GC/MS record of target molecule **22**, where M^+ peak is observed along with other anticipated fragments caused by the loss of the alkyl groups. The peaks also possess typical isotope pattern.

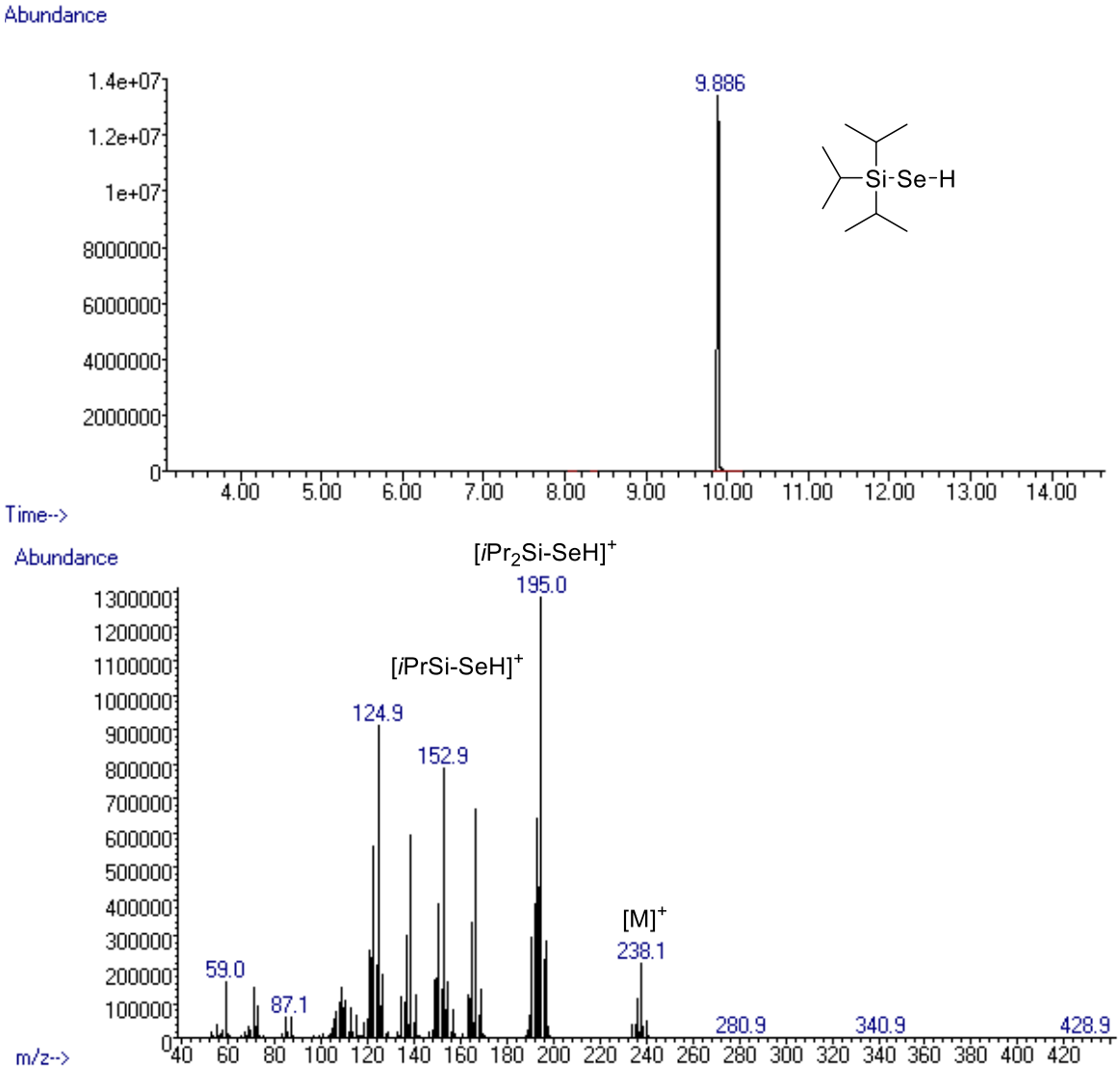

Figure 22. GC/MS record of molecule **22**.

^{1}H-NMR spectra of **22** (*Figure 23*) showed an undistinguished multiplet of the *iso*propyl group at 0.98–1.04 ppm. Singlet with very low chemical shift at –2.81 ppm belongs to the proton attached to the selenium.

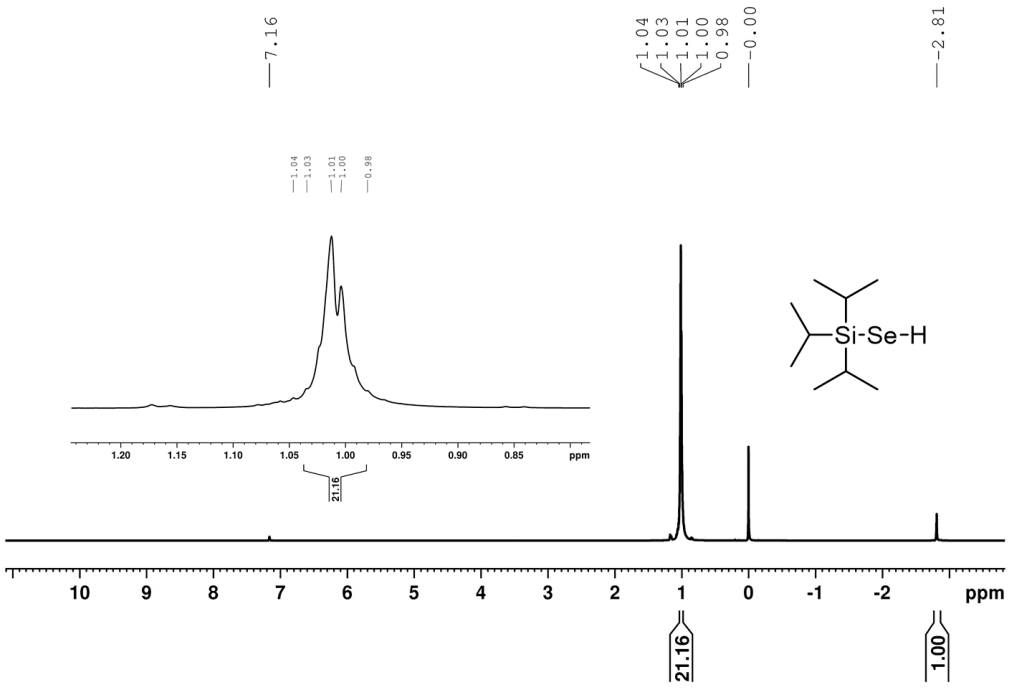

Figure 23. ^{1}H-NMR spectra (400 MHz, 25 °C, C_6D_6) of **22**.

^{13}C-NMR (APT) spectra were very simple showing two signals at 13.96 and 18.72 ppm. Similarly, only one signal at 32.22 ppm was observed in ^{29}Si-NMR spectra. Both spectra are shown in *Figure 24.*

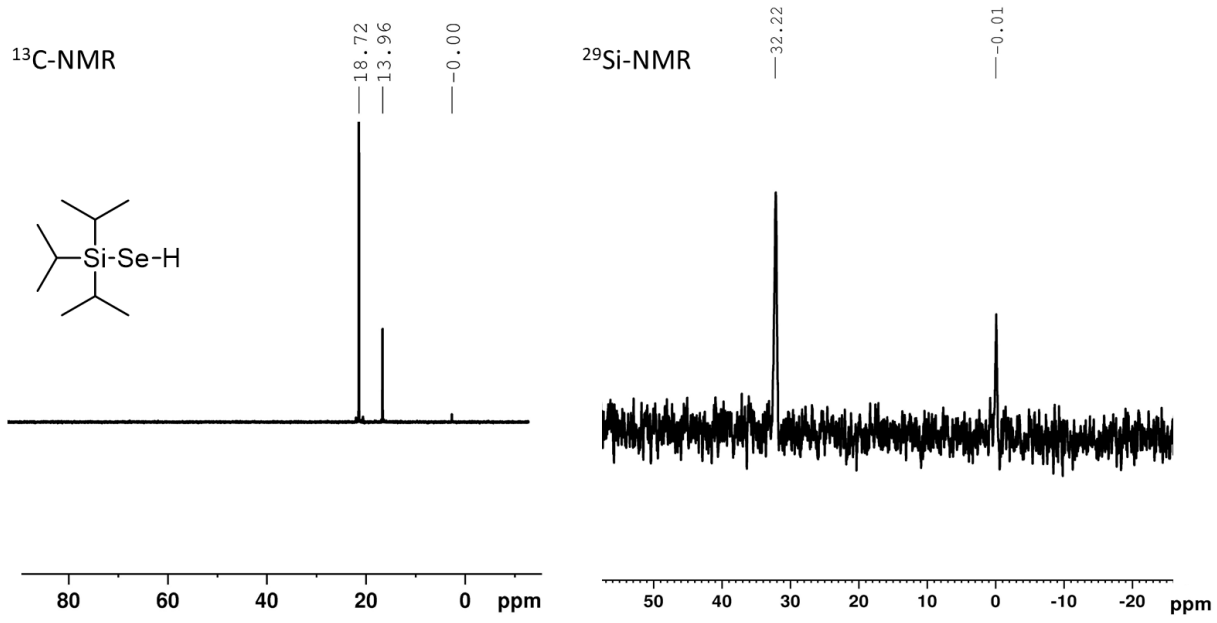

Figure 24. ^{13}C-NMR APT (100 MHz, 25 °C, C_6D_6) and ^{29}Si-NMR (99 MHz, 25°C, C_6D_6) of **22**.

Gated ^{77}Se-NMR spectra shown in *Figure 25* confirmed direct Se-H coupling resulting in a doublet at –420.7 ppm with interaction constant J = 47.17 Hz.

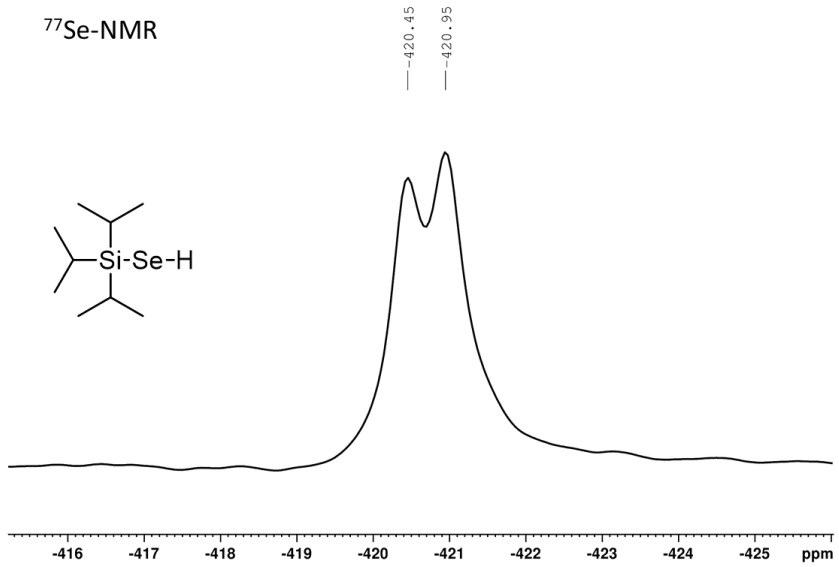

Figure 25. ^{77}Se-NMR (95 MHz, 25 °C, C_6D_6, gated) of **22**.

In general, the NMR spectra of target selenides are not complicated due to their simple structure, which, on the other hand, ensures their low molecular weight and high volatility. One interesting observation that worth mentioning here is Si-Se coupling, which was observed for cyclic silylselenide **20**. The ^{29}Si- and ^{77}Se-NMR spectra shown in *Figure 26* revealed the interaction constant $J \approx 250$ Hz. Silylselenide **20** is the only molecule with this type of ^{29}Si-^{77}Se interaction observed within prepared series of products.

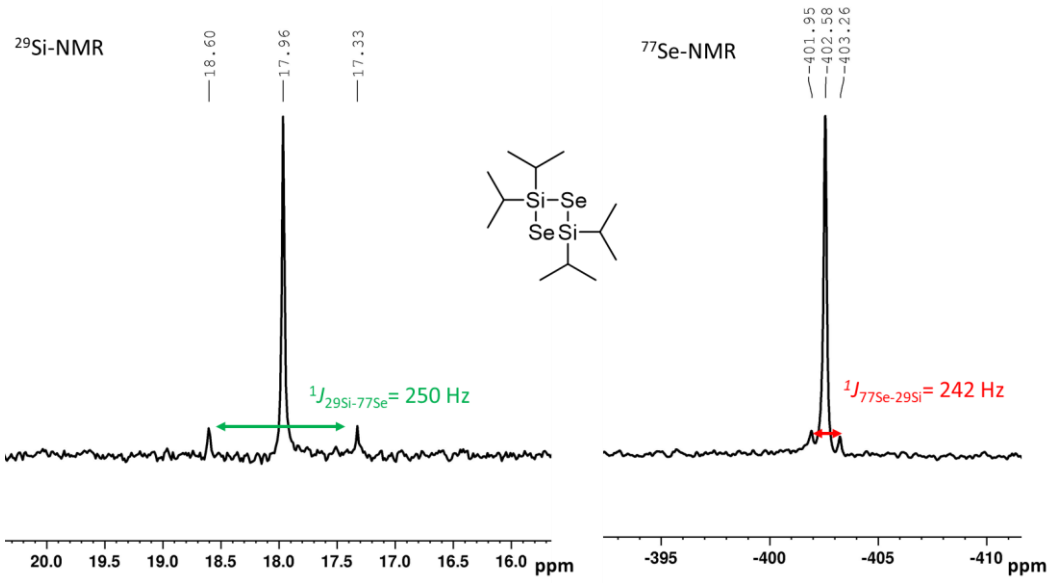

Figure 26. ^{29}Si-NMR (80 MHz, 25°C, C_6D_6) and ^{77}Se-NMR (76 MHz, 25 °C, C_6D_6) of **20**.

13.3 Thermal analysis

High volatility and thermal stability are the key parameters for successful ALD precursor utilization. To study these characteristics, Differential Scanning Calorimetry (DSC) and Thermogravimetric analysis (TG) were employed. The measurements were performed in N_2 atmosphere and laboratory pressure.

Molecules **9**, **10**, and **19** exhibited smooth evaporation that decrease with larger molecular weight (*Figure 27*). Compound **10** is solid at laboratory temperature with melting point at 145 °C and boiling around 275 °C. Compounds **9** and **19** are liquids at 25 °C that boil at 170 or 200 °C, respectively.

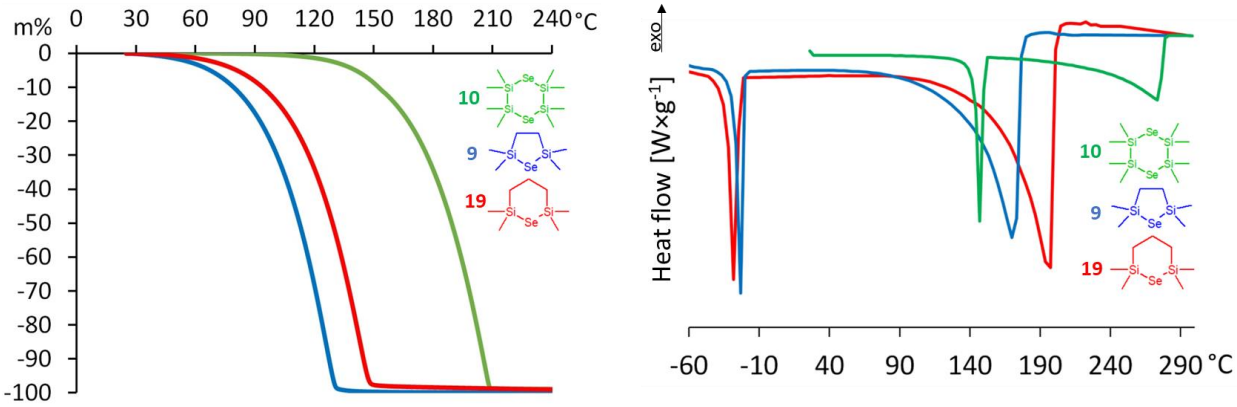

Figure 27. TGA (left) and DSC (right) curves of **9** (blue), **10** (green), and **19** (red).

DSC curve of **11** (*Figure 28*) revealed glass transition at –55 °C, melting at –21 °C, and complete evaporation at 200 °C. The two revealed melting points and relatively wide evaporation peak of **14** is another proof of this inseparable mixture. Compounds **15** and **20** were evaporated smoothly but at higher temperatures around 285 and 310 °C.

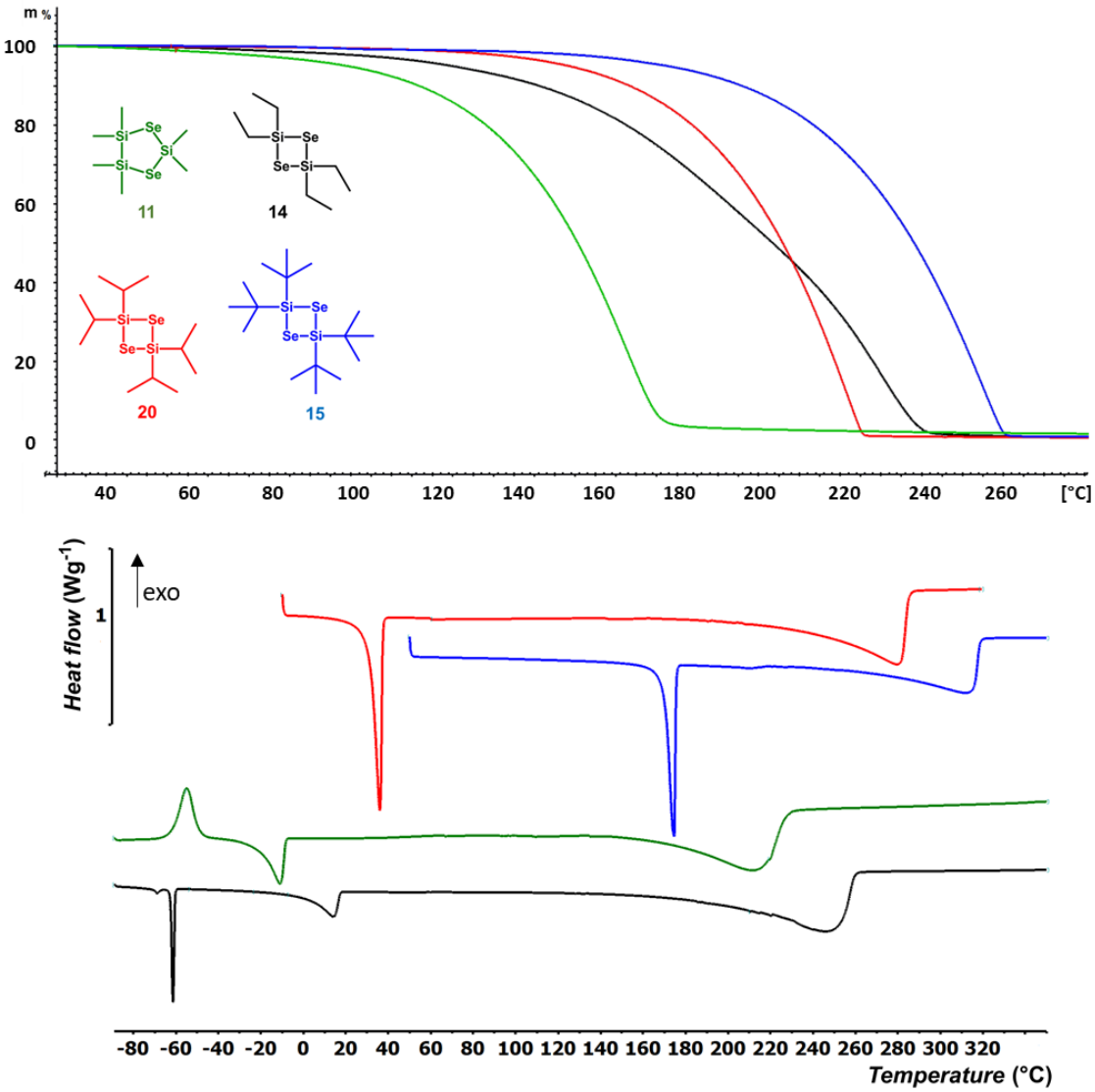

Figure 28. TGA (top) and DSC (bottom) curves of **11** (green), **14** (black), **15** (blue), and **20** (red).

Slightly broadened evaporation peaks seen in DSC curves (*Figure 29*) of **22** and **23** indicates additional thermal process taking place around boiling point. It is more pronounced in TG analysis. I suspected formation of two symmetrical molecules and this idea was confirmed by heating **22** to 180 °C for 15 hours at ambient pressure. Under such condition, a formation of bis(tri*iso*propylsilyl)selenide **3** is observed accompanied by release of H_2Se (*Scheme 18*). This is in contrast to the synthesis of **22** carried out at 250 °C (see above), where none side products were observed. However, the reaction was heavily pressurized in a pressure vessel. Compound **24** underwent glass transition at –35 °C, melting, and subsequent boiling at 345 °C.

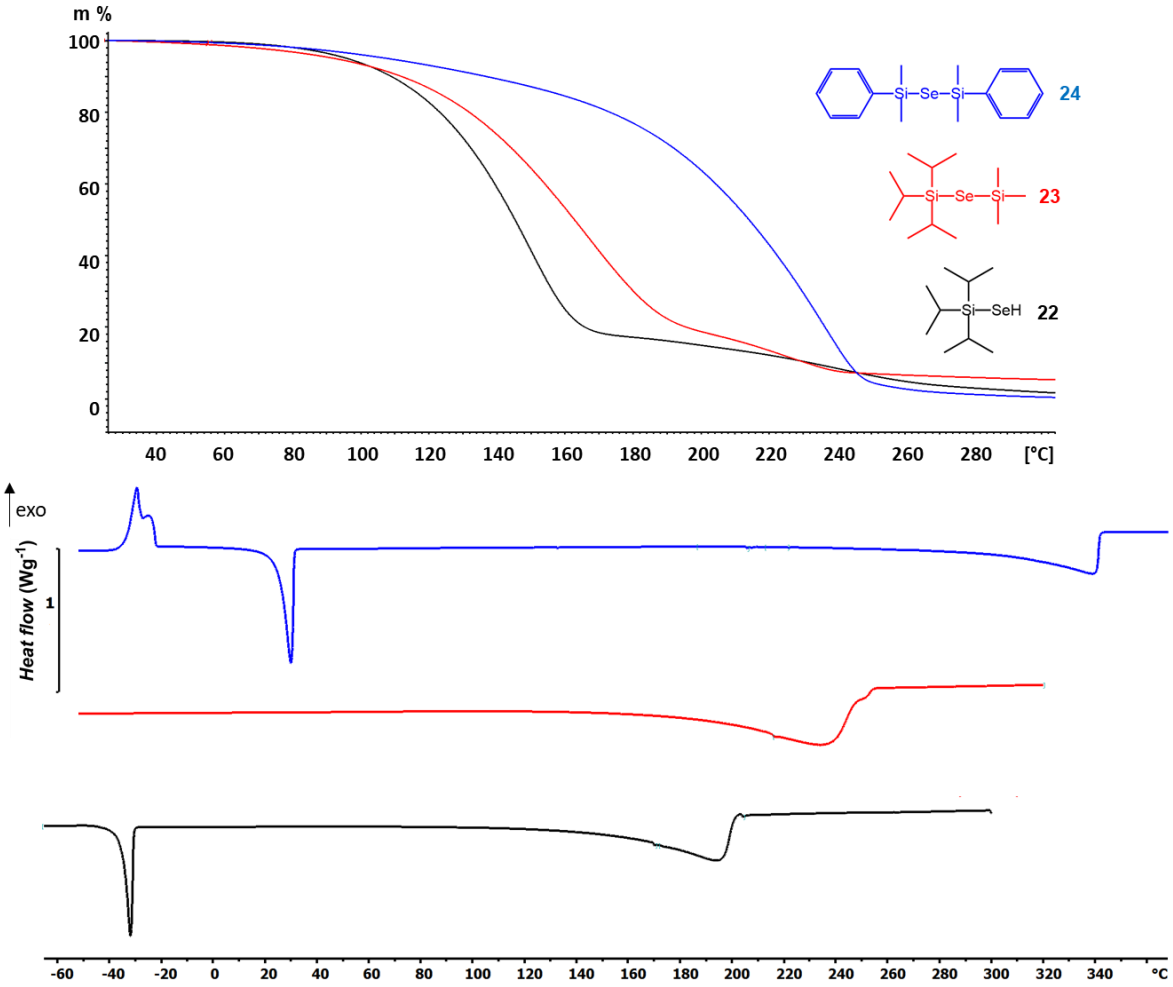

Figure 29. TGA (top) and DSC (bottom) curves of **22** (black), **23** (red) and ***24*** (blue).

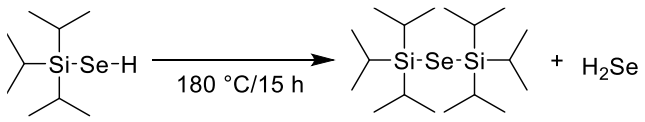

22 **3**

Scheme 18. Proposed thermal decomposition of **22**.

Figure 30 illustrates boiling points determined by DSC as function of the structure, while *Table 2* contains a complete dataset of obtained thermal properties. It is no surprise, that boiling point steadily increases with extended molecule mass and elongated alkyl chains. Most of the prepared compounds seems to be thermally stable with the exception of **22** and **23** that started to decompose at 160 °C and 185 °C, respectively. Molecule **11** showed wider peak in DSC, but an additional thermal process was identified by TG analysis. To fully ensure thermal stability of prepared selenium precursors, I plan to examine them by TGA interconnected to GC/MS. This would further disclose volatility, eventual decomposition products and hidden thermal processes.

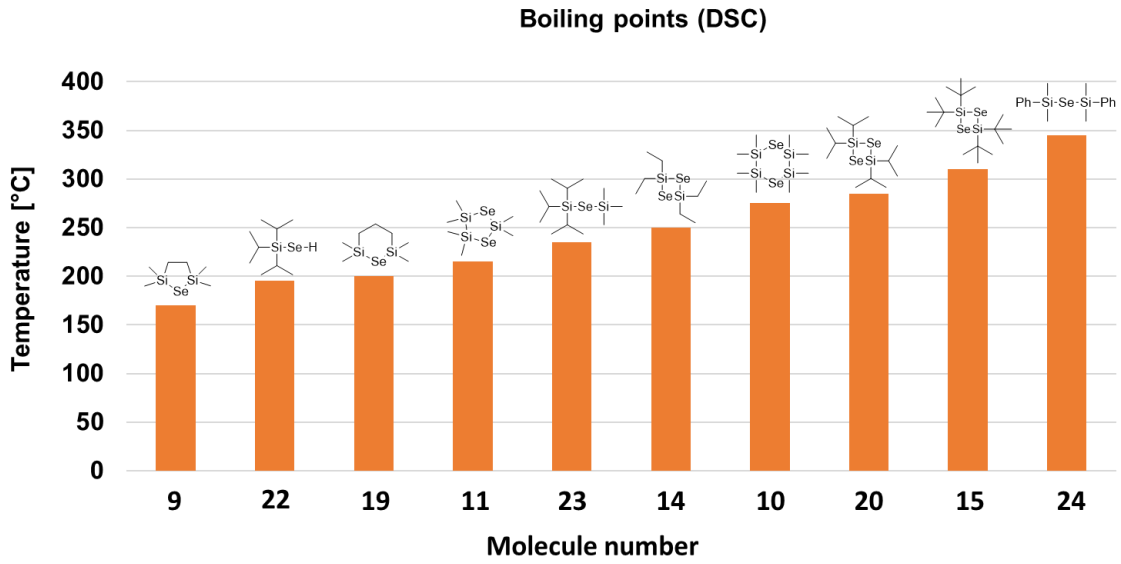

Figure 30. Overview of boiling points of products determined by DSC.

Table 2. Thermal properties of prepared molecules.

Molecule	Temperature of crystallization (DSC) [°C]	Melting point (DSC) [°C]	Temperature of glass transition (DSC) [°C]	Temperature close to the boiling point (DSC) [°C]	Boiling point (distillation) [°C (pressure)]
9	–62	–27	–90	170	85 (20 torr)
10	-	145	-	275	-
11	–62	–21	–55	215	95–100 (1 torr)
14	–64; 0	–62; 2	-	250	120–140 (1 torr)
15	157	170	-	310	-
19	–85	–32	–89	200	95 (20 torr)
20	3	32	-	285	-
22	–67	–32	-	195	80–85 (5 torr)
23	-	-	-	235	100–105 (2 torr)
24	-	25	–45	345	160–165 (2 torr)

13.4 Deposition of $MoSe_2$ with gALD

After first insight into fundamental thermal properties, four candidates **9**, **10**, **19** and **20** were selected to be screened by gALD experiments that were performed by our fellow research group of Dr. J. M. Macák at the University of Pardubice. The deposition process was carried out in custom ALD reactor on annealed TiO_2 foils, TiO_2 nanotubes or Si/SiO_2 silicon wafers as a substrate with reaction temperature 300 °C. Sequential introducing of selenium precursor and $MoCl_5$ (with N_2 purges in between) were aimed to deposit thin films of $MoSe_2$ according to ligand exchange reaction shown in *Scheme 19*.

10

Scheme 19. Formation of $MoSe_2$ thin film by reaction of $MoCl_5$ with cyclic precursor **10** as an example.

Cyclic precursor **9** was evaporated to the reaction chamber already at 35 °C at the pressure of 1–2 torr. *Figure 31* shows SEM picture with polycrystalline flaky structure, which is typical for $MoSe_2$ and was further confirmed by Raman spectroscopy. Closer surface compositional analysis using XPS unfortunately revealed presence of significant chlorine impurities along with elemental selenium. This suggest that the reactivity of **9** is not high enough within the used conditions and the exchange of ligands is incomplete. Presence of selenium would also point to a partial decomposition process. Precursor **10** needed higher temperature for evaporation (120 °C), but the prepared $MoSe_2$ thin films possessed high quality with minimum level of impurities. A detailed characterization of the as-prepared nanofilms and deposition conditions were already published.[141]

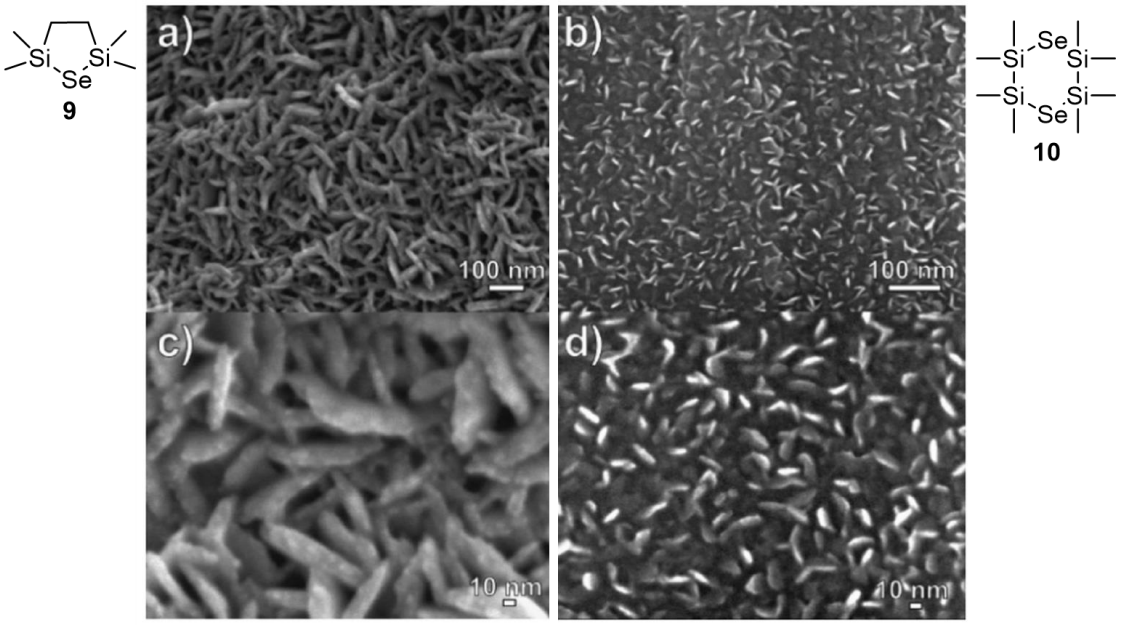

Figure 31. SEM images of $MoSe_2$ (400 cycles) deposited using $MoCl_5$ and **9** (left: a, c) or **10** (right: b, d).

In contrast to five-membered cycle **9**, six-membered silylselenide **19** did not provide any deposition of $MoSe_2$. Increased temperature for evaporation from 45 to even 155 °C, which should ensure large oversaturation of the surface, had no effect. Thus, it seems that **19** is too stable to react at the given conditions.

Four-membered cycle **20** bearing two selenium atoms was the last tested gALD precursor. Its slightly lower volatility required evaporation temperature of 120 °C. *Figure 32* represents SEM images of the as-deposited $MoSe_2$ on two different substrates including cross-sectional SEM, where typical out-of-plane oriented flaky nanosheet structure is clearly visible. Investigation of different pulse lengths ensures finding the right condition for saturated reaction in ALD regime. If temperature was lowered from 300 to 200 °C, the morphology changed to granular and presence of Se-Se bonds or Se^0 emerged in the XPS spectra. This means that morphology and surface reactions are temperature dependent. Nevertheless, deposition at 300 °C provided high-quality $MoSe_2$ thin films with no residual chlorine detected meaning good ligand exchange. A detailed characterization and deposition conditions were already published.[142]

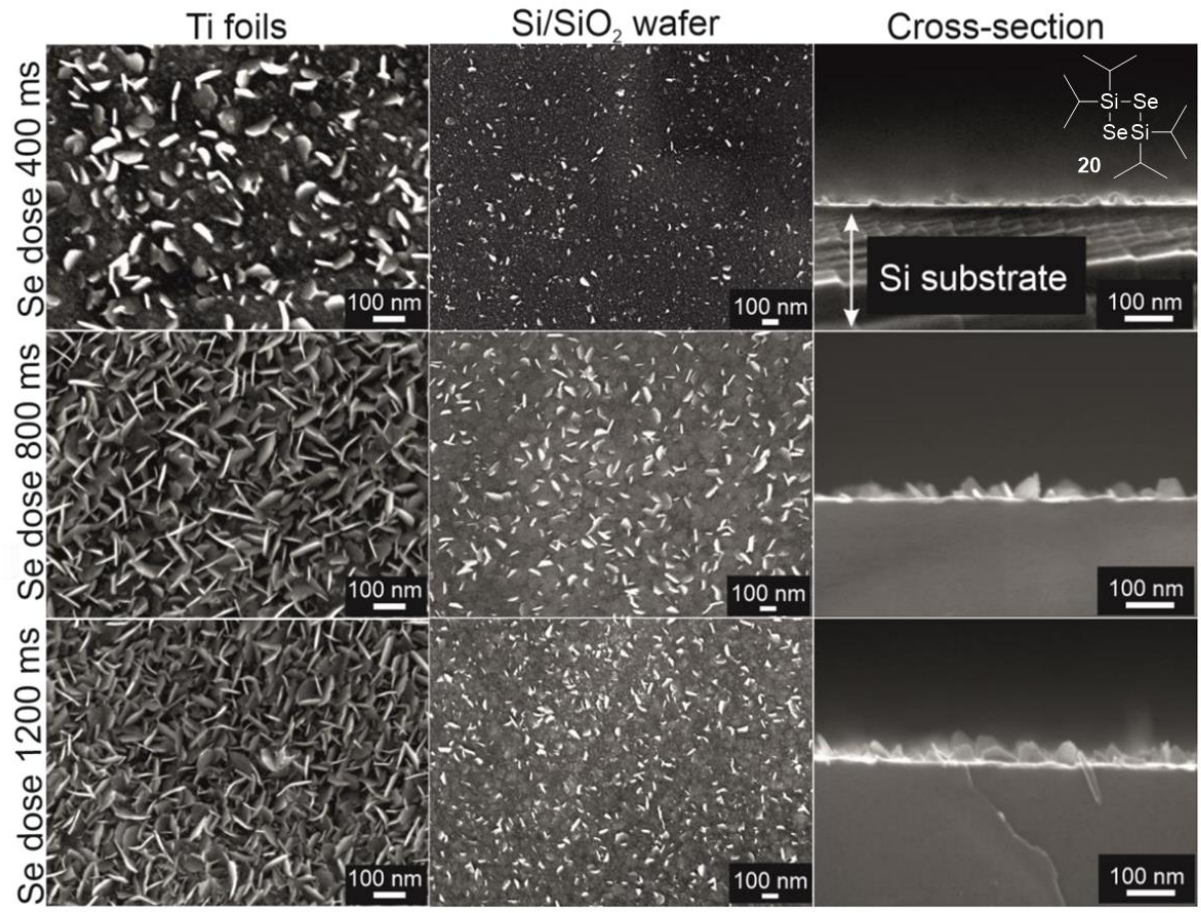

Figure 32. SEM and cross-section SEM images of $MoSe_2$ (800 cycles) deposited using $MoCl_5$ and various pulse lengths of **20** on different substrates.

13.5 Deposition of Sb_2Se_3 using sALD

Suitability of prepared Se-precursors for sALD was examined during my internship at the Friedrich-Alexander-University Erlangen-Nűrnberg under guidance of prof. Julien Bachmann. Sb_2Se_3 has been chosen as a target material because of its high application potential as photon-absorbing layer in thin film solar cells. It has been prepared by reacting selected Se precursors with $SbCl_3$ according to *Scheme 20*.

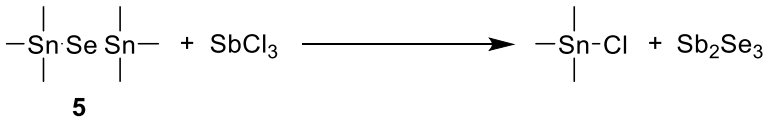

Scheme 20. Reaction of $SbCl_3$ with stanylselenide **5** resulting in Sb_2Se_3 thin film.

The deposition was carried out using self-made sALD system composed of steel reaction chamber, peristaltic pump, Teflon tubing, and Schlenk flasks connected to the nitrogen filled Schlenk line to maintain the inert atmosphere during the whole process. *Figure 14* shows schematic interpretation of the system, while *Figure 33* depicts its real photograph and a detail of the steel chamber with two different substrates. The chamber allowed deposition on substrates with size up to 10 × 20 mm.

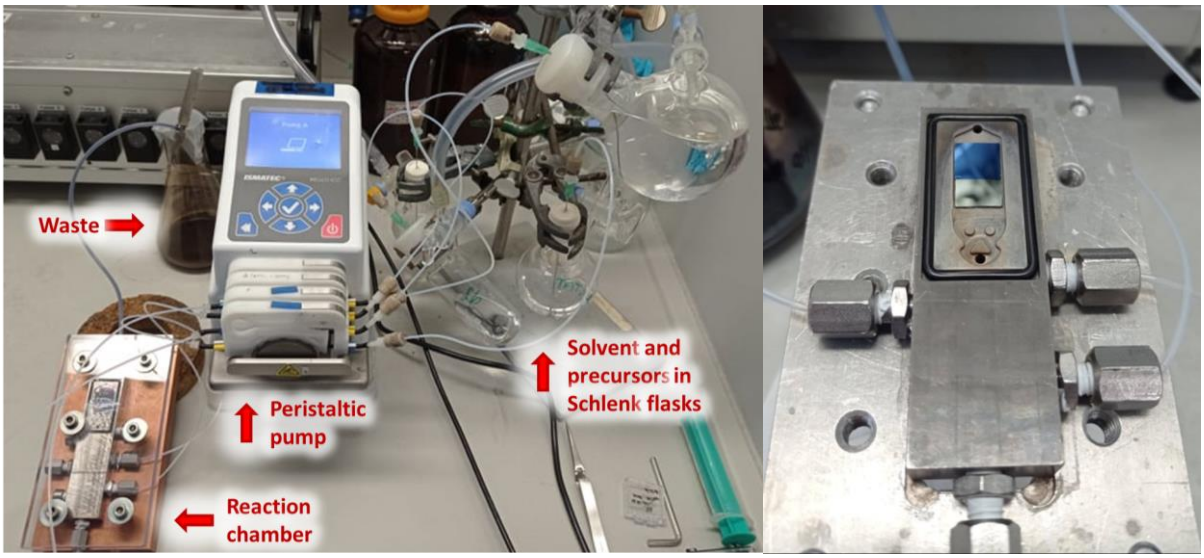

Figure 33. A photograph of the used sALD setup (left) and opened steel sALD reaction chamber with two different substrates (right)

The deposition was carried out in an injection mode, where line called *Solvent 1* (see *Figure 34*) brings continuous flow of the solvent (1 ml/min) and precursors are injected to this stream sequentially by the separate inlets with flowrate of 0.8 ml/min. The *Solvent 2* line (0.8 ml/min) is activated between each precursor pulse to ensure complete purge of the chamber and preventing mixing of precursors. To clarify the protocol, *Figure 34 (right)* depicts the dosage as a function of time. Used precursor concentration is 1 mmol/l, unless otherwise

stated. The length of optimal pulse and purge was determined during ALD study (see below). The thicknesses were determined by ellipsometry.

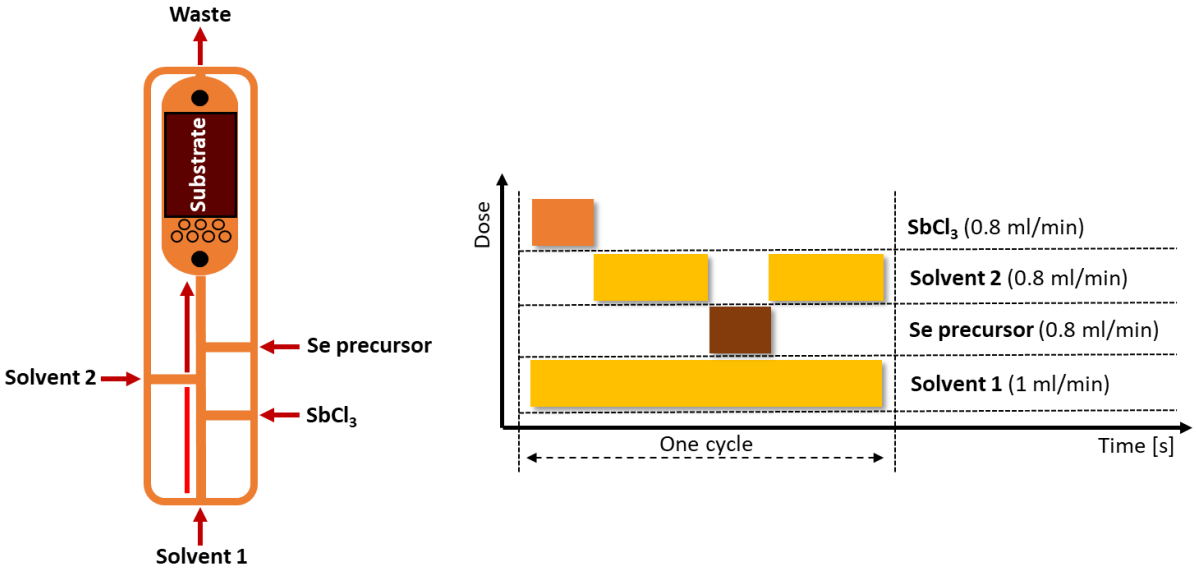

Figure 34. Scheme of the reaction chamber (left) and schematic representation of pulse-purge protocol (right) using selenium precursor and $SbCl_3$ for Sb_2Se_3 deposition.

Unlike gALD, sALD does not demand high volatility and thermal stability, thus the selection of selenium precursors was based on ease of preparation, handling, and economical aspects. Solubility is also important, however the selected selenides shown on *Figure 35* are well soluble in wide range of organic solvents. Hexane was used as solvent because it possesses several advantages. Most importantly, it dissolves $SbCl_3$, which is very good counter-precursor for the tested selenides. Hexane is also easily dried by distillation over Na/K alloy. Moreover, it is inert to the tubing system and have a suitable viscosity.

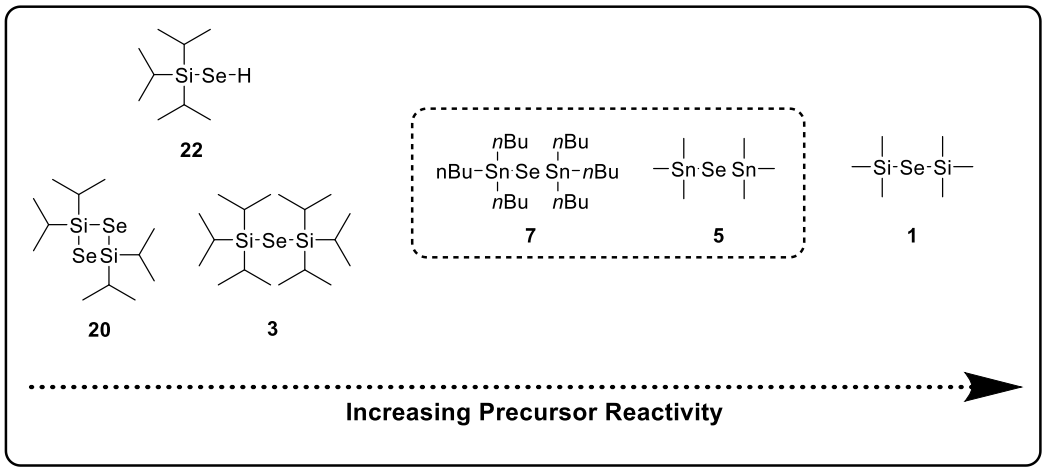

Figure 35. Structure of tested Se-precursors and their relative reactivity.

The initial experiments have shown that reactivity of bis(trimethylsilyl)selenide **1**, a benchmark gALD Se-precursor, is very similar to bis(trimethylstanyl)selenide **5**. Larger bis(tributylstanyl)selenide **7** showed lower growth rate, due to larger and sterically hindered butyls. Selenides **3**, **20**, and **22** afforded none or very poor deposition. This was very surprising, especially for **20** as it was successfully applied in gALD. Although **5** provided slightly larger growth per cycle than **7**, the latter was preferred. The reason is that higher reactivity of **5** caused inhomogeneity during the nucleation and further increasing the number of cycles led to a thickness gradient with thicker film at the side located closer to the solution inlet. Slightly lower reactivity of larger butyl derivate **7** elegantly solved this problem. The saturation behaviour and optimal length of pulse and purge were determined by performing series of experiments using different dosage intervals of precursors and solvent introduction. Si/SiO_2 wafer was used as a substrate. *Figure 36* shows that surface is saturated with pulse around 20 seconds and chamber is purged after 60 seconds. For most of the later experiments 90 seconds long purge was kept to avoid mixing the precursors. The stable, linear growth rate of 0.85 Å/c was achieved with increasing number of cycles, which is a typical feature of ALD growth type.

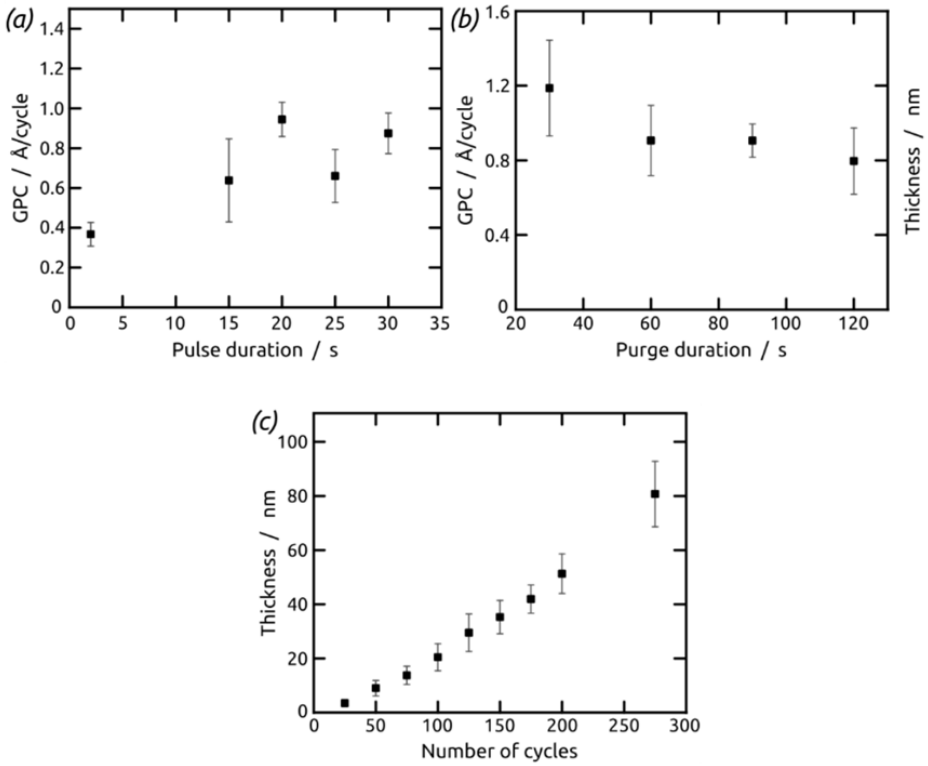

Figure 36. Effect on growth caused by parameter variation. (a) pulse variation (20 cycles, 90 seconds purge), (b) purge variation (20 cycles, 20 seconds pulse). (c) demonstration of linear growth (20 seconds pulse, 90 seconds purge).

Growth characteristics are highly dependent on substrate type. Substrate effect was observed during deposition on various substrates including Si/SiO_2, Si/SiO_2 treated with piranha solution before use (mixture of H_2SO_4 and H_2O_2), TiO_2 (crystalline anatase form), TiO_2 dipped in $ZnCl_2$ solution, amorphous Sb_2S_3, and crystalline Sb_2S_3 (*Figure 37*). The highest growth rate and also good reproducibility were achieved using both types of TiO_2, however *Figure 37b* and *37c* revealed that the difference in growth rates is distinguished only at the initial stage of deposition and stabilize once the whole substrate surface is completely covered. This is further confirmed by SEM images (*Figure 37d* and *e*) showing identical morphology on both substrates.

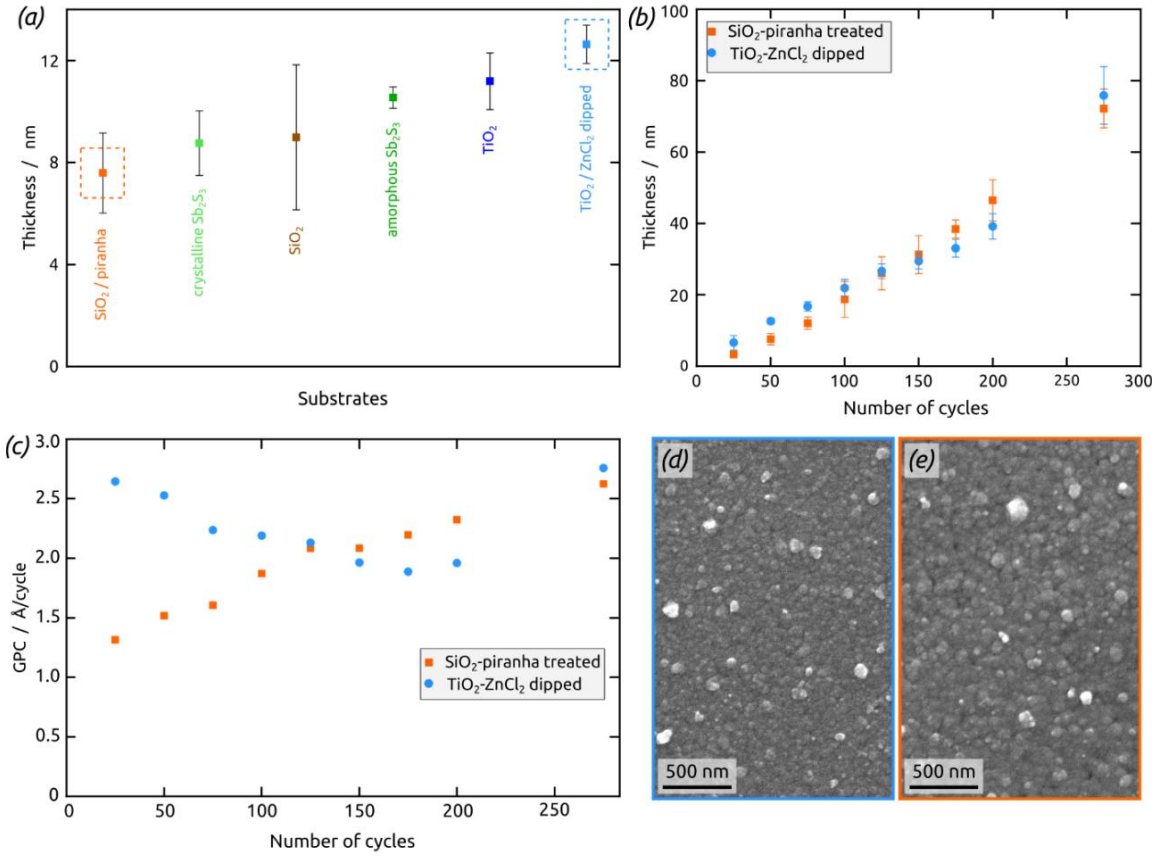

Figure 37. Effect of the substrate to growth characteristics using $SbCl_3$ and **7**. Thickness of films after 50 cycles on six different substrates (a); full growth study on two selected substrates (b and c); scanning electron micrographs of Sb_2Se_3 films obtained after 275 sALD cycles on piranha-cleaned SiO_2 wafer (d) and a $ZnCl_2$-dipped, TiO_2-coated wafer (e).

EDX analysis of layers prepared by reaction of **7** in *Figure 38* revealed chlorine incorporation in as-deposited (amorphous) films. This might be caused by incomplete reaction of precursors or leftovers of $SbCl_3$ stuck in film cavities. Incorporation of tin is not observed. Nevertheless, annealing the sample (300 °C for 5 minutes, N_2 atmosphere) resulted in crystallization of the material and a total removal of residual chlorine impurities.

The composition remains slightly superstoichiometric even after annealing. Interestingly, if **5** was used as selenium source, no chlorine impurities were present.

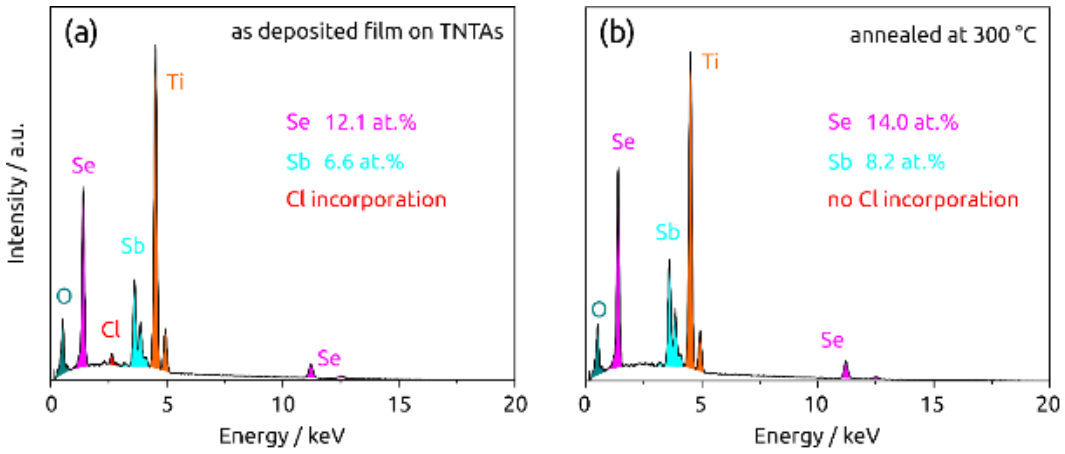

Figure 38. EDX measurements of Sb_2Se_3 prepared using **7** (100 cycles) on TiO_2 nanotubes (TNTAs): (a) as deposited; (b) after annealing (300 °C, 5 min).

The reaction outcome of sALD can be tuned by varying the used solvent. Increasing relative polarity of the solvent (hexane→chlorobenzene→dichloromethane) decreased the nucleation density on the substrate surface. This is clearly visible on both AFM and SEM images shown in *Figure 39*. Hexane seems to be an ideal choice to achieve good uniformity.

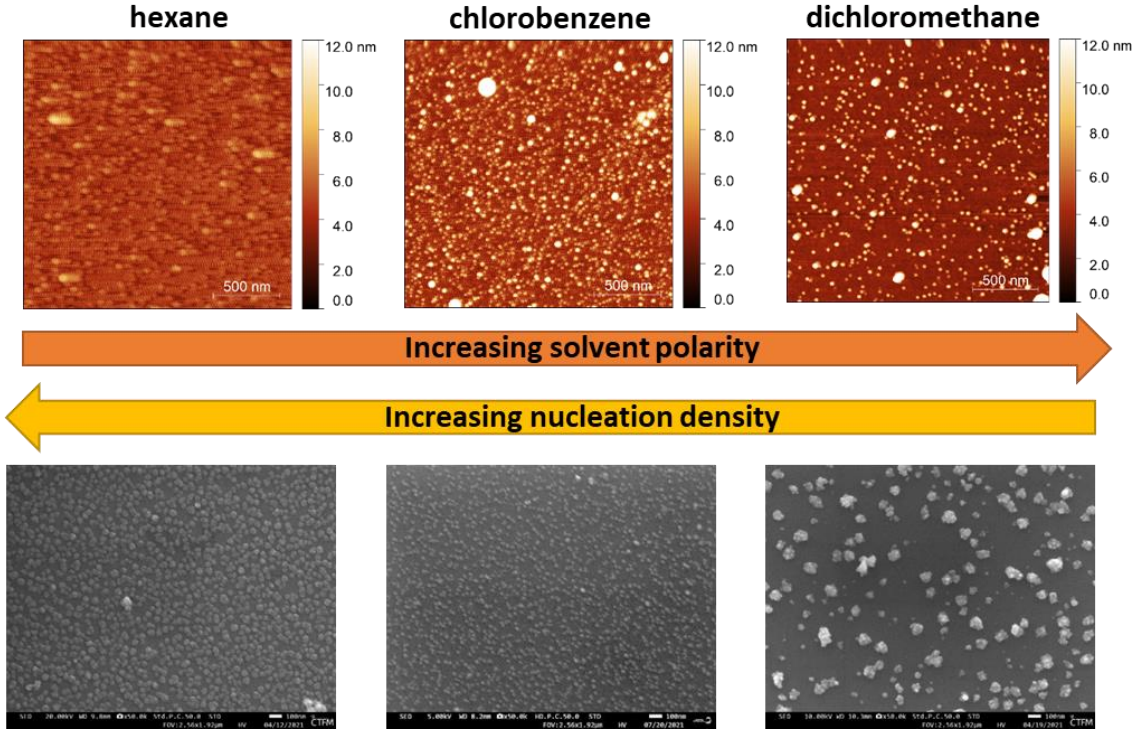

Figure 39. Solvent effect on the nucleation density using $SbCl_3$ and **5**. Top: AFM images of Sb_2Se_3 (5 cycles). Bottom: SEM images of Sb_2Se_3 (50 cycles).

13.6 Upscaling the Sb_2Se_3 sALD deposition

sALD is useful tool for thin films deposition, however, to prove its utility for specific applications, the technique must be able to reach beyond laboratory scale and provide uniform thin layers on large-scale substrates. Hence, a homebuilt sALD setup based on a modified slot-die coater has been used for upscaling the Sb_2Se_3 sALD; see *Figure 40* for its schematic representation and a real photograph. The whole setup was placed under inert conditions in N_2 flow-box. Precursors and solvent were transported via a peristaltic pump and Teflon tubes. The flowrates of two precursor solutions and the purge solvent were set to 1.75 ml/min with precursor concentration 1 mmol/l. Less volatile octane was used as a solvent to prevent evaporation from the substrate, which might cause uneven distribution of liquid. This setup allows to perform deposition on up to 10×10 cm substrates or whole 4-inch silicon wafer. The mobility of printing head also ensures even distribution of precursors, which allows to use more reactive bis(trimethylstanyl)selenide **5** without uniformity loss. $SbCl_3$ was used as a source of antimony.

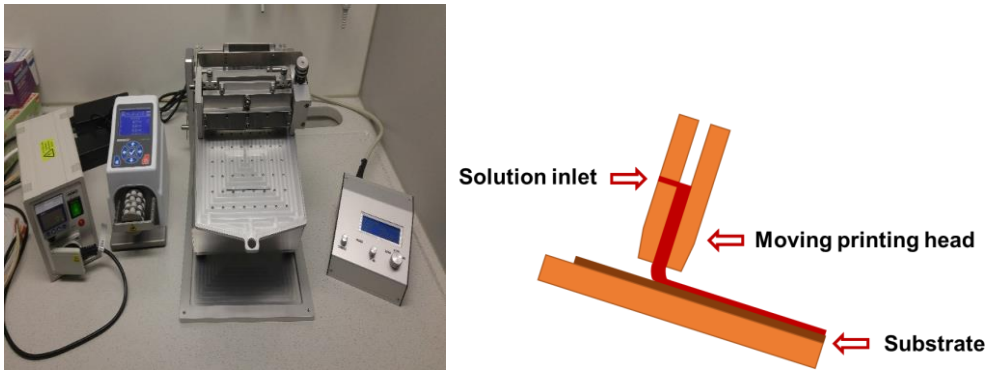

Figure 40. Schematic representation of slot-die type sALD setup printing head (right) and its real photograph (left).

The performed sALD study (*Figure 41*) revealed linear growth with GPC around 1.5 Å per cycle. The best conditions used for the deposition were optimized as 10 seconds pulse with 120 seconds purge. A high growth rate visible in *Figure 41a* indicates that 120 seconds purge was not enough for longer 20 seconds pulse. However, extending the purge to 200

seconds resulted in saturated regime again (see the orange highlighted datapoint).

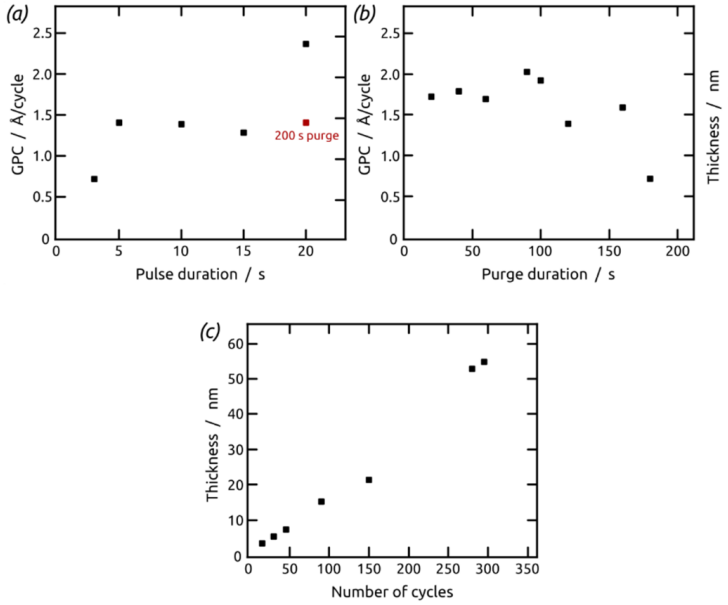

Figure 41. Effect on growth of $SbCl_3$ and **5** in slot-die printer setup caused by parameter variation: (a) pulse variation (50 cycles, 120 seconds purge), (b) purge variation (50 cycles, 10 seconds pulse), (c) demonstration of linear growth (10 seconds pulse, 120 seconds purge).

Detailed characterization of as-grown and annealed Sb_2Se_3 thin films was carried out by means of XRD, SEM, EDX, XPS, and Raman spectroscopy. To investigate the effect of annealing of the films, GI-XRD was performed of as-deposited and annealed Sb_2Se_3 on TiO_2 nanotubes (TNTAs). The amorphous nature of the as-grown material (*Figure 42*, red curve) was confirmed. In contrast, well-defined signals of crystalline orthorhombic Sb_2Se_3 arise after annealing (*Figure 42*, black curve). These characteristics correspond well to the reported pattern (COD 9007437). The signals at 25.4, 38.0, and 48.1° can be attributed to the TiO_2 substrate (anatase-phase, COD 1526931). *Figure 43* shows SEM images of the prepared layers that are relatively rough before annealing, but become smooth after thermal treatment with grains up to 1 µm.

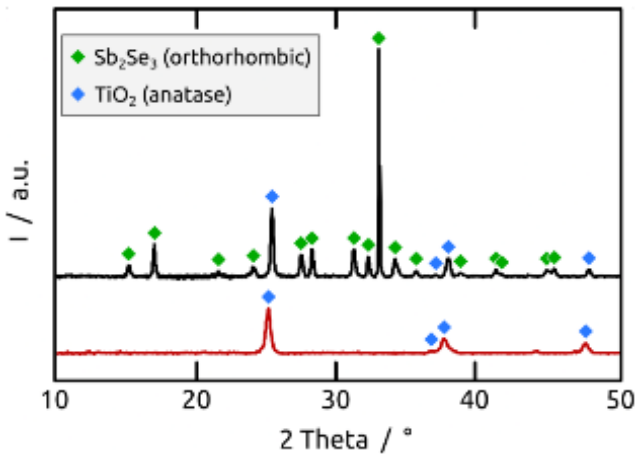

Figure 42. GI-XRD diffractogram of Sb_2Se_3 prepared by 150 sALD cycles on TiO_2 nanotubes before (red curve) and after annealing at 300 °C for 5 min in N_2 atmosphere (black curve).

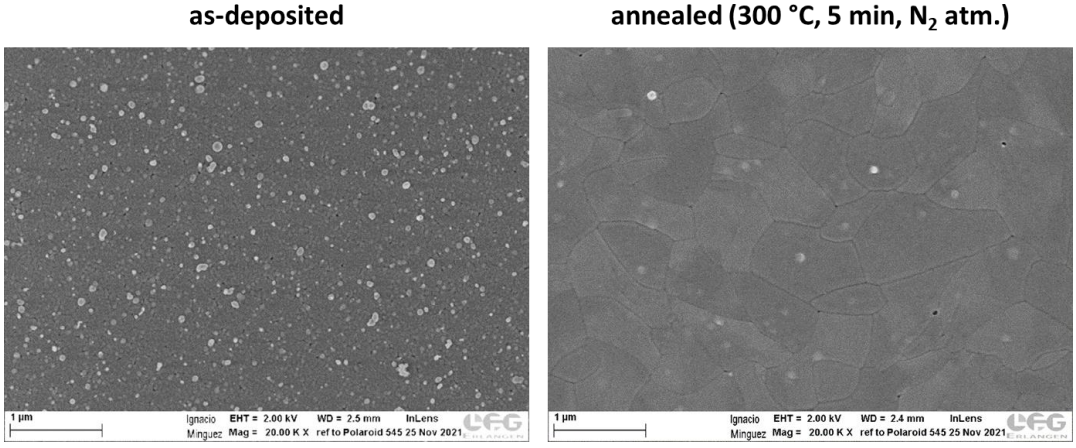

Figure 43. SEM images of Sb_2Se_3 (350 cycles) on Si/SiO_2 wafer before and after annealing.

Sb_2Se_3 deposited on Si substrates (with thin native oxide to avoid electrostatic charging) were further investigated by XPS before and after annealing (300 °C, 5 min, N_2). The signals expected for Sb and Se were found, whereas the absence of Sn and Cl signals proved the purity of the Sb_2Se_3 films (*Figure 44a*). A negligible contribution of oxide-bound Sb is found at 34.1 eV and 35.3 eV, which is attributed to surface oxidation to Sb_2O_3 (*Figure 44b*). This contribution disappears upon annealing (*Figure 44c*). The Sb/Se ratio was determined to be approximately 1, which confirms a Se deficiency in the Sb_2Se_3 films, at least in the high-vacuum conditions under the X-ray beam. In summary, the analyses provided evidence for the sALD growth of films that are affected by superficial oxidation in the amorphous as-grown state, whereas annealing to the crystalline state stabilizes a single-phase antimony selenide state.

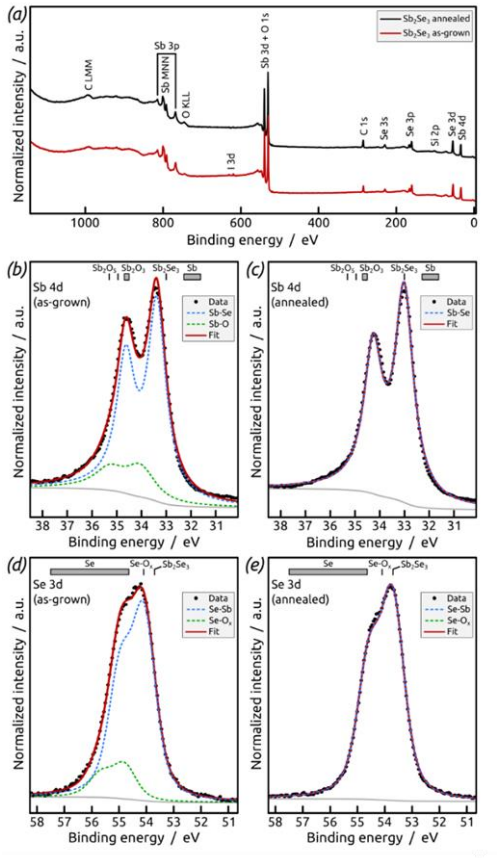

Figure 44. XPS of Sb_2Se_3 on native Si wafer (300 cycles). (a) Survey spectrum, (b) Sb 4d core level spectrum of as-grown Sb_2Se_3, (c) Sb 4d core level spectrum of annealed Sb_2Se_3, (d) Se 3d core level spectrum of as-grown Sb_2Se_3, (e) Se 3d core level spectrum of annealed Sb_2Se_3.

The uniformity of deposited layer was determined by ellipsometry area imaging. For this purpose, silicon wafer of 10 cm diameter (4 inch) was decorated with 80 cycles of Sb_2Se_3 using the same conditions, as mentioned above. The measurement excluded edges of the wafer recording 7 × 7 cm area in total. The mean of obtained thickness corresponds to 11,3 nm (± 0,9 nm). *Figure 45* presents attained results in greater detail. Section *a)* reveals the cut-off and depicts direction of two examined scanning lines, whereas *b)* reveal observed thickness profile. Part *c)* shows thickness graphically. Horizontal thickness is uniform meanwhile slight shift in film thickness is observed in direction of the printing head movement (from top to the bottom).

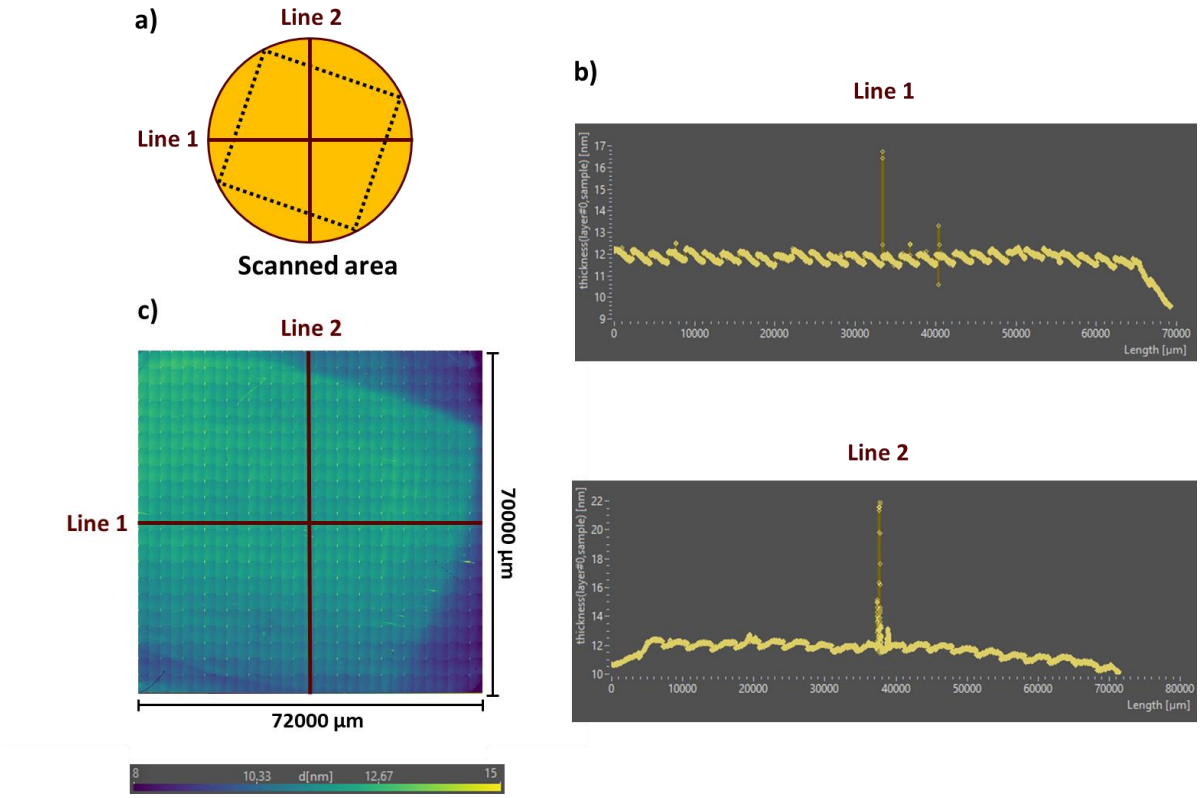

Figure 45. Ellipsometry area imaging of the whole 4-inch wafer scale deposition.

13.7 Deposition of $MoTe_2$ by gALD

The current portfolio of Te-precursors is very narrow, which significantly complicates ALD of metal tellurides. In 2009, bis(trialkylsilyl)tellurides were reported along with their selenium analogues.[69] Nevertheless, these molecules proved to be extremely sensitive to air and light, thus very difficult to prepare and handle. Based on my gained experience with selenides, cyclic silyltelluride **25** was designed and prepared according to *Scheme 21*. This compound was previously reported by Herzog[88] but I intended to use it as Te-precursor and verify its reactivity to produce metal telluride thin films. Higher stability and easier handling were also expected. DSC measurement of **25** (*Figure 45*) revealed crystallization temperature at 114 °C, melting at 153 °C and smooth evaporation around 255 °C, which is surprisingly a bit lower than its selenium analogue **10** (275 °C). The precursor is stable and does not show any decomposition after one month, when stored under argon atmosphere.

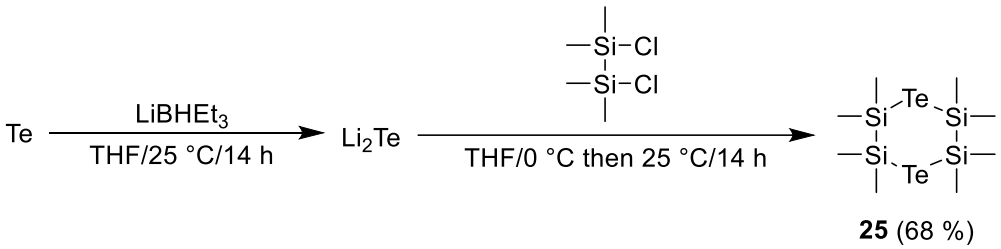

Scheme 21. Preparation of cyclic silyltelluride **25**.

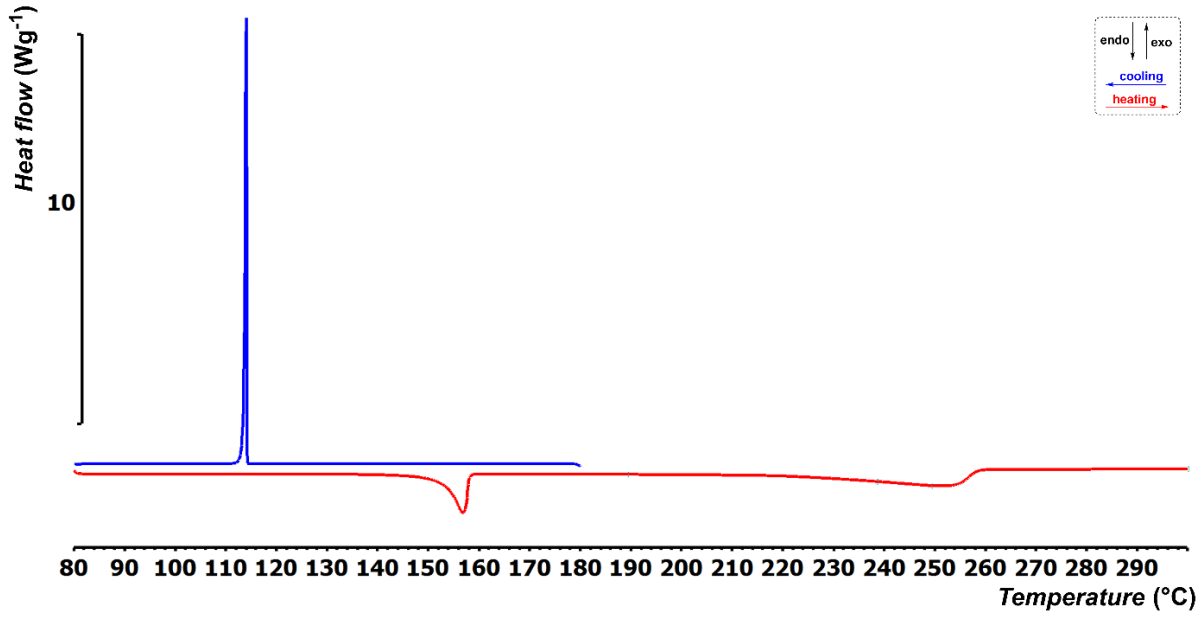

Figure 46. DSC curve of silyltelluride **25**.

The reaction in gALD performed at J. M. Macák research group was carried out in a custom flow-ALD reactor, where **25** reacted with $MoCl_5$ according to the reaction in *Scheme 22*.

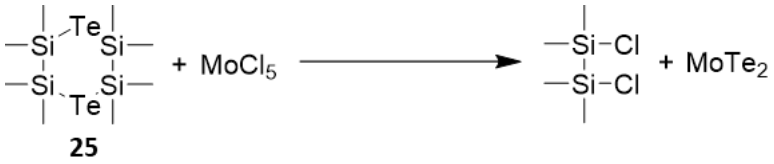

25

Scheme 22. Reaction of $MoCl_5$ with **25** resulting in $MoTe_2$ thin film.

The used substrates included Si/SiO_2 wafer, TiO_2 foils, and TiO_2 nanotubes; the reaction temperature was 270 °C. The growth rate seems to be somewhat lower, thus relatively high temperature for evaporation of **25** (175 °C) was necessary to provide sufficient vapor pressure and high amount of precursor in the chamber. This might be solved by using stopflow-ALD reactor in the future. Nevertheless, $MoTe_2$ was successfully deposited using gALD for the first time and demonstrated good efficiencies for electrocatalysis (HER) and photocatalysis (methylene blue photo-decomposition). $MoTe_2$ typical flaky structure are presented on SEM images shown in *Figure 46*. Detailed analyses and aforementioned catalytic performances were published.[143]

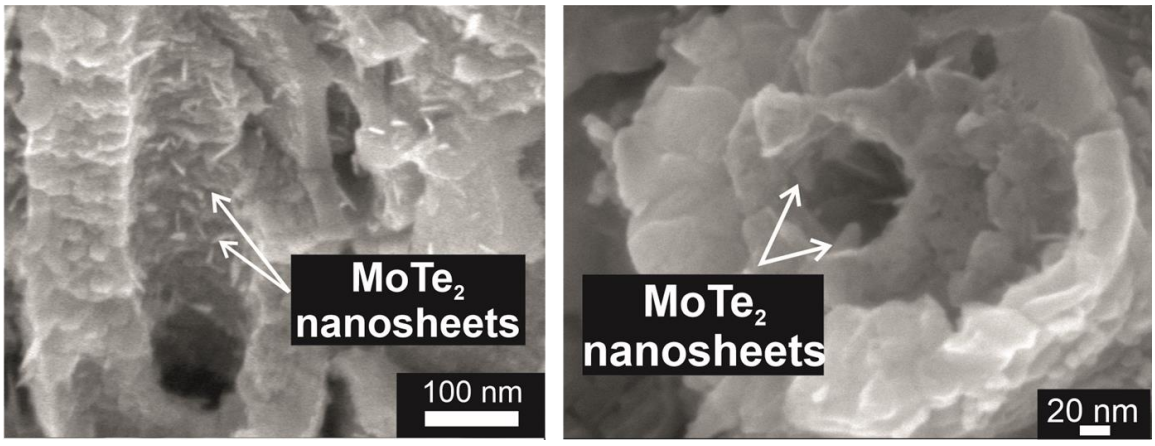

Figure 47. SEM image of $MoTe_2$ prepared in gALD using $MoCl_5$ and **25** on TiO_2 nanotubes (1500 cycles).

14 Conclusion

The dissertation focuses on organoselenium compounds and their modern applications, especially in thin film preparation by Atomic Layer Deposition. Its mechanism, characteristics, and challenges were discussed. A selection of the right ALD precursor is crucial for the successful deposition, thus an idealized precursor has been defined. Literature research aiming to review the existing and possible selenium precursors for ALD has been performed. The later section of the theoretical part is devoted to solution-based deposition methods and utilization of prepared selenide thin films.

The experimental part demonstrates synthesis of cyclic silyl-selenides as a potential ALD precursor. The structure-property tuning is directed towards organoselenium molecules with sufficient reactivity, volatility, thermal stability, and improved air-stability; a trade-off between these properties was targeted. Compounds **15** and **20** were prepared via a newly developed reaction pathway. Reported synthesis of silyl-selenoles exploiting trialkylsilanes was modified. By this way, two silyl-selenides **2** and **24** and tri*iso*propylsilyl-selenol **22** were obtained. Precursor **22** was characterized for the first time, while it offers interesting application in ALD due to its high volatility and economical synthesis. Another modification was proposed for stannyl-selenides, where the developed reaction pathway allows to prepare bis(trialkylstanyl)selenides from readily available, air-stable, and inexpensive starting materials in near to quantitative yields.

All of the prepared materials were analysed by GC/MS and heteronuclear NMR. The basic thermal behaviour was studied using DSC and TG analyses. It was shown that molecules **15** and **24** possess boiling points over 300 °C, which is considered as too high. The remaining molecules are considered volatile enough to be used in the standard ALD reactor. Thermal stability of asymmetric compounds **22** and **23** is limited, because of self-reaction forming two symmetric products.

Testing of the selected selenides **9**, **10**, **19** and **20** in gALD revealed rather lower reactivity of **9** and **19**, while **10** and **20** are good candidates for preparation of $MoSe_2$ thin layers. Bis(trialkylstanyl)selenides **5** and **6** were successfully utilized in sALD for Sb_2Se_3 deposition by the reaction with $SbCl_3$. An ALD study revealing suitable conditions was performed and a typical linear growth was achieved. The differences caused by the effect of various substrates and solvents were addressed. Using optimized conditions, the deposition process was up-scaled allowing Sb_2Se_3 deposition on 10×10 cm silicon wafer with satisfying uniformity. Properties and composition of the manufactured thin layers were studied and confirmed by ellipsometry, SEM, AFM, EDX, XPS, and XRD. In addition, my further synthetic attempts resulted in preparation of cyclic silyl-telluride **25**, which was characterized

and successfully used in gALD. Its reaction with $MoCl_5$ led to deposition of $MoTe_2$, reported for the first time by gALD.

Research outcomes achieved within my dissertation, including spectral data of all prepared target molecules were published in the following articles:

Charvot J., Pokorný D., Zazpe R., Krumpolec R., Pavliňák D., Hromádko L., Přikryl J., Rodriguez-Pereira J., Klikar M., Jelínková V., Macák J. M., Bureš F. *ChemPlusChem* **2020**, 85, 576-579. (Cyclic Silylselenides: Convenient Selenium Precursors for Atomic Layer Deposition).

Charvot J., Pokorný D., Klikar M., Jelínková V., Bureš F. *Molecules* **2020**, 25, 5212. (Towards Volatile Organoselenium Compounds with Cost-Effective Synthesis).

Charvot J., Zazpe R., Macák J. M., Bureš F. *ACS Omega* **2021**, 6, 6554-6558 (Organoselenium Precursors for Atomic Layer Deposition).

Charvot J., Zazpe R., Krumpolec R., Rodriguez-Pereira J., Pavliňák D., Pokorný D., Klikar M., Jelínková V., Macák J. M., Bureš F. *RSC Adv.* **2021**, 11, 22140-22147. (Deposition of $MoSe_2$ flakes using cyclic selenides).

Zazpe R., Sopha H., Charvot J., Krumpolec R., Rodriguez-Pereira J., Michalička J., Mistrík J., Bača D., Motola M., Bureš F., Macák J. M. *Appl. Mater. Today* **2021**, 23, 101017. (2D $MoTe_2$ Nanosheets by Atomic Layer Deposition: Excellent Photo- Electrocatalytic Properties).

I have also significantly participated on the following publications:

Rodriguez-Pereira J., Zazpe R., Charvot J., Bureš F., Macak J. M. *Surf. Sci. Spectra* **2020**, 27, 024006. (Molybdenum Diselenide Thin Films Grown by Atomic Layer Deposition: An XPS Analysis).

Zazpe R., Krumpolec R., Sopha H., Rodriguez-Pereira J., Charvot J., Hromádko L., Kolíbalová E., Michalička, Pavliňák D., Motola M., Přikryl J., Krbal M., Bureš F., Macak J. M. *ACS Appl. Nano Mater.* **2020**, 3, 12034-12045. (Atomic Layer Deposition of $MoSe_2$ Nanosheets on TiO_2 Nanotube Arrays for Photocatalytic Dye Degradation and Electrocatalytic Hydrogen Evolution).

Zazpe R., Charvot J., Krumpolec R., Hromádko L., Pavliňák D., Dvorak D., Knotek P., Michalicka J., Přikryl J., S. Ng, Jelínková V., Bureš F., Macák J. M., *FlatChem* **2020**, 21, 100166. (Atomic Layer Deposition of $MoSe_2$ Using New Selenium Precursors).

15 References

[1] O. Pierson, Hugh, *Handbook of Chemical Vapor Deposition (CVD), Principles, Technology, and Applications.*, Noyes Publications, New Jersey, **1992**.

[2] L. Sun, G. Yuan, L. Gao, J. Yang, M. Chhowalla, H. Gharahcheshmeh, Meysam, K. Gleason, Karen, S. Choi, Yong, H. Hong, Byung, Z. Liu, *Nat Rev Methods Primers.* **2021**, *1*, 5.

[3] H. Liu, D. S. Dandy, *Diamond Chemical Vapor Deposition: Nucleation and Early Growth Stages*, Noyes Publications, Colorado, USA, **1995**.

[4] R. L. Puurunen, *Chem. Vap. Depos.* **2014**, *20*, 332–344.

[5] M. Ritala, J. Niinistö, *ECS Trans.* **2009**, *25*, 641–652.

[6] H. C. M. Knoops, T. Faraz, K. Arts, W. M. M. Kessels, *J. Vac. Sci. Technol. A* **2019**, *37*, 030902.

[7] S. M. George, *Chem. Rev.* **2009**, *110*, 111–131.

[8] J. Vos, M, F, A. J. M. Mackus, W. M. M. Kessels, "Atomic layer deposition process development," DOI DOI: 10.6100/alddatabasecan be found under https://www.atomiclimits.com/2019/02/12/atomic-layer-deposition-process-development-10-steps-to-successfully-develop-optimize-and-characterize-ald-recipes/, **2019**.

[9] J. Bachmann, *Atomic Layer Deposition in Energy Conversion Applications*, Wiley-VCH Verlag GmbH & Co. KGaA, Weinheim, Germany, **2017**.

[10] A. Rautiainen, M. Lindblad, L. B. Backman, R. L. Puurunen, *Phys. Chem. Chem. Phys.* **2002**, *4*, 2466–2472.

[11] H. Kim, S. M. Rossnagel, *J. Vac. Sci. Technol. A Vacuum, Surfaces, Film.* **2002**, *20*, 802–808.

[12] N. E. Richey, C. De Paula, S. F. Bent, *J. Chem. Phys.* **2020**, *152*, 040902.

[13] R. L. Puurunen, W. Vandervorst, *J. Appl. Phys.* **2004**, *96*, 7686–7695.

[14] K. E. Elers, T. Blomberg, M. Peussa, B. Aitchison, S. Haukka, S. Marcus, *Chem. Vap. Depos.* **2006**, *12*, 13–24.

[15] N. Pinna, M. Knez, *Atomic Layer Deposition of Nanostructured Materials*, Wiley-VCH Verlag GmbH & Co. KGaA, Weinheim, Germany, **2012**.

[16] K. Arts, H. Thepass, M. A. Verheijen, R. L. Puurunen, W. M. M. Kessels, H. C. M. Knoops, *Chem. Mater.* **2021**, *33*, 5002–5009.

[17] R. Zazpe, R. Krumpolec, H. Sopha, J. Rodriguez-Pereira, J. Charvot, L. Hromádko, E. Kolíbalová, J. Michalička, D. Pavliňák, M. Motola, J. Přikryl, M. Krbal, F. Bureš, J. M. Macak, *ACS Appl. Nano Mater.* **2020**, *3*, 12034–12045.

[18] A. J. M. Mackus, M. J. M. Merkx, W. M. M. Kessels, *Chem. Mater.* **2019**, *31*, 2–12.

[19] S. E. Atanasov, B. Kalanyan, G. N. Parsons, *J. Vac. Sci. Technol. A Vacuum, Surfaces, Film.* **2016**, *34*, 01A148.

[20] J. Kwon, M. Saly, M. D. Halls, R. K. Kanjolia, Y. J. Chabal, *Chem. Mater.* **2012**, *24*, 1025–1030.

[21] S. McDonnell, R. C. Longo, O. Seitz, J. B. Ballard, G. Mordi, D. Dick, J. H. G. Owen, J. N. Randall, J. Kim, Y. J. Chabal, K. Cho, R. M. Wallace, *J. Phys. Chem. C* **2013**, *117*, 20250–20259.

[22] M. J. M. Merkx, S. Vlaanderen, T. Faraz, M. A. Verheijen, W. M. M. Kessels, A. J. M. MacKus, *Chem. Mater.* **2020**, *32*, 7788–7795.

[23] P. O. Oviroh, R. Akbarzadeh, D. Pan, R. A. M. Coetzee, T. C. Jen, *Sci. Technol. Adv. Mater.* **2019**, *20*, 465–496.

[24] J. V. Sci, S. T. Barry, J. Sundqvist, *J. Vac. Sci. Technol. A* **2021**, *39*, 051001.

[25] S. M. George, B. Yoon, A. A. Dameron, *Acc. Chem. Res.* **2009**, *42*, 498–508.

[26] S. Yoo, C. Yoo, E. S. Park, W. Kim, Y. K. Lee, C. S. Hwang, *J. Mater. Chem. C* **2018**, *6*, 5025–5032.

[27] K. Zhang, A. D. R. Pillai, K. Bollenbach, D. Nminibapiel, W. Cao, H. Baumgart, T. Scherer, V. S. K. Chakravadhanula, C. Kübel, V. Kochergin, *ECS J. Solid State Sci. Technol.* **2014**, *3*, 207–212.

[28] J. Hämäläinen, M. Ritala, M. Leskelä, *Chem. Mater.* **2014**, *26*, 786–801.

[29] T. S. Tripathi, J. Lahtinen, M. Karppinen, *Adv. Mater. Interfaces* **2018**, 5, 1701366.

[30] S. ichi Ohta, S. Kobayashi, F. Kaneko, K. ichi Kashiro, *J. Cryst. Growth* **1990**, *106*, 166–174.

[31] W. Faschinger, P. Juza, S. Ferreira, H. Zajicek, A. Pesek, H. Sitter, K. Lischka, *Thin Solid Films* **1993**, *225*, 270–274.

[32] T. Yao, T. Takeda, *Appl. Phys. Lett.* **1986**, *48*, 160.

[33] E. Kurtz, H. D. Jung, T. Hanada, Z. Zhu, T. Sekiguchi, T. Yao, *J. Cryst. Growth* **1998**, *184/185*, 242–247.

[34] J. Ihanus, E. Lambers, P. H. Holloway, M. Ritala, M. Leskelä, *J. Cryst. Growth* **2004**, *260*, 440–446.

[35] Y. K. Ezhovskii, *Russ. J. Phys. Chem* **2014**, *88*, 1580–1584.

[36] M. Ahonen, M. Pessa, T. Suntola, *Thin Solid Films* **1980**, *65*, 301–307.

[37] Y. Cao, T. Wähler, H. Park, J. Will, A. Prihoda, N. Moses Badlyan, L. Fromm, T. Yokosawa, B. Wang, D. M. Guldi, A. Görling, J. Maultzsch, T. Unruh, E. Spiecker, M. Halik, J. Libuda, J. Bachmann, *Adv. Mater. Interfaces* **2020**, *7*, 2001493.

[38] R. Browning, N. Kuperman, R. Solanki, V. Kanzyuba, S. Rouvimov, *Semicond. Sci. Technol.* **2016**, *31*, 095002.

[39] H. Kim, *J. Vac. Sci. Technol. B Microelectron. Nanom. Struct.* **2003**, *21*, 2231.

[40] R. L. Puurunen, *J. Appl. Phys.* **2005**, *97*, 121301.

[41] H. Salami, A. Uy, A. Vadapalli, C. Grob, V. Dwivedi, R. A. Adomaitis, *J. Vac. Sci. Technol. A* **2019**, *37*, 010905.

[42] A. V. Uvarov, A. S. Gudovskikh, V. N. Nevedomskiy, A. I. Baranov, D. A. Kudryashov, I. A. Morozov, J. P. Kleider, *J. Phys. D Appl. Phys.* **2020**, *53*, 345105.

[43] B. B. Burton, D. N. Goldstein, S. M. George, *J. Phys. Chem. C* **2009**, *113*, 1939–1946.

[44] J. Bachmann, J. Escrig, K. Pitzschel, J. M. M. Moreno, J. Jing, D. Görlitz, D. Altbir, K. Nielsch, *J. Appl. Phys.* **2009**, *105*, 07B521.

[45] E. Dashjav, M. Lipińska-Chwałek, D. Grüner, G. Mauer, M. Luysberg, F. Tietz, *Surf. Coatings Technol.* **2016**, *307*, 428–435.

[46] J. P. Niemelä, G. Marin, M. Karppinen, *Semicond. Sci. Technol.* **2017**, *32*, 093005.

[47] H. H. Sønsteby, J. E. Bratvold, V. A.-L. K. Killi, D. Choudhury, J. W. Elam, H. Fjellvåg, O. Nilsen, *J. Vac. Sci. Technol. A* **2020**, *38*, 060804.

[48] M. Utriainen, M. Kröger-Laukkanen, L. S. Johansson, L. Niinistö, *Appl. Surf. Sci.* **2000**, *157*, 151–158.

[49] T. S. Tripathi, C. S. Yadav, M. Karppinen, *APL Mater.* **2016**, *4*, 046106.

[50] K. B. Klepper, O. Nilsen, H. Fjellvåg, *Thin Solid Films* **2007**, *515*, 7772–7781.

[51] J. J. Senkevich, F. Tang, D. Rogers, J. T. Drotar, C. Jezewski, W. A. Lanford, G. C. Wang, T. M. Lu, *Chem. Vap. Depos.* **2003**, *9*, 5.

[52] Z. Golrokhi, P. A. Marshall, S. Romani, S. Rushworth, P. R. Chalker, R. J. Potter, *Appl. Surf. Sci.* **2017**, *399*, 123–131.

[53] D. M. Hausmann, E. Kim, J. Becker, R. G. Gordon, *Chem. Mater.* **2002**, *14*, 4350–4358.

[54] K. H. Kim, D. B. Farmer, J. S. M. Lehn, P. Venkateswara Rao, R. G. Gordon, *Appl. Phys. Lett.* **2006**, *89*, 133512.

[55] K. Kukli, J. Niinistö, A. Tamm, M. Ritala, M. Leskelä, *J. Vac. Sci. Technol. B Microelectron. Nanom. Struct.* **2009**, *27*, 226.

[56] M. Mäkelä, T. Hatanpää, K. Mizohata, K. Meinander, J. Niinistö, J. Räisänen, M. Ritala, M. Leskelä, *Chem. Mater.* **2017**, *29*, 2040–2045.

[57] M. B. E. Griffiths, D. Zanders, M. A. Land, J. D. Masuda, A. Devi, S. T. Barry, *J. Vac. Sci. Technol. A* **2021**, *39*, 032409.

[58] J. Charvot, R. Zazpe, J. M. Macak, F. Bureš, *ACS Omega* **2021**, *6*, 6554–6558.

[59] Z. Guo, R. Zhao, S. Yan, W. Xiong, J. Zhu, K. Lu, X. Wang, *Chem. Mater.* **2021**, *33*, 2478–2487.

[60] W. S. Rees, D. M. Green, T. J. Anderson, E. Bretschneider, *Mater. Res. Soc. Symp. Proc.* **1992**, *242*, 281–286.

[61] C. D. Lee, B. H. Lim, C. Lim, H. L. Park, C. H. Chung, S. K. Chang, *J. Cryst. Growth* **1992**, *117*, 148–151.

[62] A. Yoshikawa, M. Kobayashi, S. Tokita, *Phys. Status Solidi* **1994**, *82/83*, 316–321.

[63] R. Browning, N. Kuperman, B. Moon, R. Solanki, *Electronics* **2017**, *6*, 27.

[64] V. E. Drozd, I. O. Nikiforova, V. B. Bogevolnov, A. M. Yafyasov, E. O. Filatova, D. Papazoglou, *J. Phys. D. Appl. Phys.* **2009**, *42*, 125306.

[65] N. D. Boscher, C. J. Carmalt, I. P. Parkin, *J. Mater. Chem.* **2006**, *16*, 122–127.

[66] N. D. Boscher, C. J. Carmalt, R. G. Palgrave, J. J. Gil-Tomas, I. P. Parkin, *Chem. Vap. Depos.* **2006**, *12*, 692–698.

[67] Y. Noda, T. Ishikawa, M. Yamabe, Y. Hara, *Appl. Surf. Sci.* **1997**, *113/114*, 28–32.

[68] H. Fujiwara, H. Kiryu, I. Shimizu, *J. Appl. Phys.* **1995**, *77*, 3927–3933.

[69] V. Pore, T. Hatanpää, M. Ritala, M. Leskelä, *J. Am. Chem. Soc.* **2009**, *131*, 3478–3480.

[70] S. Ng, M. Krbal, R. Zazpe, J. Prikryl, J. Charvot, F. Dvořák, L. Strizik, S. Slang, H. Sopha, Y. Kosto, V. Matolin, F. K. Yam, F. Bures, J. M. Macak, *Adv. Mater. Interfaces* **2017**, 1701146.

[71] J. H. Jeong, D. J. Choi, *Mater. Sci. Semicond. Process.* **2016**, *54*, 42–50.

[72] T. Sarnet, T. Hatanpää, M. Vehkamäki, T. Flyktman, J. Ahopelto, K. Mizohata, M. Ritala, M. Leskelä, *J. Mater. Chem. C* **2015**, *3*, 4820–4828.

[73] K. Lee, S. Lee, *Nanotechnology* **2021**, *32*, 245202.

[74] C. Yoo, W. Kim, J. W. Jeon, E. S. Park, M. Ha, Y. K. Lee, C. S. Hwang, *ACS Appl. Mater. Interfaces* **2020**, *12*, 23110–23118.

[75] W. Kim, S. Yoo, C. Yoo, E. Park, J. Jeon, Y. J. Kwon, K. S. Woo, H. J. Kim, Y. K. Lee, C. S. Hwang, *Nanotechnology* **2018**, *29*, 365202.

[76] M. Krbal, J. Prikryl, R. Zazpe, F. Dvorak, F. Bures, J. M. Macak, *Phys. Status Solidi - Rapid Res. Lett.* **2018**, *12*, 1800023.

[77] R. Zazpe, J. Charvot, R. Krumpolec, L. Hromádko, D. Pavliňák, F. Dvorak, P. Knotek, J. Michalicka, J. Přikryl, S. Ng, V. Jelínková, F. Bureš, J. M. Macak, *FlatChem* **2020**, *21*, 100166.

[78] J. Charvot, Organic Selenium Compounds as Precursors for Atomic Layers Deposition, Diploma thesis, University of Pardubice, **2018**.

[79] T. Hantapää, V. Pore, M. Ritala, M. Leskelä, *Electrochem. Soc.* **2009**, *25*, 609–616.

[80] L. Syper, J. Mlochowski, *Tetrahedron* **1988**, *44*, 6119–6130.

[81] J. A. Gladysz, J. L. Hornby, J. E. Garbe, *J. Org. Chem.* **1978**, *43*, 1204–1208.

[82] M. R. Detty, M. D. Seidler, *J. Org. Chem.* **1982**, *47*, 1354–1356.

[83] J. E. Drake, B. M. Glavinčevski, R. T. Hemmings, *Can. J. Chem.* **1980**, *58*, 2161–2166.

[84] L. Han, F. Mirzaei, M. Tanaka, *Organometallics* **2000**, *3*, 722–724.

[85] S. Vyzanakin, N, N. Bocharkev, M, P. Sanina, L, *J. Gen. Chem. USSR* **1966**, *36*, 175.

[86] N. Mahuli, D. Halder, A. Paul, S. K. Sarkar, *Chem. Mater.* **2019**, *31*, 7434–7442.

[87] C. Li, L. Zhu, P. Tong, X. Zeng, *Method for Preparing Selenium Dimethyl*

Dithiocarbamate as Rubber Vulcanization Accelerator, **2016**, CN 105367468 A.

[88] U. Herzog, G. Rheinwald, *J. Organomet. Chem.* **2001**, *627*, 23–36.

[89] U. Herzog, U. Böhme, *Silicon Chem.* **2003**, *2*, 77–92.

[90] D. P. Thompson, P. Boudjouk, *J. Chem. Soc. Chem. Commun.* **1987**, *19*, 1466–1497.

[91] M. Weidenbruch, L. Kirmaier, E. Kroke, W. Saak, *Zeitschrift fur Anorg. und Allg. Chemie* **1997**, *623*, 1277–1280.

[92] T. I. Kuckmann, M. Hermsen, M. Bolte, M. Wagner, H.-W. Lerner, *Inorg. Chem.* **2005**, *44*, 3449–3458.

[93] S. Vyzanakin, N, N. Bochkarov, M, J. Sanina, *J. Gen. Chem. USSR* **1968**, *38*, 410.

[94] K. Grenader, B. Schüpbach, A. Peters, O. Kümmel, O. Halter, A. Terfort, *Adv. Synth. Catal.* **2012**, *354*, 2653–2658.

[95] J. E. Greene, *Appl. Phys. Rev.* **2014**, *1*, 041302.

[96] O. Graniel, J. Puigmartí-Luis, D. Muñoz-Rojas, *Dalt. Trans.* **2021**, *50*, 6373–6381.

[97] P. K. Nair, M. T. S. Nair, V. M. García, O. L. Arenas, Y. Peña, A. Castillo, I. T. Ayala, O. Gomezdaza, A. Sánchez, J. Campos, H. Hu, R. Suárez, M. E. Rincón, *Sol. Energy Mater. Sol. Cells* **1998**, *52*, 313–344.

[98] C. D. Lokhande, *Mater. Chem. Phys.* **1991**, *27*, 1–43.

[99] M. T. S. Nair, P. K. Nair, H. M. K. K. Pathirana, R. A. Zingaro, E. A. Meyers, *J. Electrochem. Soc.* **1993**, *140*, 2987–2994.

[100] Y. F. Nicolau, *Appl. Surf. Sci.* **1985**, *22/23*, 1061–1074.

[101] M. Pathan, H, D. Lockhande, C, *Bull. Mater. Sci.* **2004**, *27*, 85–111.

[102] S. P. Ratnayake, J. Ren, E. Colusso, M. Guglielmi, A. Martucci, E. Della Gaspera, *Small* **2021**, *2101666*,

[103] Y. Wu, D. Döhler, M. Barr, E. Oks, M. Wolf, L. Santinacci, J. Bachmann, *Nano Lett.* **2015**, *15*, 6379–6385.

[104] I. Kundrata, K. Fröhlich, L. Vančo, M. Mičušík, J. Bachmann, *Beilstein J. Nanotechnol.* **2019**, *10*, 1443–1451.

[105] V. M. Koch, M. K. S. Barr, P. Büttner, I. Mínguez-Bacho, D. Döhler, B. Winzer, E. Reinhardt, D. Segets, J. Bachmann, *J. Mater. Chem. A* **2019**, *7*, 25112.

[106] Y. Cao, S. Zhu, J. Bachmann, *Dalt. Trans.* **2021**, *50*, 13066–13072.

[107] M. Mattinen, M. Leskelä, M. Ritala, *Adv. Mater. Interfaces* **2021**, *8*, 2001677.

[108] J. Cai, X. Han, X. Wang, X. Meng, *Matter* **2020**, *2*, 587–630.

[109] G. H. Park, K. Nielsch, A. Thomas, *Adv. Mater. Interfaces* **2019**, *6*, 1800688.

[110] K. Thakar, S. Lodha, *Mater. Res. Express* **2019**, *7*, 014002.

[111] Q. Fu, J. Han, X. Wang, P. Xu, T. Yao, J. Zhong, W. Zhong, S. Liu, T. Gao, Z. Zhang, L. Xu, B. Song, *Adv. Mater.* **2020**, 1907818.

[112] C. K. Sumesh, S. C. Peter, *Dalt. Trans.* **2019**, *48*, 12772.

[113] U. Gupta, C. N. R. Rao, *Nano Energy* **2017**, *41*, 49–65.

[114] Y. Yin, Y. Zhang, T. Gao, T. Yao, X. Zhang, J. Han, X. Wang, Z. Zhang, P. Xu, P. Zhang, X. Cao, B. Song, S. Jin, *Adv. Mater.* **2017**, 1700311.

[115] X. Zhang, S. Y. Teng, A. C. M. Loy, B. S. How, W. D. Leong, X. Tao, *Nanomaterials* **2020**, *10*, 1012.

[116] J. Cavin, A. Ahmadiparidari, L. Majidi, A. S. Thind, S. N. Misal, A. Prajapati, Z. Hemmat, S. Rastegar, A. Beukelman, M. R. Singh, K. A. Unocic, A. Salehi-Khojin, R. Mishra, *Adv. Mater.* **2021**, *33*, 2100347.

[117] T. K. Todorov, S. Singh, D. M. Bishop, O. Gunawan, Y. S. Lee, T. S. Gershon, K. W. Brew, P. D. Antunez, R. Haight, *Nat. Commun.* **2017**, *8*, 682.

[118] M. Tao, H. Hamada, T. Druffel, J.-J. Lee, K. Rajeshwar, *ECS J. Solid State Sci. Technol.* **2020**, *9*, 125010.

[119] A. Zakutayev, J. D. Major, X. Hao, A. Walsh, J. Tang, T. K. Todorov, L. H. Wong, E. Saucedo, *J. Phys. Energy 3* **2021**, *3*, 032003.

[120] K. Zeng, D. J. Xue, J. Tang, *Semicond. Sci. Technol.* **2016**, *31*, 063001.

[121] Z. Li, X. Liang, G. Li, H. Liu, H. Zhang, J. Guo, J. Chen, K. Shen, X. San, W. Yu, R. E. I. Schropp, Y. Mai, *Nat. Commun.* **2019**, *10*, 125.

[122] I. Gharibshahian, A. A. Orouji, S. Sharbati, *Sol. Energy Mater. Sol. Cells* **2020**, *212*, 110581.

[123] K. Brazier, “A thermoelectric circuit composed of materials of different Seebeck coefficient (p-doped and n-doped semiconductors), configured as a thermoelectric generator.,” can be found under https://commons.wikimedia.org/wiki/File:Thermoelectric_Generator_Diagram.svg, **2008**.

[124] R. Freer, A. V. Powell, *J. Mater. Chem. C* **2020**, *8*, 441.

[125] S. Twaha, J. Zhu, Y. Yan, B. Li, *Renew. Sustain. Energy Rev.* **2016**, *65*, 698–726.

[126] T. R. Wei, C. F. Wu, F. Li, J. F. Li, *J. Mater.* **2018**, *4*, 304–320.

[127] C. de Mello Donegá, *Chem. Soc. Rev.* **2011**, *40*, 1512–1546.

[128] H. Zhong, T. Mirkovic, G. D. Scholes, in *Compr. Nanosci. Technol.*, Elsevier Inc., **2010**, pp. 153–201.

[129] C. B. Murray, D. J. Norris, M. G. Bawendi, *J. Am. Chem. Soc.* **1993**, *115*, 8706–8715.

[130] A. N. Beecher, X. Yang, J. H. Palmer, A. L. Lagrassa, P. Juhas, S. J. L. Billinge, J. S. Owen, *J. Am. Chem. Soc.* **2014**, *136*, 10645–10653.

[131] N. Revaprasadu, M. A. Malik, P. O’Brien, M. M. Zulu, G. Wakefield, *J. Mater. Chem.* **1998**, *8*, 1885–1888.

[132] N. Revaprasadu, M. Azad Malik, J. Carstens, P. O’Brien, *J. Mater. Chem.* **1999**, *9*, 2885–2888.

[133] S. Razzaque, M. D. Khan, M. Aamir, M. Sohail, S. Bhoyate, R. K. Gupta, M. Sher, J. Akhtar, N. Revaprasadu, *Inorg. Chem.* **2021**, *60*, 1449–1461.

[134] W. Bryks, S. C. Smith, A. R. Tao, *Chem. Mater.* **2017**, *29*, 3653–3662.

[135] Y. Liu, H. Y. Zhang, L. X. Chen, X. W. He, *J. Chem. Res. - Part S* **2000**, 216–217.

[136] Y. Liu, H. Y. Zhang, *Chinese J. Chem.* **2000**, *18*, 66–68.

[137] O.-J. Jung, *J. Korean Enviromental Sci. Soc.* **1996**, *2*, 211–220.

[138] T. Chatterjee, V. S. Shetti, R. Sharma, M. Ravikanth, *Chem. Rev.* **2017**, *117*, 3254–3328.

[139] T. Shimizu, M. Kawaguchi, T. Tsuchiya, K. Hirabayashi, N. Kamigata, *J. Org. Chem.* **2005**, *70*, 5036–5044.

[140] S. K. Pushpan, S. Venkatraman, V. G. Anand, J. Sankar, H. Rath, T. K. Chandrashekar, *Proc. Indian Acad. Sci. Chem. Sci.* **2002**, *114*, 311–338.

[141] J. Charvot, D. Pokorný, R. Zazpe, R. Krumpolec, D. Pavliňák, L. Hromádko, J. Přikryl, J. Rodriguez-Pereira, M. Klikar, V. Jelínková, J. M. Macak, F. Bureš, *Chempluschem* **2020**, *85*, 576–579.

[142] J. Charvot, R. Zazpe, R. Krumpolec, J. Rodriguez-Pereira, D. Pavliňák, D. Pokorný, M. Klikar, V. Jelínková, J. M. Macak, F. Bureš, *RSC Adv.* **2021**, *11*, 22140.

[143] R. Zazpe, H. Sopha, J. Charvot, R. Krumpolec, J. Rodriguez-Pereira, J. Michalička, J. Mistrík, D. Bača, M. Motola, F. Bureš, J. M. Macak, *Appl. Mater. Today* **2021**, *23*, 101017.

16 Data for the library database

Název práce	Organické sloučeniny selenu a jejich moderní využití.
Autor práce	Ing. Jaroslav Charvot
Obor	Organická chemie
Rok obhajoby	2022
Vedoucí práce	prof. Ing. Filip Bureš, Ph.D.
Anotace	Tato disertační práce se zabývá sloučeninami selenu a jejich aplikací při tvorbě tenkých vrstev. První část práce představuje vybrané depoziční metody s bližším zaměřením na technologii Atomic Layer Deposition (ALD), její charakteristiky, využití a obecné požadavky na ALD prekurzor. Ve větším detailu je pak studována příprava a vlastnosti organických sloučenin selenu s již popsaným či potenciálním využitím v ALD. V experimentální části práce bylo připraveno několik silylselenidů, silylselenolů, stanylselenidů a jednoho silylteluridu. Charakterizace cílových molekul byla provedena pomocí GC/MS a multinukleární magnetické rezonance. Syntéza a strukturní analýza je doplněna o studii základních termických vlastností (DSC a TGA), které jsou pro využití v ALD zcela klíčové. Vybrané selenidy byly v poslední části práce testovány při tvorbě tenkých vrstev $MoSe_2$ a Sb_2Se_3.
Klíčová slova	Selen, syntéza, ALD, depozice, tenké vrstvy